พอลิเมอร์ฐานเมทัลโลซาเลนสำหรับรีดักชันของคาร์บอนไดออกไซด์

นายชีรวัฒน์ แก้วใหญ่

วิทยานิพนธ์นี้เป็นส่วนหนึ่งของการศึกษาตามหลักสูตรปริญญาวิทยาศาสตรมหาบัณฑิต
สาขาวิชาปิโตรเคมีและวิทยาศาสตร์พอลิเมอร์
คณะวิทยาศาสตร์ จุฬาลงกรณ์มหาวิทยาลัย
ปีการศึกษา 2560

METALLOSALEN-BASED POLYMERS FOR REDUCTION OF CARBON DIOXIDE

Mr. Cherawat Kaewyai

A Thesis Submitted in Partial Fulfillment of the Requirements

for the Degree of Master of Science Program in Petrochemistry and Polymer Science

Faculty of Science

Chulalongkorn University

Academic Year 2017

Thesis Title	METALLOSALEN- BASED POLYMERS FOR REDUCTION OF CARBON DIOXIDE
By	Mr. Cherawat Kaewyai
Field of Study	Petrochemistry and Polymer Science
Thesis Advisor	Associate Professor Patchanita Thamyongkit, Dr.rer.nat.

Accepted by the Faculty of Science, Chulalongkorn University in Partial Fulfillment of the Requirements for the Master's Degree

.....Dean of the Faculty of Science

(Associate Professor Polkit Sangvanich, Ph.D.)

THESIS COMMITTEE

.....Chairman

(Associate Professor Nuanphun Chantarasiri, Ph.D.)

.....Thesis Advisor

(Associate Professor Patchanita Thamyongkit, Dr.rer.nat.)

.....Examiner

(Associate Professor Sirilux Poompradub, Ph.D.)

.....External Examiner

(Assistant Professor Vachiraporn Ajavakom, Ph.D.)

ชีรวัฒน์ แก้วใหญ่ : พอลิเมอร์ฐานเมทัลโลซาเลนสำหรับรีดักชันของคาร์บอนไดออกไซด์ (METALLOSALEN-BASED POLYMERS FOR REDUCTION OF CARBON DIOXIDE) อ.ที่ปรึกษาวิทยานิพนธ์หลัก: รศ. ดร.พัชณิตา ธรรมยงค์กิจ, 112 หน้า.

งานวิจัยนี้แสดงการสังเคราะห์ชุดของคอปเปอร์และนิกเกิลซาเลนที่มีโครงสร้างโมเลกุลแบบไม่สมมาตรที่มีหมู่แทนที่เป็นอนุพันธ์ของไทโอฟีน และพิสูจน์เอกลักษณ์โดยเทคนิคนิวเคลียร์แมกเนติกเรโซแนนซ์สเปกโตรสโกปีและแมสสเปกโตรเมตรี ความสามารถในการเป็นตัวเร่งปฏิกิริยาด้วยเคมีไฟฟ้าในระบบเอกพันธุ์ของสารประกอบเป้าหมายสำหรับรีดักชันของคาร์บอนไดออกไซด์ถูกตรวจสอบด้วยเทคนิคไซคลิกโวลแทมเมตรี การศึกษาทางเคมีไฟฟ้าแสดงให้เห็นว่าสารประกอบเป้าหมายมีความสามารถในการเป็นตัวเร่งปฏิกิริยาสำหรับรีดักชันของคาร์บอนไดออกไซด์เนื่องจากการเพิ่มขึ้นอย่างมีนัยสำคัญของค่ากระแสไฟฟ้าภายใต้ภาวะที่อิ่มตัวด้วยคาร์บอนไดออกไซด์เทียบกับภายใต้ภาวะที่อิ่มตัวด้วยไนโตรเจน ผลการศึกษายังแสดงให้เห็นว่าการแทรกตัวของพันธะสามของคาร์บอน-คาร์บอนระหว่างหมู่ที่มาจากไทโอฟีนและโครงสร้างหลักของซาเลนนำไปสู่ความต้องการศักย์ไฟฟ้ารีดักชันที่ลดลง ในขณะที่การเพิ่มของวงไทโอฟีนไม่มีอิทธิพลอย่างมีนัยสำคัญในด้านนี้ นอกจากนี้ การเติมน้ำร้อยละ 3 เพื่อเป็นแหล่งโปรตอนส่งผลให้เกิดการเพิ่มมากขึ้นของค่ากระแสไฟฟ้าที่ใช้ในการรีดักชันของคาร์บอนไดออกไซด์อีกด้วย ผลการศึกษาจากปฏิกิริยาพอลิเมอร์ไรเซชันทางเคมีไฟฟ้าของสารประกอบเป้าหมายผ่านหมู่ที่มาจากไทโอฟีนให้พอลิเมอร์ฐานเมทัลโลซาเลนที่ต้องการ ในกระบวนการพอลิเมอร์ไรเซชัน แสดงให้เห็นว่าการเพิ่มของวงไทโอฟีนนำไปสู่ความต้องการศักย์ไฟฟ้าออกซิเดชันที่ลดลง ในขณะที่อนุพันธ์ที่มีหมู่เชื่อมต่อที่เป็นพันธะสามของคาร์บอน-คาร์บอนต้องการศักย์ไฟฟ้าออกซิเดชันที่มากขึ้น อย่างไรก็ตาม ภาวะในกระบวนการพอลิเมอร์ไรเซชันยังจำเป็นต้องได้รับการปรับปรุงเพิ่มเติม เพื่อให้ได้รับฟิล์มที่มีประสิทธิภาพมากขึ้นสำหรับรีดักชันของคาร์บอนไดออกไซด์

สาขาวิชา ปิโตรเคมีและวิทยาศาสตร์พอลิเมอร์ ลายมือชื่อนิสิต .....

ปีการศึกษา 2560 ลายมือชื่อ อ.ที่ปรึกษาหลัก .....

5871939123 : MAJOR PETROCHEMISTRY AND POLYMER SCIENCE
KEYWORDS: SALEN / METALLOSALEN / ELECTROCHEMICAL REDUCTION / CARBON DIOXIDE / ELECTROPOLYMERIZATION

CHERAWAT KAEWYAI: METALLOSALEN-BASED POLYMERS FOR REDUCTION OF CARBON DIOXIDE. ADVISOR: ASSOC. PROF. PATCHANITA THAMYONGKIT, Dr.rer.nat., 112 pp.

In this research, a series of novel asymmetric copper- and nickel-salens bearing thiophene-based substituents were successfully synthesized and characterized by nuclear magnetic resonance spectroscopy and mass spectrometry. Homogeneous electrocatalytic activities of these monomers toward reduction of CO_2 were investigated using cyclic voltammetry technique. Electrochemical studies showed these salen monomers are able to serve as catalysts in the electrochemical reduction of CO_2 due to the significantly increase of the current observed under CO_2-saturated condition, compared with those found under the N_2-saturated one. Results also revealed that insertion of the carbon-carbon triple-bond between the thiophene-based substituents and the salen core led to the lower required reduction potential, while the additional thiophene rings did not significantly influence in this aspect. Furthermore, addition of 3% of H_2O as a proton source resulted in even higher current enhancement in the reduction of CO_2. Electropolymerization of the target monomers through their thiophene-based units gave desirable metallosalen-based polymers in most cases. In the polymerization process, results showed that the introduction of bithiophenyl rings led to the lower required oxidation potential, while the derivatives containing carbon-carbon triple-bond spacers required higher oxidation potential than those having the thiophene-based substituents directly linked to the salen cores. However, further optimization of the polymerization condition is required to obtain more efficient films for the reduction of CO_2.

Field of Study: Petrochemistry and Polymer Science Student's Signature .....
Advisor's Signature .....

Academic Year: 2017

ACKNOWLEDGEMENTS

First of all, I would like to express my deep appreciation to my advisor Assoc. Prof. Dr. Patchanita Thamyongkit for her kind guidance, valuable advice, extensive support and encouragement during my research. Her valuable advice are not only in the research methodologies but also in other methodologies of my life and the successful thesis could not be achieved without her.

Secondly, I would like to thank Assoc. Prof. Dr. Nuanphan Chantarasiri for serving as the chairman, Assoc. Prof. Dr. Sirilux Poompradub for serving as examiner, and Asst. Prof. Dr. Vachiraporn Ajavakom for serving as external examiner, and for all of their valuable suggestions in this research

Additionally, I would like to thank Dr. Parichatr Vanalabhpatana for serving an opportunity to access her laboratory and research facility for electrochemical experiments.

Most importantly, special thanks also give to all members in the research and the neighbour group for valuable friendship and helpfulness.

Finally, I would like to express my deep sense of appreciation to my beloved family for their inspiration, understanding, great support and encouragement in every part of my study.

CONTENTS

Page

Page

Page

LIST OF FIGURES

LIST OF SCHEMES

LIST OF TABLES

LIST OF ABBREVIATIONS

°C	: degree Celcius
calcd	: calculated
$CDCl_3$	: deuterated chloroform
CO_2	: carbon dioxide
^{13}C-NMR	: carbon nuclear magnetic resonance spectroscopy
CV	: cyclic voltammetry
DMF	: *N,N′*-dimethylformamide
d	: doublet (NMR)
dd	: doublet of doublet (NMR)
ECR	: electrochemical reduction
E_{onset}	: onset potential
E_{peak}	: peak potential
HR-ESI-MS	: high-resolution electrospray ionization mass spectrometry
g	: gram(s)
h	: hour(s)
^{1}H-NMR	: proton nuclear magnetic resonance spectroscopy
Hz	: hertz
J	: coupling constant
m/z	: mass to charge ratio
MALDI-TOF-MS	: matrix-assisted laser desorption ionization-time of flight-mass spectrometry
CH_2Cl_2	: dichloromethane
m	: multiplet (NMR)
MHz	: megahertz
min	: minute(s)

mmol	: millimole(s)
mg	: milligram(s)
mL	: milliliter(s)
ε	: molar absorptivity
$mV \cdot s^{-1}$	: millivolt(s) per second
N_2	: nitrogen
NHE	: normal hydrogen electrode
nm	: nanometer(s)
ppm	: parts per million
QRE	: quasi-reference electrode
rt	: room temperature
s	: singlet (NMR)
t	: triplet (NMR)
V	: volt(s)
vs.	: *versus*
mA	: milliampere(s)
mL	: milliliter(s)
δ	: chemical shift
% yield	: percentage yield

CHAPTER I

INTRODUCTION

In the present scenario, the world has global warming problem because of a concentration of greenhouse gases in the atmosphere that absorbed the sunlight and solar radiation without letting them bounce off the surface's earth. Carbon dioxide (CO_2), is a one of greenhouse gases which has been released continuously from human activities,[1] including burning of fuel in industry and household. Subsequent climate change leads to ecological impacts, such as a change the amount of carbon in vegetations, sea-level rise, hotter heat waves, and more frequent natural disaster.[2-5] Because of this, there are several researches trying to find out ways to reduce CO_2 in the atmosphere by conversion of CO_2 to value added products.

The electrocatalytic reduction (ECR) of CO_2 is an attractive way to reduce and convert CO_2 to several fuels and chemicals,[6-9] such as carbon monoxide (CO), alcohol, aldehyde and hydrocarbon.[10-11] CO and/or formate ($HCOO^-$) were obtained from two-electron reduction of CO_2 system, whereas methanol (CH_3OH) and methane (CH_4) were obtained from six and eight-electron reduction of CO_2, respectively.[12-14] Many types of metals, such as copper (Cu), ruthenium (Ru) and molybdenum (Mo), have been studied for the ECR of CO_2 owing to their ability to proceed multi-electron transfer to reduce CO_2, but one of common drawbacks of this process is large overpotential required for the formation of desired products. Consequently, metal complexes become of interest so as to reduce the overpotential by well-designed ligand and suitable central metal to improve catalytic properties.[15] One of attractive metal complexes for the ECR of CO_2 is metal-salen complexes, also called as metallosalen. In the past few years, the metallosalen was investigated as catalyst for ECR of CO_2 to give many possible products could be obtained including CO, CH_4, ethylene (C_2H_4), ethane (C_2H_6), depending on applied potential and central metal of metallosalen.[16] Copper (Cu) and nickel (Ni) were used to form metallosalen electrocatalysts. Cu(0) is well known to facilitate the formation of hydrocarbons,[17-18] while Ni(0) reportedly promotes in H_2 production with slight formation of CO.[19]

In this work, we are interested in synthesizing and investigating monomers and polymers of the metallosalen for the ECR of CO_2. The target monomers contain thiophene-based substituents on peripheral phenol rings, and a Cu(II) or Ni(II) metal center as shown in **Figure I–1**. Thiophene is known to be easy to electrochemically polymerize to give polythiophene that has conductive property.[20] Polythiophene derivatives had been used in various applications, such as *organic light-emitting diodes* (OLEDs),[21-27] solar cells[28-35] and chemical sensors.[36-40] The metallosalen-embedded polythiophenes was previously synthesized by electropolymerization with lower potential, affording conductive polymer.[41-42] Moreover, it was efficiently used for the ECR of O_2 to give H_2O and H_2O_2 as products.[43]

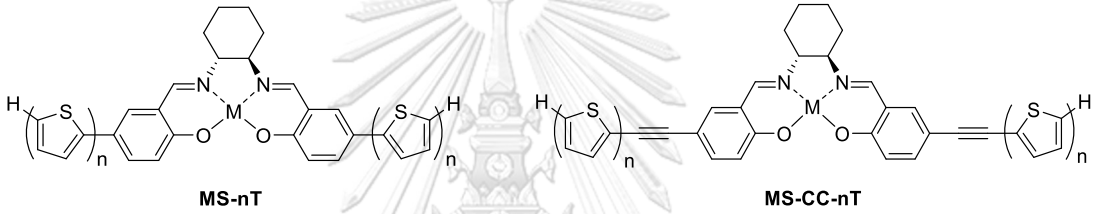

Figure I–1: Structures of the target molecules

Since it was found that unsymmetrical metallosalens served as versatile asymmetric catalysts leading to highly reactive and enantioselective catalytic reactions,[44-48] the target salens for this work are designed to have a cyclohexyl stereocenter in the molecules. The resulting monomers will be subject to electropolymerization. Both monomers and polymers will be investigated for their physical properties and electrochemical properties, and their catalytic abilities for the ECR of CO_2.

1.1 Objectives of this research

Synthesis and investigation of physical and electrochemical properties, as well as their catalytic abilities towards the ECR of CO_2 of unsymmetrical metallosalen monomers and polymers.

1.2 Scopes of this research

Each target unsymmetrical metallosalen monomers contains thienyl or bithiophenyl *para*-substituents on its phenolic groups and a Cu(II) or Ni(II) metal center as shown in **Figure I–1**. All target monomers will be characterized by spectroscopic techniques, including ^{1}H- and ^{13}C-nuclear magnetic resonance (NMR) spectroscopy, and mass spectrometry. The polymerization will be performed by cyclic voltammetry (CV). Both target monomers and polymers will be studied for their possible use as catalysts for the ECR of CO_2.

CHAPTER II

THEORY AND LITERATURE REVIEWS

2.1 Electrochemical reduction of CO_2

The ECR of CO_2 is the conversion of CO_2 into the fuel or others value added chemicals.[49-56] Considering thermodynamics of this reaction, the reduction of CO_2 by proton-coupled multi-electron processes are normally more favorable than single-electron step process because the latter requires high energy to convert CO_2 to $CO_2^{\bullet-}$. Moreover, several thermodynamically stable products are produced in the proton-coupled multi-electron processes,[57] corresponding to equations (1)–(6) from calculation of the standard reduction potential (E^o) in a 1 M aqueous solution of other solutes at pH 7 *vs.* normal hydrogen electrode (NHE) at 25°C under 1 atm gas pressure.[58]

$$CO_2 + e^- \longrightarrow CO_2^{\bullet-} \qquad E^o = -1.90\ V \quad (1)$$

$$CO_2 + 2H^+ + 2e^- \longrightarrow HCOOH \qquad E^o = -0.61\ V \quad (2)$$

$$CO_2 + 2H^+ + 2e^- \longrightarrow CO + H_2O \qquad E^o = -0.53\ V \quad (3)$$

$$CO_2 + 4H^+ + 4e^- \longrightarrow HCHO + H_2O \qquad E^o = -0.48\ V \quad (4)$$

$$CO_2 + 6H^+ + 6e^- \longrightarrow CH_3OH + H_2O \qquad E^o = -0.38\ V \quad (5)$$

$$CO_2 + 8H^+ + 8e^- \longrightarrow CH_4 + 2H_2O \qquad E^o = -0.24\ V \quad (6)$$

In kinetic aspect, a major challenge is a formation of nuclei and chemical bonds to convert CO_2 into other carbon-based molecules. Two mechanistic pathways have been proposed: one is the conversion of CO_2 to syngas (CO/H_2), followed by transformation to liquid fuel, such as gasoline, by Fisher-Tröpsch technologies;[59] and the other is the direct conversion of CO_2 to liquid fuel, such as methanol, by electrocatalytic processes. Efficient electrocatalysis of CO_2 requires fast electron transfer at an electrode surface and acceleration of a chemical conversion.[60] As a result, both electron transfer and chemical kinetics must be optimized, or in other words, the electrocatalysts must exhibit good thermodynamic match between the redox potential for the electron transfer reaction and the chemical reaction that is being catalyzed.[61]

Several groups of organometallic compounds were reported to be efficient electrocatalysts for reduction of CO_2 because of their high efficiencies, selectivities and turnover numbers,[6] for example metal complexes of porphyrins,[62-69] phthalocyanines,[70-76] cyclams,[77-83] phosphines,[84-93] bipyridines,[94-101] and salen ligands.[16]

2.2 Cyclic voltammetry (CV)

CV is a one of the most widely used techniques to determine the efficiency of the electrocatalysts for the ECR of CO_2[102] due to its non-destructive nature, versatility and informative details that can be relatively quickly extracted. Furthermore, it can be used for a wide range of applications in organic and inorganic chemistry as well as material development.[103-104] In addition, both qualitative and quantitative information about analyte in the electrochemical reaction can be obtained from this technique.[105] The electrochemical cell consists of three electrodes, *i.e.* a working electrode (WE), a counter electrode (CE) (also called as an auxiliary electrode) and a reference electrode (RE), which are immersed in an electrolyte solution[106] as depicted in **Figure II–1a**. During measurement, oxidation and/or reduction of the analyte occur at the WE surface corresponding to applied potential (E_{appl}). CV consists of the linearity of potential scanning with a triangular waveform,[106] sweeping through a potential range and reversing the direction of the sweep in a cyclic wave as depicted in **Figure II–1b**. The E_{appl} value is simultaneously measured across the WE and the RE having a large resistance and therefore no passing current. The current is then measured in response to E_{appl} across the WE and the CE, resulting in a plot between the current response and E_{appl}, which is called a cyclic voltammogram[105] as shown in **Figure II–1c**. A forward scan produces cathodic peak current (I_{pc}) for reducing the analyte in a range of E_{appl} with a maximum cathodic current called cathodic peak potential (E_{pc}). On the other hand, a reverse scan produces anodic peak current (I_{pa}) for oxidizing the reduced form of the analyte back to the original form with a maximum anodic current as anodic peak potential (E_{pa}).

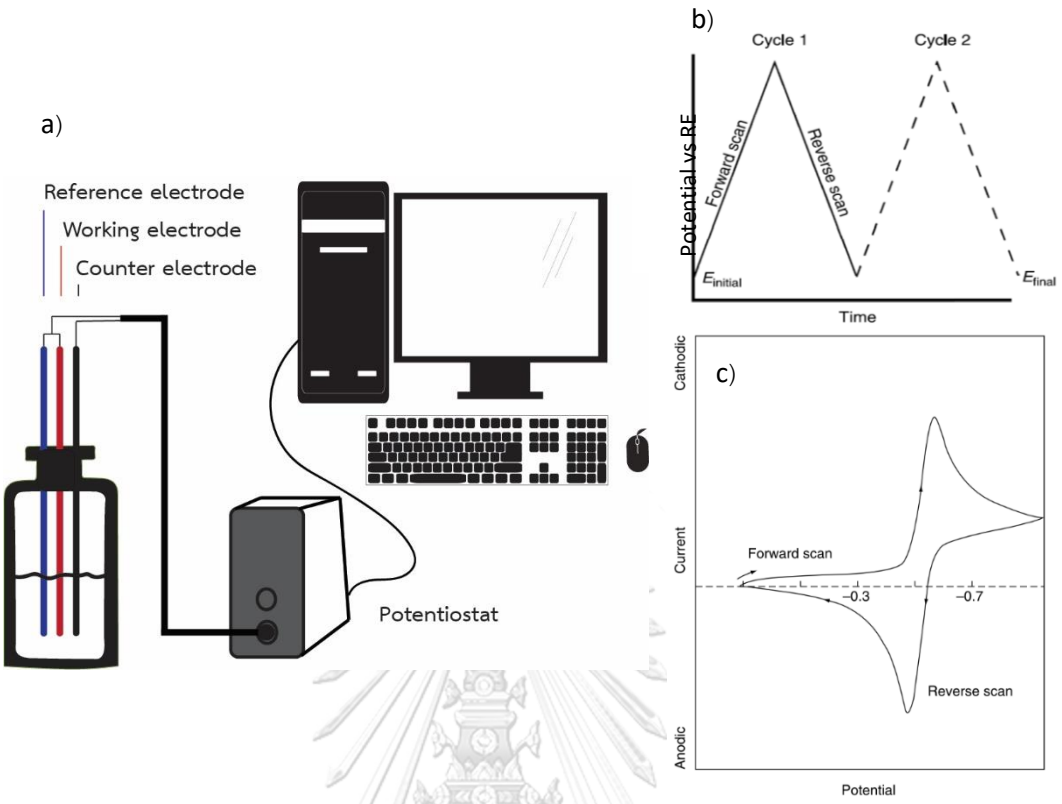

Figure II–1: a) Three-electrode cell setup, b) the triangular waveform signal[106] and c) the cyclic voltammograms.[105]

In a study of the electrocatalytic activity for the CO_2 reduction, the cyclic voltammogram of the electrocatalyst under a dry inert atmosphere (Ar or N_2) should show a reversible or quasi-reversible redox couple. When CO_2 was added in system, the diffusion limited current should increase significantly, while the potential shifts anodically, and the reversibility in the return oxidation wave may lose because of the chemical reaction between CO_2 and the electrocatalyst. For instance, **Figure II–2a** shows a cyclic voltammogram of cobalt(II)-tetraphenylporphyrin (**CoTPP**).[107] When the **CoTPP** solution was saturated with CO_2, the first reduction for a $Co^{II}P/Co^{I}P$ step was unaffected but the second reduction for a $Co^{I}P/Co^{0}P$ step exhibited significant increase in current, compared with that obtained in the Ar-saturated condition. This catalytic reduction of CO_2 took place at a potential about 0.3 V less negative than that required for direct reduction of CO_2 in a similar solution without **CoTPP** (–2.02 *vs*. –2.32 V, *vs.* saturated calomel electrode (SCE)) (**Figure II–2b**). These results indicated that **CoTPP** can lower overpotential and increase the reaction kinetics of the CO_2 reduction.

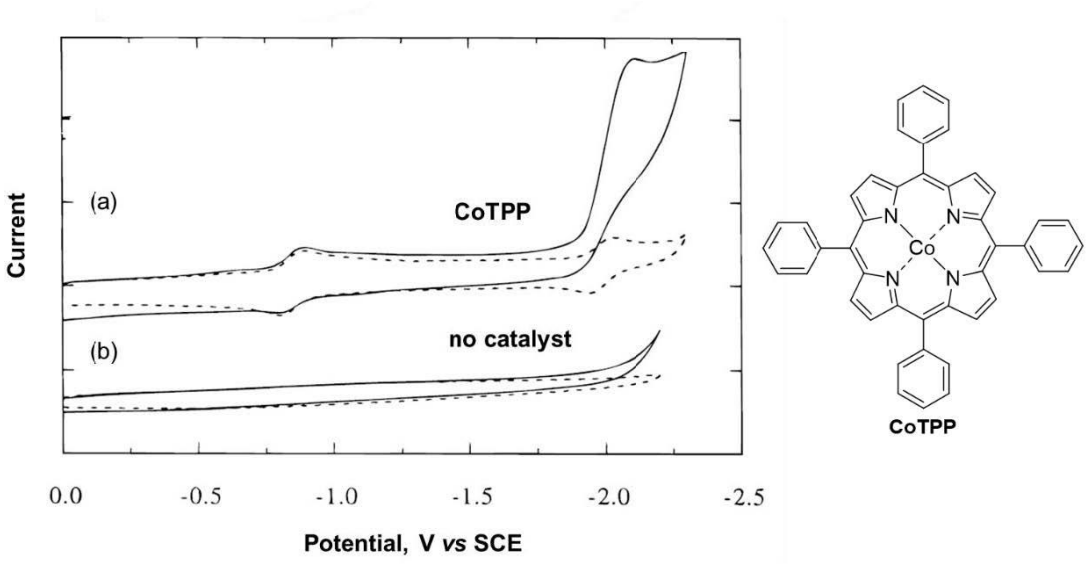

Figure II–2: Cyclic voltammograms of a 0.1 M tetrapropylammonium perchlorate (nPr_4NClO_4) solutions having (a) 0.5 mM **CoTPP** and (b) no catalyst under saturation with Ar (dotted line) and with CO_2 (solid line). A scan rate was 100 $mV \cdot s^{-1}$ and a current scale was 100 μA/division.[107]

2.3 Electropolymerization

Electropolymerization has been studied for a long time because of its several advantages,[108-109] e.g. it is a catalyst-free procedure, it provides direct deposition of a doped polymer onto an electrode surface, control of film thickness is quite easy *in situ* characterization of the polymerization by electrochemical and/or spectroscopic techniques is possible. Moreover, rate of initiation can be easily controlled by varying electrochemical parameters and it can be carried out under mild condition. A great number of experiments have been performed in organic solvent (non-aqueous) systems with various kinds of supporting electrolytes. The widely used organic solvents include dimethylformamide (DMF), dimethylsulfoxide (DMSO) and acetonitrile (ACN),[110-111] while the examples of the commonly used supporting electrolytes are tetra-butylammonium phosphate (TBAP), tetraethylammonium tetrafluoroborate (Et_4NBF_4), tetraethylammonium perchlorate (Et_4NClO_4) and tetrabutylammonium perchlorate ($n Bu_4NClO_4$). Recently, aqueous systems have been of interest for the electropolymerization due to environmental friendliness and economic advantage.[112-115] However, the selection of the solvent systems depends on the solubility of the monomers.

The electropolymerization can be classified according to occurrence of the polymer. If the polymer forms at a cathode, it will be called electroreduction polymerization (ERP). If the polymer forms at an anode, it will be called electrooxidation polymerization (EOP). In general, the EOP of organic materials has received more interest than the ERP because the formation of the polymer often occurs by the oxidation of the aromatic compounds.[116] The examples of compounds that can be polymerized by the EOP include pyrrole,[117-119] thiophene,[120] Indole,[121] furan,[122] benzene and derivatives,[123-125] while the compounds that can be polymerized by ERP include methyl methacrylate,[126] acrylonitrile and methacrylonitrile.[127-128]

2.4 Metallosalen

Salen is an anionic tetradentate ligand and widely used in coordination chemistry and homogeneous catalysis.[47] The name of salen is an abbreviation from salicylaldehyde and ethylenediamine, which are substrates for condensation to give salen ligand.[129] The salen ligand is a yellow micaceous solid that is favorably soluble in polar organic solvents. The structure of the salen ligand generally consists of two phenoxy groups connected by two methyne carbons *via* two imine bridges, which are formed by condensation between carbonyl group at *ortho*-positions of the phenoxy groups and amine groups of the ethylenediamine[130-131] (**Figure II–3**).

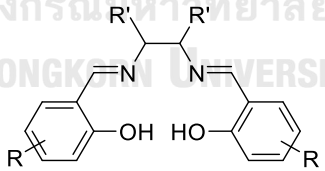

Figure II–3: A general structure of the salen ligand

There are several methods for structural modification of the salen ligands, including the substitution on the phenoxy groups or the ethylene bridge[132-134] and the metalation to give a complex called a metallosalen. Metallosalens were well known as chemical catalyst in various reactions such as enantioselective pinacol coupling[47], copolymerization,[135-137] enantioselective Nazarov cyclization,[138] asymmetric sulfimidation and sigmatropic rearrangement.[139] Later, the catalytic efficiency of metallosalen was improved by substitution on salen ligand in order to use as a catalyst

for copolymerization between cyclohexene oxide and CO_2.[140-141] Moreover, the substitution of acetylene derivatives on the metallosalen structure at peripheral phenol rings was investigated for catalytic efficiency in Henry reaction.[142-143]

2.4.1 Synthesis of metallosalen

Synthesis of the metallosalen was reported for the first time in 1933 by Pfeiffer and co-workers.[130] In 1950, Diehl[131] suggested a simple route of synthesis of the salen ligand *via* condensation between salicylaldehyde and ethylenediamine in hot ethanol (**Scheme II–1**).

Scheme II–1: Synthesis of the salen ligand under a Diehl's condition.

Later, condensation between salicylaldehyde derivatives and 1,2-diamine derivatives in ethanol in the similar manner was reported to give the corresponding salen ligands as precipitates in 50–80% yield (**Scheme II–2**). The metallosalens can be quantitatively prepared via metallation between the salen ligands and various metal salts in appropriate solvents[140-141] (**Scheme II–3**).

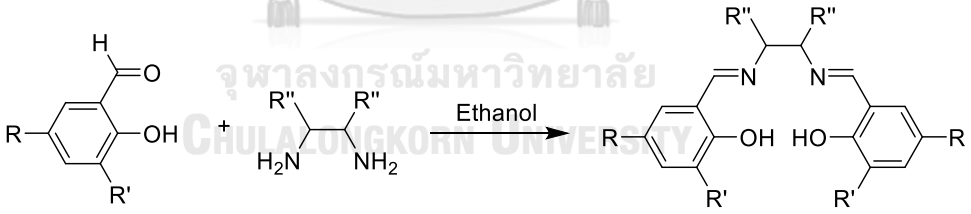

Scheme II–2: Synthesis of substituted-salen ligands

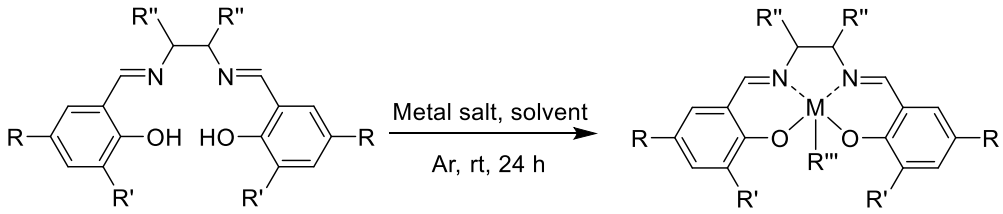

Scheme II–3: Metallation of substituted-metallosalens

2.5 Thiophene

Thiophene is a five-membered ring heterocyclic aromatic compound, which can be polymerized to be polythiophene (**Figure II-4**), which exhibits conductive properties.[20] Its conductive properties are caused by delocalization of electrons throughout its conjugated backbone. Furthermore, high environmental stability and well-established structural modification of polythiophene enable great developments of its derivatives for several electronic applications,[144] such as capacitors,[145-151] light-emitting diodes,[152-161] field-effect transistors,[162-167] solar cells[168-175] and electrochromic device.[176-183]

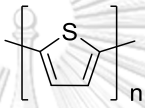

Figure II–4: A structure of polythiophene.

Polythiophenes can be prepared by means of two routes, chemical and electrochemical synthesis.[109] In case of chemical synthetic routes, nickel- and palladium-based cross coupling chemistry are adapted to the efficient synthesis of polythiophene and its derivatives. Two important features of these cross-coupling reactions are selective C-C bond formation and regioselectivity of the catalyst. **Scheme II–4** shows published preparation procedures of polythiophenes using nickel- and palladium-based catalysts. The upper route involves in the formation of two intermediates by reacting a 2,5-dibromothiophene derivative with Rieke zinc (Zn*) under a Rieke's method.[184] The resulting Zn-complexes were accessed in the cross-coupling reaction using $Pd(PPh_3)_4$, affording a corresponding polythiophene derivative. The lower way starts from synthesis of intermediates through Grignard metathesis, followed by nickel-catalyzed coupling reaction to get the corresponding polymer.[185]

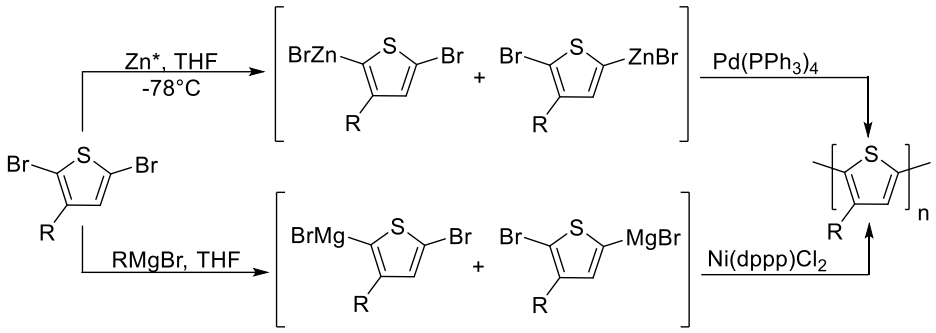

Scheme II–4: Syntheses of polythiophene derivatives through Rieke's (upper)[184] and Grignard's (lower) routes.[185]

As regards the electrochemical polymerization, the cyclic voltammograms and the proposed mechanism of the electropolymerization of thiophene are depicted in **Figure II–5**. The electrochemical processes of thiophene starts from the oxidation step generating cation radical species, followed by coupling and aromatization to form its dimer. After that, a sequence of subsequent dimerization steps proceeds to the formation of oligomers and polymers. The cyclic voltammogram shows a current density increased as more polythiophene was formed on the electrode surface.[186]

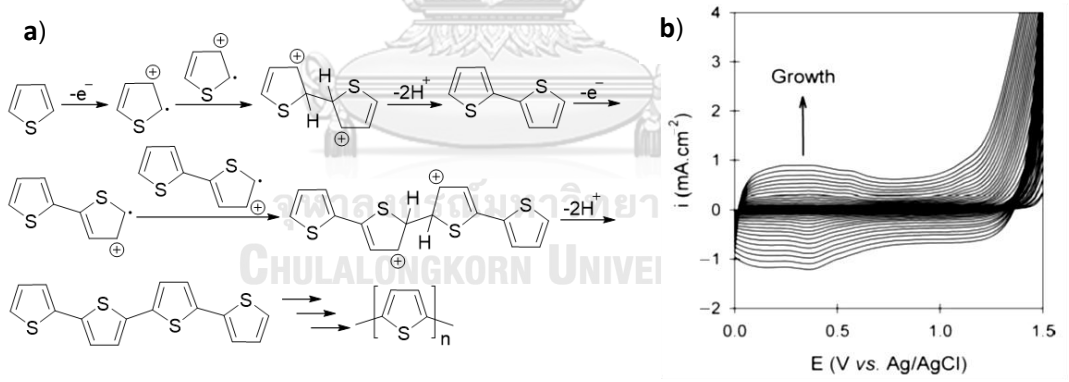

Figure II–5: a) Proposed mechanism of the electropolymerization of thiophene and b) the corresponding cyclic voltammograms.[186]

2.6 Thiophene-substituted metallosalen derivatives

In 1998, Kingsborough and Swager[41] studied electroactivity of the thiophene-substituted cobalt-salen (**CoS-T**) which was synthesized through the palladium-based cross coupling, followed by the condensation and the cobalt metallation (**Scheme II–**

5). After that, **CoS-T** was successfully polymerized by oxidative polymerization, while no film growth was observed for the metal-free derivative.

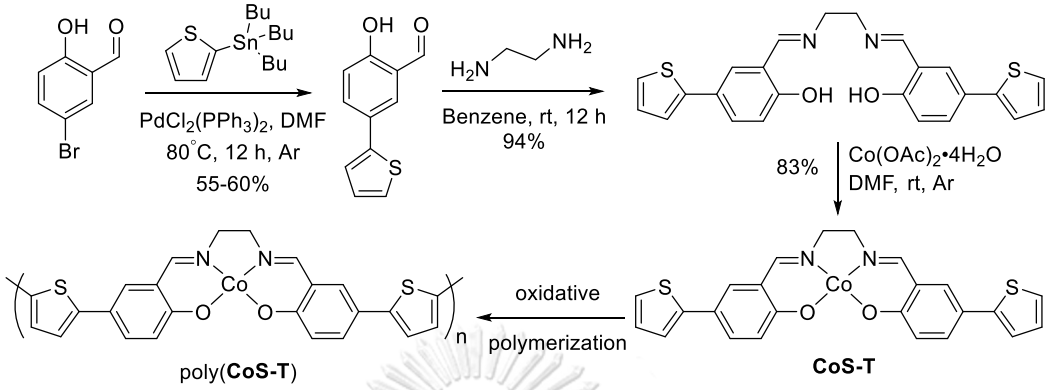

Scheme II–5: Synthesis and oxidative polymerization of **CoS-T**

Furthermore, EDOT-substituted cobalt-salen (**CoS-EDOT**), where EDOT stands for 3,4-ethylenedioxythiophene (**Figure II–6**), was synthesized and polymerized in the similar manner as **CoS-T**. Compared with the cyclic voltammograms of electro-polymerization of **CoS-T**, those of **CoS-EDOT** showed overall decrease in the oxidation potential as depicted in **Figure II–7**, indicating that a more electron-rich EDOT led to easier oxidative polymerization. In addition, an EDOT-substituted cobalt-salen polymer (poly(**CoS-EDOT**)) was investigated for the electrocatalytic activity for oxygen (O_2) reduction. The result showed that poly(**CoS-EDOT**) was a highly conducting hybrid material capable of O_2 reduction by four-electron reduction process to produce H_2O and H_2O_2.[43]

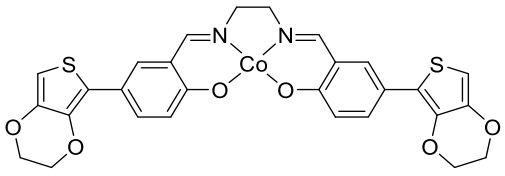

Figure II–6: A structure of **CoS-EDOT**

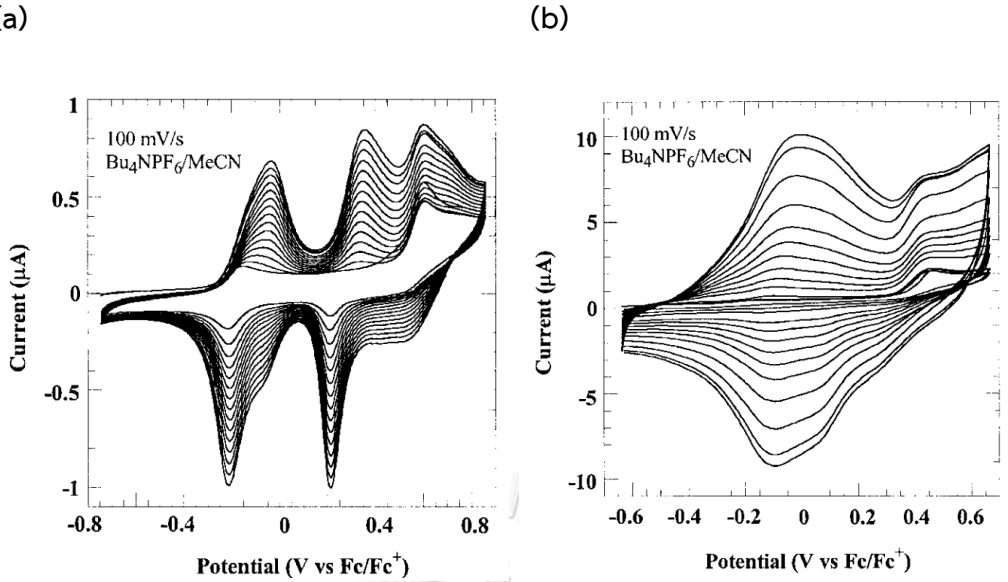

Figure II–7: Cyclic voltammograms of oxidative polymerization of (a) **CoS-T** and (b) **CoS-EDOT**[41]

In 2006, asymmetric thiophene-derivatives metallosalens **1**, **2** and **3** (**Figure II–8**) were synthesized and polymerized to investigate effects of their structures on the electroactivity.[187] The [*1S*,*2S*]-cyclohexyl bridge was introduced to these molecules to improve the catalytic activities for Nozaki-Hiyama-Kishi reaction and enantioselectivities of the metallosalen,[188] which was found that asymmetric metallosalen gave better those properties than symmetric one.[189-190] Moreover, thienyl rings were used to improve the stability, reversibility of redox couples and conductivity of the resulting polymers.[41-42]

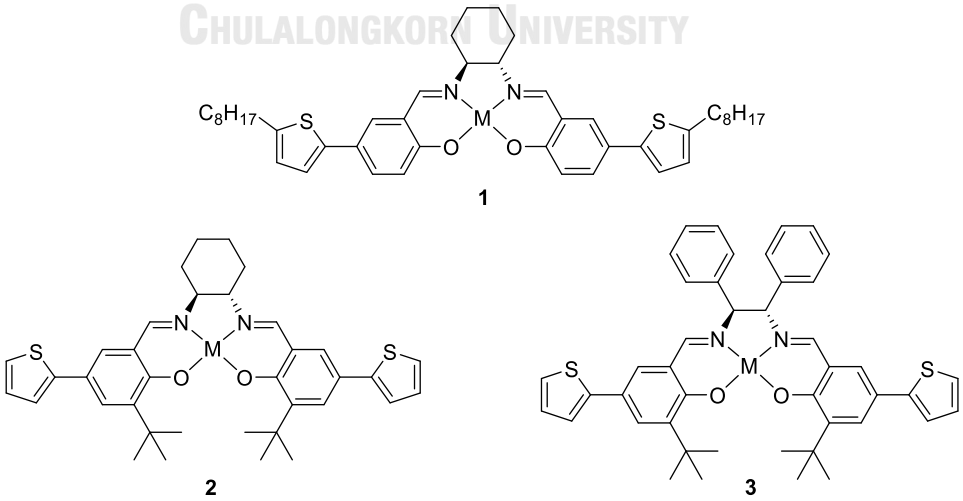

Figure II–8: Structures of **1**, **2** and **3**

CHAPTER III

EXPERIMENTS

3.1 Synthesis

3.1.1 Materials and methods

All chemicals were commercially available and used as received unless noted otherwise.

^{1}H- and ^{13}C-NMR spectra were recorded on a Varian Mercury 400 NMR Spectrometer and a Bruker Avance 400 NMR Spectrometer respectively and obtained in $CDCl_3$. Chemical shifts (δ) were reported in parts per million (ppm) relative to the residual $CHCl_3$ signal (7.26 ppm for ^{1}H-NMR spectroscopy and 77.0 ppm for ^{13}C-NMR spectroscopy.

Mass spectra were obtained using high-resolution electrospray ionization (HR-ESI) and matrix-assisted laser desorption ionization time-of-flight (MALDI-TOF) mass spectrometers using α-dithranol as a matrix.

3.1.2 2-Hydroxy-5-thiophen-2-yl-benzaldehyde (H-1T-B)

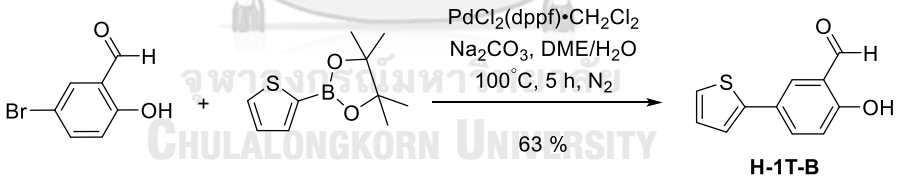

H-1T-B

Following a reported procedure[188] with slight modification by using a protected boronic acid derivative instead of thiophenyl-2-boronic acid, a mixture of 5-bromosalicyladehyde (0.396 g, 1.97 mmol), 2-(4,4,5,5-tetramethyl-1,3,2-dioxaborolan-2-yl)-thiophene (0.496 g, 2.36 mmol), [1,1′-bis(diphenylphosphino)ferrocene]dichloro-palladium(II) complex with CH_2Cl_2 ($PdCl_2$(dppf)·CH_2Cl_2, 0.082 g, 0.10 mmol) and sodium carbonate (Na_2CO_3, 0.209 g, 1.97 mmol) in dimethoxyethane (DME)/water (3/1, 6 mL, degassed with N_2) was stirred under N_2 atmosphere at 100 °C for 5 h. After cooling to room temperature, the reaction mixture was poured into deionized water (20 mL). The aqueous mixture was extracted with CH_2Cl_2 (3x15 mL), and the combined organic

phase was dried over anhydrous $MgSO_4$. The solvent was removed under reduced pressure and the resulting crude was purified by column chromatography over silica gel (diethyl ether (Et_2O)/hexanes 1/1) to give a yellow powder. After recrystallization in hexanes, compound **H-1T-B** was obtained as yellow crystals (0.254 g, 63%). m.p. 108–110 °C. ^{1}H NMR δ 7.00 (d, *J* = 8.4 Hz, 1H), 7.04–7.11 (m, 1H), 7.20–7.24 (m, 1H), 7.24–7.28 (m, 1H), 7.70–7.76 (m, 2H), 9.90 (s, 1H), 11.00 (s, 1H) (**Figure A–1**); ^{13}C NMR δ 118.3, 120.7, 122.9, 124.7, 126.9, 128.2, 130.6, 134.6, 142.6, 161.0, 196.5 (**Figure A–2**). These characterization data are consistent with those described in a published report.[188]

3.1.3 2-Hydroxy-5-(2,2′-bithiophen-5-yl)-benzaldehyde (H-2T-B)

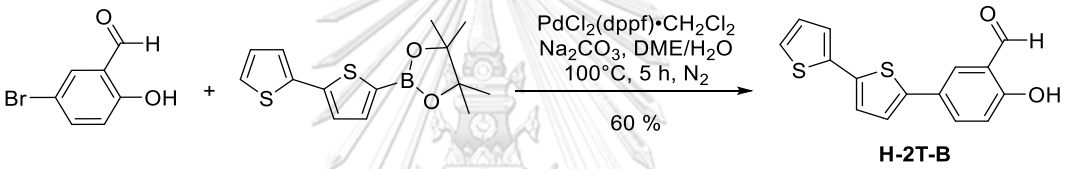

H-2T-B

In a similar manner to the synthesis of **H-1T-B**, a mixture of 5-bromosalicyladehyde (0.396 g, 1.97 mmol), 5-(4,4,5,5-tetramethyl-1,3,2-dioxaborolan-2-yl)-2,2′-bithiophene (0.689 g, 2.36 mmol), $PdCl_2(dppf)\cdot CH_2Cl_2$ (0.082 g, 0.10 mmol) and Na_2CO_3 (0.209 g, 1.97 mmol) in DME/H_2O (3/1, 6 mL, degassed with N_2) was stirred under N_2 atmosphere at 100 °C for 5 h. After above-mentioned work-up process, the resulting crude was purified by column chromatography over silica gel (CH_2Cl_2/hexanes 1/1) to provide dark yellow powder. After recrystallization in hexanes, compound **H-2T-B** was obtained as a dark yellow solid (0.338 g, 60%). m.p. 179–181 °C. ^{1}H NMR δ 7.02–7.05 (m, 2H), 7.14 (s, 1H), 7.19 (d, *J* = 2.4 Hz, 1H), 7.23 (d, *J* = 4.0 Hz, 1H), 7.24–7.26 (m, 1H), 7.73–7.77 (m, 2H), 9.95 (s, 1H), 11.01 (s, 1H) (**Figure A–3**); ^{13}C NMR δ 118.5, 120.8, 123.6, 123.9, 124.7, 124.8, 126.7, 128.0, 130.4, 134.3, 136.8, 137.2, 141.3, 161.2, 196.5 (**Figure A–4**); HR-ESI-MS *m/z*: [M^+] calcd for $C_{15}H_{10}O_2S_2$, 286.0122; found, 286.0123 (**Figure A–5**).

3.1.4 2-Hydroxy-5-(2-(thiophen-2-yl)-ethyn-1-yl)-benzaldehyde (H-CC-1T-B)

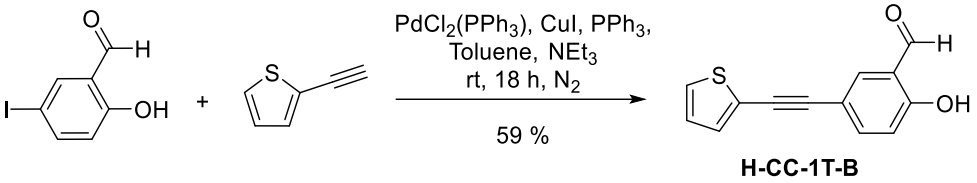

H-CC-1T-B

Following a reported procedure,[191] a mixture of 5-iodosalicyladehyde[192] (0.496 g, 2.00 mmol), 2-ethynylthiophene (0.270 g, 2.50 mmol), bis[triphenylphosphine]-dichloropalladium(II) ($PdCl_2(PPh_3)_3$, 0.070 g, 0.10 mmol), CuI (0.038 g, 0.20 mmol) and PPh_3 (0.052 g, 0.20 ,mmol) in toluene (6 mL, degassed with N_2) was stirred at room temperature for 15 min. After that, triethylamine (NEt_3, 3 mL) was added slowly, and then a mixture was stirred under N_2 atmosphere at room temperature for 18 h. Then, the reaction mixture was poured into CH_2Cl_2 (25 mL) and the resulting solution was extracted with a saturated aqueous solution of NH_4Cl (3x15 mL) and a saturated aqueous solution of NaCl (1x15 mL). The combined organic phase was dried over anhydrous $MgSO_4$ and the solvent was removed under reduced pressure. The resulting crude was purified by column chromatography over silica gel (CH_2Cl_2/hexanes 1/4) to give an off-white powder which was recrystallized in hexanes to yield compound **H-CC-1T-B** as white crystals (0.268 g, 59%). m.p. 103–105 °C. ^{1}H NMR δ 6.95–7.05 (m, 2H), 7.23–7.34 (m, 2H), 7.64 (dd, *J* = 8.8, 2.0 Hz, 1H), 7.73 (d, *J* = 1.6 Hz, 1H), 9.88 (s, 1H), 11.12 (s, 1H) (**Figure A–6**); ^{13}C NMR δ 82.3, 91.3, 115.0, 118.3, 120.7, 123.1, 127.3, 127.5, 132.1, 136.9, 139.7, 161.6, 196.1 (**Figure A–7**); HR-ESI-MS *m/z*: [M^+] calcd for $C_{13}H_8O_2S$, 228.0245; found, 228.0240 (**Figure A–8**).

3.1.5 2-Hydroxy-5-(2-(2,2′-bithiophen-5-yl)-ethyn-1-yl)-benzaldehyde (H-CC-2T-B)

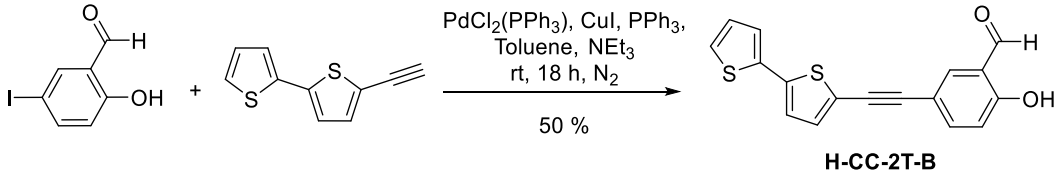

H-CC-2T-B

In a similar manner to synthesis of **H-CC-1T-B**, a mixture of 5-iodosalicyladehyde[192] (0.496 g, 2.00 mmol), 5-ethynyl-2,2′-bithiophene[193] (0.476 g, 2.50 mmol), $PdCl_2(PPh_3)$ (0.070 g, 0.10 mmol), CuI (0.038 g, 0.20 mmol) and PPh_3 (0.052 g,

0.20 ,mmol) in toluene (6 mL, degassed with N_2) was stirred at room temperature for 15 min, NEt_3 (3 mL) was added slowly, and then a mixture was stirred continuously under N_2 atmosphere at room temperature for 18 h. After above-mentioned work-up process, the resulting crude was purified by column chromatography over silica gel (Ch_2Cl_2/hexanes 1/2) to give yellow powder which was recrystallized in hexanes to yield compound **H-CC-2T-B** as a light-yellow solid (0.310 g, 50%). m.p. 146–148 °C. ^{1}H NMR δ 6.99 (d, *J* = 8.4 Hz, 1H), 7.03 (dd, *J* = 5.2, 3.6 Hz, 1H), 7.07 (d, *J* = 3.6 Hz, 1H), 7.17 (d, *J* = 4.0 Hz, 1H), 7.20 (d, *J* = 2.8 Hz, 1H), 7.23–7.26 (m, 1H), 7.64 (dd, *J* = 8.4, 1.6 Hz, 1H), 7.73 (d, *J* = 1.6 Hz, 1H), 9.88 (s, 1H), 11.13 (s, 1H) (**Figure A–9**); ^{13}C NMR δ 82.3, 92.3, 115.0, 118.4, 120.7, 121.7, 123.7, 124.4, 125.2, 128.1, 133.0, 136.8, 139.2, 139.7, 161.7 196.1 (**Figure A–10**); HR-ESI-MS *m/z*: [M^+] calcd for $C_{17}H_{10}O_2S_2$, 310.0122; found, 310.0127 (**Figure A–11**).

3.1.6 General procedure for salen ligand formation

Following a reported procedure,[188] to a solution of a salicylaldehyde derivative (1.70 equivalent) in ethanol (15 mL) was treated with (*S,S*)-1,2-cyclohexanediamine (1.00 equivalent) at 60 ºC for 1.5 h. After the reaction mixture was cooled to room temperature, the resulting solid was filtered, washed with ethanol, methanol and hexane, and recrystallized in chloroform and hexane to afforded desired products.

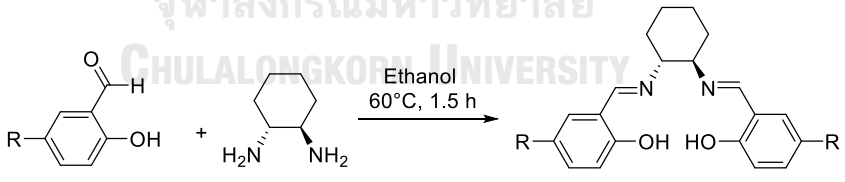

H_2S-1T (65%) **H_2S-2T** (55%) **H_2S-CC-1T** (52%) **H_2S-CC-2T** (49%)

3.1.6.1 (*S,S*)-*N,N′*-bis(salicylidene-5-thiophen-2-yl)-cyclohexane-1,2-diamine (H_2S-1T)

H-1T-B (0.402 g, 1.97 mmol) was reacted with (*S,S*)-1,2-cyclohexanediamine (0.116 g, 1.02 mmol) to give the title compound as a yellow crystal (0.312 g, 65%); m.p.

115–117 °C. ^{1}H NMR δ 1.45–1.53 (m, 2H), 1.68–1.80 (m, 2H), 1.84–2.03 (m, 4H), 3.31–3.38 (m, 2H), 6.91 (d, *J* = 8.4 Hz, 2H), 7.00–7.04 (m, 2H), 7.10–7.14 (m, 2H), 7.18 (d, *J* = 4.8 Hz, 2H), 7.37 (s, 2H), 7.44–7.52 (m, 2H), 8.30 (s, 2H), 13.38 (s, 2H) (**Figure A–12**); ^{13}C NMR δ 24.2, 33.1, 72.8, 117.5, 118.7, 122.2, 123.9, 125.6, 128.0, 128.9, 130.2, 143.8, 160.7, 164.6 (**Figure A–13**); MALDI-TOF-MS *m/z*: found, 486.586 (100) [M^+]; calcd avg mass, 486.648 (M^+; M = $C_{28}H_{26}N_2O_2S_2$) (**Figure A–14**). These characterization data are consistent with those described in a published report.[188]

3.1.6.2 (*S,S*)-*N,N′*-bis(salicylidene-5-(2,2′-bithiophen-5-yl)-cyclohexane-1,2-diamine (H_2S-2T)

H-2T-B (0.292 g, 1.02 mmol) was reacted with (*S,S*)-1,2-cyclohexanediamine (0.069 g, 0.60 mmol) to give the title compound as a light orange crystal (0.183 g, 55%); m.p. 240–242 °C. ^{1}H NMR δ 1.47–1.60 (m, 2H), 1.70–1.81 (m, 2H), 1.86–2.04 (m, 4H), 3.33–3.39 (m, 2H), 6.92 (d, *J* = 8.4 Hz, 2H), 6.98–7.04 (m, *J* = 3.4 Hz, 2H), 7.08 (d, *J* = 3.6 Hz, 2H), 7.15 (d, *J* = 2.8 Hz, 2H), 7.19 (d, *J* = 4.0 Hz, 2H), 7.24–7.29 (m, 2H), 7.35 (d, *J* = 1.6 Hz, 2H), 7.47 (dd, *J* = 8.4, 2.0 Hz, 2H), 8.30 (s, 2H), 13.40 (s, 2H) (**Figure A–15**); ^{13}C NMR δ 24.3, 33.1, 72.8, 117.7, 118.8, 122.8, 123.5, 124.3, 124.6, 125.3, 127.9, 128.6, 129.9, 135.8, 137.6, 142.6, 160.9, 164.7 (**Figure A–16**); MALDI-TOF-MS *m/z* (%): found, 650.646 (100) [M^+]; calcd avg mass, 650.888 (M^+; M = $C_{36}H_{30}N_2O_2S_4$) (**Figure A–17**); HR-ESI-MS *m/z*: [$(M+H)^+$] calcd for $C_{36}H_{30}N_2O_2S_4$, 651.1263; found, 651.1261 (**Figure A–18**).

3.1.6.3 (*S,S*)-*N,N′*-bis(salicylidene-5-(2-(thiophen-2-yl)-ethyn-1-yl)-cyclohexane-1,2-diamine (H_2S-CC-1T)

H-CC-1T-B (0.233 g, 1.02 mmol) was reacted with (*S,S*)-1,2-cyclohexanediamine (0.069 g, 0.60 mmol) to give the title compound as a light-yellow crystal (0.243 g, 52%); m.p. 193–195 °C. ^{1}H NMR δ 1.35–1.44 (m, 2H), 1.58–1.69 (m, 2H), 1.78–1.90 (m, 4H), 3.21–3.28 (m, 2H), 6.80 (d, *J* = 8.4 Hz, 2H), 6.89–6.93 (m, 2H), 7.15 (d, *J* = 2.4 Hz, 2H), 7.17 (d, *J* = 5.2 Hz, 2H), 7.26 (s, 2H), 7.30–7.34 (m, 2H), 8.14 (s, 2H), 13.49 (s, 2H) (**Figure A–19**); ^{13}C NMR δ 24.2, 33.0, 72.6, 81.2, 92.5, 113.2, 117.6, 118.6, 123.7, 127.0, 127.2, 131.6, 134.8, 135.5, 161.6, 164.18 (**Figure A–20**); MALDI-TOF-MS *m/z* (%): found, 534.713

(100) [M^+]; calcd avg mass, 534.692 (M^+; M = $C_{32}H_{26}N_2O_2S_2$) (**Figure A–21**); HR-ESI-MS *m/z*: [$(M+H)^+$] calcd for $C_{32}H_{26}N_2O_2S_2$, 535.1508; found, 535.1505 (**Figure A–22**).

3.1.6.4 (*S,S*)-*N,N′*-bis(salicylidene-5-(2-(2,2′-bithiophen-5-yl)-ethyn-1-yl)-cyclohexane-1,2-diamine (H_2S-CC-2T)

H-CC-2T-B (0.317 g, 1.02 mmol) was reacted with (*S,S*)-1,2-cyclohexanediamine (0.069 g, 0.60 mmol) to give the title compound as a dark yellow crystal (0.390 g, 49%); m.p. 129–131 °C. ^{1}H NMR δ 1.45–1.54 (m, 2H), 1.68–1.78 (m, 2H), 1.85–2.01 (m, 4H), 3.32–3.38 (m, 2H), 6.89 (d, *J* = 8.4 Hz, 2H), 7.00–7.03 (m, 2H), 7.04 (d, *J* = 3.6 Hz, 2H), 7.11 (d, *J* = 3.6 Hz, 2H), 7.18 (d, *J* = 2.4 Hz, 2H), 7.23 (d, *J* = 4.0 Hz, 2H), 7.32–7.36 (m, 2H), 7.40 (dd, *J* = 8.4, 1.6 Hz, 2H), 8.23 (s, 2H), 13.59 (s, 2H) (**Figure A–23**); ^{13}C NMR δ 24.1, 32.9, 72.5, 81.2, 93.5, 113.1, 117.5, 118.5, 122.2, 123.5, 124.1, 124.9, 127.9, 132.3, 134.7, 135.4, 136.8, 138.5, 161.6, 164.0 (**Figure A–24**); MALDI-TOF-MS *m/z* (%): found, 699.010 (100) [M^+]; calcd avg mass, 698.932 (M^+; M = $C_{40}H_{30}N_2O_2S_4$) (**Figure A–25**); HR-ESI-MS *m/z*: [$(M+H)^+$] calcd for $C_{40}H_{30}N_2O_2S_4$, 699.1263; found, 699.1269 (**Figure A–26**).

3.1.7 General procedure for salen complexation

Following a reported procedure,[188] a solution of salen ligand (0.50 mmol) in CH_2Cl_2 (30 mL) was reacted with $Ni(OAc)_2$ or $Cu(OAc)_2$ (0.55 mmol, 1.1 mol equivalent) in MeOH (15 mL) at room temperature. After 5 h, the reaction mixture was poured into water (25 mL), and the separated organic phase was extracted with a saturated aqueous solution of NH_4Cl (3x15 mL) and a saturated aqueous solution of NaCl (3x15 mL). The combined extract was dried over anhydrous $MgSO_4$, and the solvent was removed under reduced pressure. The resulting crude was filtered and washed with methanol and hexane to afford the desired product.

CuS-1Th (0.219 g, 80%), a dark green solid; m.p. > 250 °C. MALDI-TOF-MS *m/z* (%): found, 547.748 (100) [M^+]; calcd avg mass, 548.178 (M^+; M = $C_{28}H_{24}CuN_2O_2S_2$) (**Figure A–27**).

NiS-1Th (0.231 g, 85%), a dark yellow solid; m.p. > 250 °C. MALDI-TOF-MS *m/z* (%): found, 542.257 (100) [M^+]; calcd avg mass, 543.325 (M^+; M = $C_{28}H_{24}N_2NiO_2S_2$) (**Figure A–28**).

CuS-2Th (0.249 g, 70%), a brown green solid; m.p. > 250 °C. MALDI-TOF-MS *m/z* (%): found, 711.954 (100) [M^+]; calcd avg mass, 712.418 (M^+; M = $C_{36}H_{28}CuN_2O_2S_4$) (**Figure A–29**).

NiS-2Th (0.255 g, 73%), a brown yellow solid; m.p. > 250 °C. MALDI-TOF-MS *m/z* (%): found, 705.727 (100) [M^+]; calcd avg mass, 707.565 (M^+; M = $C_{36}H_{28}N_2NiO_2S_4$) (**Figure A–30**).

CuS-CC-1T (0.223 g, 75%), a dark green solid; m.p. > 250 °C. MALDI-TOF-MS *m/z* (%): found, 594.774 (100) [M^+], 614.858 [$(M+Na)^+$], 659.909 [$(M+Cu)^+$]; calcd avg mass, 596.222 (M^+; M = $C_{32}H_{24}CuN_2O_2S_2$) (**Figure A–31**); HR-ESI-MS *m/z*: [$(M+H)^+$] calcd for $C_{32}H_{24}CuN_2O_2S_2$, 596.0648; found, 596.0645 (**Figure A–32**).

NiS-CC-1T (0.236 g, 80%), a dark yellow solid; m.p. > 250 °C. MALDI-TOF-MS *m/z* (%): found, 590.290 (100) [M^+]; calcd avg mass, 591.369 (M^+; M = $C_{32}H_{24}N_2NiO_2S_2$) (**Figure A–33**); HR-ESI-MS *m/z*: [$(M+H)^+$] calcd for $C_{32}H_{24}N_2NiO_2S_2$, 591.0705; found, 591.0712 (**Figure A–34**).

CuS-CC-2T (0.269 g, 71%), a brown green solid; m.p. > 250 °C. MALDI-TOF-MS *m/z* (%): found, 758.324 (100) [M^+], 823.316 [$(M+Cu)^+$]; calcd avg mass, 760.462 (M^+; M = $C_{40}H_{28}CuN_2O_2S_4$) (**Figure A–35**); HR-ESI-MS *m/z*: [$(M+H)^+$] calcd for $C_{40}H_{28}CuN_2O_2S_4$, 760.0402; found, 760.0407 (**Figure A–36**).

NiS-CC-2T (0.279 g, 74%), a brown yellow solid; m.p. > 250 °C. MALDI-TOF-MS *m/z* (%): found, 753.408 (100) [M^+]; calcd avg mass, 755.609 (M^+; M = $C_{40}H_{28}N_2NiO_2S_4$) (**Figure A–37**); HR-ESI-MS *m/z*: [$(M+H)^+$] calcd for $C_{40}H_{28}N_2NiO_2S_4$, 755.0460; found, 755.0434 (**Figure A–38**).

3.2 Electrochemistry

3.2.1 Electropolymerization

The electropolymerization was performed using a Metrohm-Autolab PGSTAT101 potentiostat in a three-electrode cell containing the ITO-coated glass as the WE, Pt plate as the CE and a silver chloride coated on silver wire (Ag/AgCl) as a quasi-reference electrode (QRE). The concentration of monomers at their maximum solubility (0.50–0.10 mM) in dry CH_2Cl_2 containing 0.1 M nBu$_4$NPF$_6$ was used. The solution was degassed with N_2 for 15 min prior to the electropolymerization. The polymerization was carried out at cyclic potential between –0.2 V and 1.8 V versus Ag/AgCl QRE at a scan rate of 100 mV•s^{-1} with the number of repeated scanning of 10 cycles.

3.3.2 ECR of CO_2

The ECR of CO_2 was performed using a Metrohm-Autolab PGSTAT101 potentiostat. For a homogeneous condition, the electrochemical reduction was conducted in the three-electrode cell containing a glassy carbon as the WE, Pt plate as the CE and the Ag/AgCl QRE. The concentration of the monomers was 0.50 mM in dry DMF containing 0.1 M nBu$_4$NPF$_6$. The electrochemical behavior of the monomers was studied by purging N_2 to the solution for 15 min prior to the measurements which were proceeded at cyclic potential between 0.0 V and –2.0 V versus Ag/AgCl QRE at a scan rate of 50 mV•s^{-1}, for 3 cycles. After that the same solution was purged with CO_2 for 15 min to determine their electrocatalyric activities for the ECR of CO_2 by using the same potential range, scan rate and number of scan. For the heterogeneous ECR of CO_2, the same cyclic voltammetry setup on that described for the monomers was used, except that the WE in this case was the polymer films on the ITO-coated glass, the electrolyte solution contained no salen monomer and the potential range was between 0.0 V and –1.7 V.

CHAPTER IV
RESULTS AND DISCUSSION

This research mainly focuses on synthesis, characterization and investigation of physical properties and electrochemical properties of novel unsymmetrical metallosalen bearing thienyl derivatives substituents, which are shown in **Figure IV–1**. Target compounds **MS–nT** consist the metallosalen bear thienyl or bithiophenyl units directly attached on their phenoxyl rings, while target compounds **MS–CC–nT** have carbon-carbon triple bonds between the metallosalen and their thienyl or bithiophenyl units. These compounds will be used as monomers for the electropolymerization. After that, the target monomers and the resulting polymers will be investigated for their possible use for electrocatalytic reduction of CO_2. Thus, in this chapter, the content includes synthesis and characterization of the target monomers, the investigation of the electrocatalytic activity of the monomers towards the ECR of CO_2, and electropolymerization of the monomers and the determination of the potential use of the resulting polymers for the ECR of CO_2.

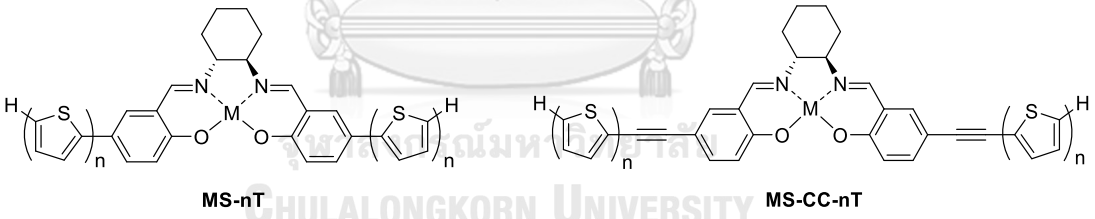

n = 1 or 2

M = Cu or Ni

Figure IV–1: Structures of the target compounds

4.1 Synthesis of salen monomers

Synthesis of **MS-nT** started with Suzuki cross-coupling of 5-bromo-salicylaldehyde with an excess amount of thiophene-2-boronic acid pinacol ester or 2,2′-bithophene-5-boronic acid pinacol ester in the presence of $PdCl_2(dppf)\cdot CH_2Cl_2$ and Na_2CO_3 in a DME/H_2O mixture[188] as depicted in **Scheme IV–1**, leading to compound **H-1T-B** or **H-2T-B** in 63% or 60%, respectively. Formation of compound **H-1T-B** was

confirmed by a ^{1}H-NMR spectrum showing a singlet peak of a hydroxyl proton at 11.00 ppm, a singlet peak of an aldehyde proton at 9.90 ppm, and a group of peaks corresponding to protons on the benzene and thiophene rings at around 7.00–7.76 ppm. These spectral data are consistent with those reported in a literature.[188] In a similar manner, a ^{1}H-NMR spectrum of **H-2T-B** showed a singlet peak of a hydroxyl proton at 11.01 ppm, a singlet peak of an aldehyde proton at 9.95 ppm, and a group of peaks indicating protons on benzene and bithiophene rings at around 7.02–7.77 ppm. Furthermore, a HS-ESI mass spectrometry showed a molecular ion peak of **H-2T-B** at *m/z* 286.0123 [$(M+H)^{+}$], comfirming successful formation of **H-2T-B**.

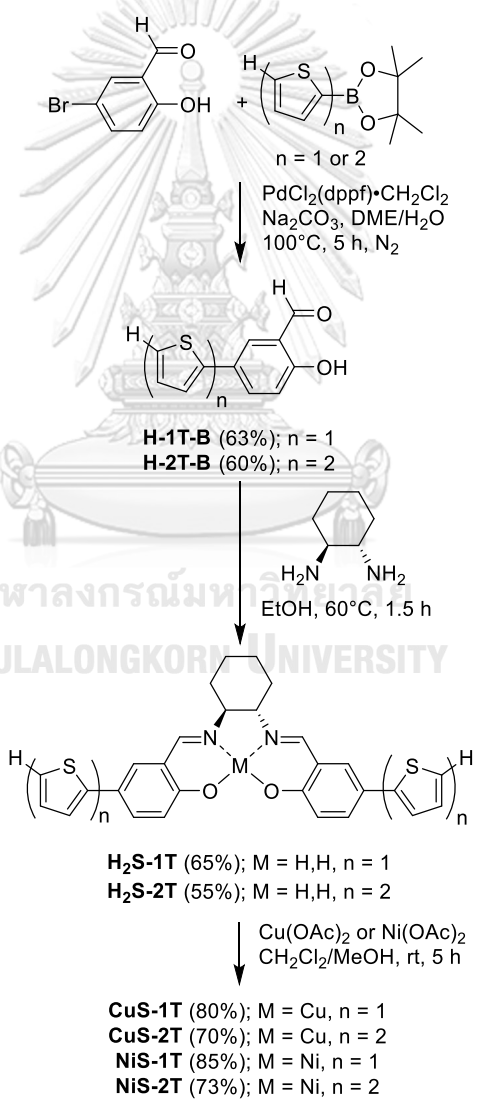

Scheme IV–1: Synthesis of **MS-nT** derivatives

After that, **H-1T-B** and **H-2T-B** were condensed with an excess amount of (*S,S*)-1,2-cyclohexanediamine at 60ºC in ethanol to avoid complication due to the co-precipitation of **H-1T-B** and **H-2T-B** with the desirable products. The reactions were completed to afford compounds **H_2S-1T** and **H_2S-2T** in 65% and 55%, respectively. Each of their ^{1}H-NMR spectra exhibited a singlet of two protons of the hydroxyl groups at 13.38–13.40 ppm due to deshielding effect from electron withdrawing phenyl rings and imine groups. Their two imine protons gave a singlet peak at 8.30 ppm, while the singlet peaks of the aldehyde protons observed in **H-1T-B** and **H-2T-B** disappeared. Besides, protons of their cyclohexane units gave three multiplet peaks at 1.47–3.39 ppm. Additionally, formation of the **H_2S-1T** and **H_2S-2T** was also confirmed by their spectra from mass spectrometry, which exhibited their molecular ion peaks at *m/z* 486.586 and 650.646, respectively. Furthermore, a HS-ESI mass spectrum showed the molecular ion peaks of **H_2S-2T** at *m/z* 651.1261 [$(M+H)^+$].

Finally, metallation of **H_2S-1T** with $Cu(OAc)_2$ or $Ni(OAc)_2$ was achieved to give **CuS-1T** or **NiS-1T** in 80% or 85% yield, respectively. Likewise, **H_2S-2T** was Cu- and Ni-metalated, resulting in **CuS-2T** and **NiS-2T** in 70% and 73%, respectively. The formation of **CuS-1T**, **NiS-1T**, **CuS-2T** and **NiS-2T** was confirmed by mass spectra, exhibiting their molecular ion peaks at *m/z* 547.748, 542.257, 711.954 and 705.727, respectively. However, the melting point of them could not be obtained because a temperature was too high to measure.

The first attempt to synthesize **MS-CC-1T** was made by Sonogashira cross-coupling of 5-bromosalicylaldehyde with an excess amount of 2-(thiophen-2-yl)-acetylene in the presence of $PdCl_2(PPh_3)_2$, CuI, and NEt_3 in refluxing THF under N_2 for 5 h.[142, 191] However, based on ^{1}H-NMR spectrometry, the desired product could not be obtained. The ^{1}H-NMR spectrum of a product separated from the reaction mixture showed a group of peaks indicating protons on thiophene rings but two peaks of protons on hydroxyl and aldehyde groups were not found. It is likely that Glaser coupling of 2-(thiophen-2-yl)-acetylene occurred, leading to a diacetylene byproduct as shown in **Scheme IV–2**.[194-195] This way be because of low reactivity of the 5-bromosalicylaldehyde.

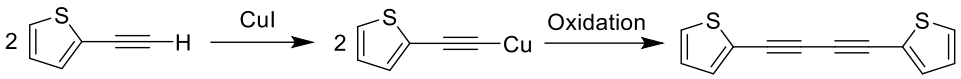

Scheme IV–2: Formation of the diacetylene byproduct

To enhance productivity of the reaction, 5-iodosalicylaldehyde[192] was therefore used instead of 5-bromosalicylaldehyde because a rate of reaction of an aryl iodide in the Sonogashira coupling was higher than an aryl bromide with a milder condition required.[196] Compounds **H-CC-1T-B** and **H-CC-2T-B** were successfully prepared in 59% and 50%, respectively, through the Sonogashira cross-coupling of 5-iodosalicylaldehyde with an excess amount of 2-ethynylthiophene and 5-ethynyl-2,2′-bithiophene,[193] respectively, in the presence of $PdCl_2(PPh_3)_2$, CuI, PPh_3 and NEt_3 in toluene at room temperature under N_2 for 18 h as shown in **Scheme IV–3**. Formation of compounds **H-CC-1T-B** and **H-CC-2T-B** was confirmed by their ^{1}H-NMR spectra showing singlet peaks of each of their hydroxyl protons at 11.12–11.13 ppm, singlet peaks of the aldehyde protons at 9.88 ppm, and multiplet signals indicating protons on their benzene and thiophene rings at around 6.99–7.73 ppm. Furthermore, HS-ESI mass spectrometry showed molecular ion peaks of **H-CC-1T-B** and **H-CC-2T-B** at *m/z* 228.040 and 310.0127 [$(M+H)^+$], respectively.

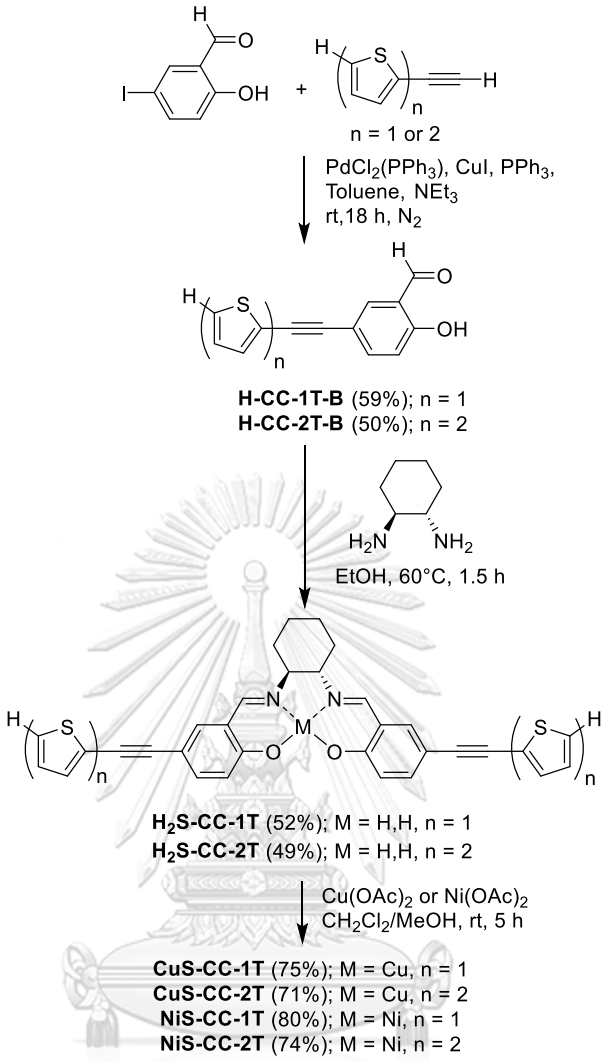

Scheme IV–3: Synthesis of **MS-CC-nT** derivatives

After that, **H-CC-1T-B** and **H-CC-2T-B** were condensed with excess amount of (*S,S*)-1,2-cyclohexanediamine at 60ºC in ethanol to avoid complication due to the co-precipitation of **H-CC-1T-B** and **H-CC-2T-B** with the desirable products. The reactions were completed to afford compounds **H_2S-CC-1T** and **H_2S-CC-2T** in 52% and 49%, respectively. Each of their ^{1}H-NMR spectra exhibited a singlet of two protons of the hydroxyl groups at 13.40–13.49 ppm due to deshielding effect from electron withdrawing phenyl rings and imine groups. Their two imine protons gave a singlet peak at 8.14–8.30 ppm, while the singlet peaks of the aldehyde protons observed in **H-CC-1T-B** and **H-CC-2T-B** disappeared. Besides, protons of their cyclohexane units gave three multiplet peaks at 1.35–3.38 ppm. Additionally, formation of the **H_2S-CC-1T** and **H_2S-CC-2T** was also confirmed by their spectra from mass spectrometry, which

exhibited their molecular ion peaks at *m/z* 534.692 and 699.010, respectively. Furthermore, a HS-ESI mass spectrum showed the molecular ion peaks of **H_2S-CC-1T** and **H_2S-CC-2T** at *m/z* 535.1505 and 699.1269 [$(M+H)^+$], respectively.

Finally, metallation of **H_2S-CC-1T** with $Cu(OAc)_2$ or $Ni(OAc)_2$ was achieved to give **CuS-CC-1T** or **NiS-CC-1T** in 75% or 80% yield, respectively. Likewise, **H_2S-CC-2T** was Cu- and Ni-metalated, resulting in **CuS-CC-2T** and **NiS-CC-2T** in 71% and 74%, respectively. The formation of **CuS-CC-1T**, **NiS-CC-1T**, **CuS-CC-2T** and **NiS-CC-2T** was confirmed by mass spectra, exhibiting their molecular ion peaks at *m/z* 596.0645, 591.0712, 760.0407 and 755.0434 [$(M+H)^+$], respectively, and the melting point of them could not be obtained because a temperature was too high to measure.

4.2 Electrochemical investigations

4.2.1 Electrochemical reduction of CO_2 of target monomers

The electrochemical reduction (ECR) of CO_2 was performed by cyclic voltammetry using the one-compartment three-electrode electrochemical cell consisting of the glassy carbon as the WE, the Pt plate as the CE and the Ag/AgCl QRE. Cyclic voltammograms were recorded in a DMF solution containing 0.1 M nBu$_4$NPF$_6$ as the supporting electrolyte at the potential between 0.0 V and –2.0 V *vs.* Ag/AgCl QRE with the scan rate of 50 $mV{\cdot}s^{-1}$. The concentration of the metallosalen analyte was 0.5 mM, which is approximately the level where most of metallosalens in the series can be dissolved (**Table IV–1**), and in case where a proton source was needed, 3% H_2O v/v was added. As for the solubility of the target metallosalen monomers in various solvents, DMF was selected as a solvent for ECR of CO_2 because of the highest solubility of the metallosalens, compared with CH_2Cl_2 and CH_3CN, and because it can mix well with water. However, due to very low solubility of **CuS-2T** and **NiS-2T**, their electrocatalytic activities could not be determined. By comparing the solubility of the **MS-nT** and **MS-CC-nT** series, results from **Table IV–1** revealed that insertion of a carbon-carbon triple bond between the peripheral thiophene rings and that salen core significantly reduced the solubility of the metallosalens in CH_2Cl_2 and DMF. Moreover, the derivatives having the bithiophenyl units were found to have less solubility than

those containing the thienyl units. Additionally, in most of the cases the copper-salen exhibited higher solubilities than their nickel-chelated analogs.

Table IV–1: Solubilities of the target metallosalen monomers in various solvents

Compound	Solubility / mM		
	CH_2Cl_2	CH_3CN	DMF
CuS-1T	0.91	0.04	2.74
NiS-1T	0.50	0.04	1.48
CuS-2T	0.04	0.01	0.04
NiS-2T	0.03	0.02	0.06
CuS-CC-1T	0.45	0.05	2.52
NiS-CC-1T	0.29	0.05	1.69
CuS-CC-2T	0.20	0.01	1.33
NiS-CC-2T	0.10	0.01	0.79

To characterize the electrochemical behavior of the target metallosalens, the electrolyte solution of each compound was purged with N_2 for 15 min prior to the measurement, while it was purged with CO_2 for 15 min to study the electrocatalytic activities for the CO_2 reduction. The cyclic voltammograms of the electrolyte solution under N_2- and CO_2-saturated condition with and without 3% H_2O are summarized in **Figure IV–2**. In comparison between N_2- and CO_2-saturated condition, results revealed that current was slightly increased in the CO_2-saturated one when the reduction potential was raised towards –2.0 V *vs.* Ag/AgCl QRE, which is attributed to transfer of a single electron proceed through the formation of carbon dioxide radical, and the current was even higher due to H_2-evolution when H_2O was added.[197-198] This observation suggested that the ECR of CO_2 in our studies was able to perform in a potential range between 0.0 V and –2.0 V *vs.* Ag/AgCl QRE.

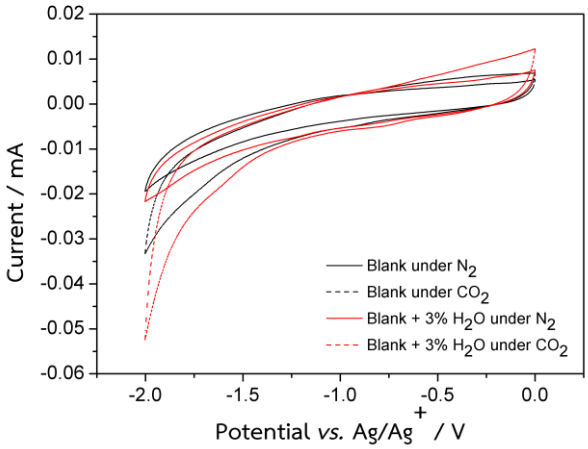

Figure IV–2: Cyclic voltammograms of the 0.1 M nBu$_4$NPF$_6$ solution in DMF under the N_2-saturated condition in the absence of H_2O (black solid line), under CO_2-saturated condition in the absence of H_2O (black dashed line), under N_2-saturated condition in the absence of H_2O (red solid line) and under the CO_2-saturated condition in the presence of H_2O (red dashed line).

Under the N_2 atmosphere in absence of H_2O, the cyclic voltammograms of **CuS-1T**, **CuS-CC-1T** and **CuS-CC-2T** showed similarly reversible reduction peaks at –1.42 V, –1.42 V and –1.35 V *vs.* Ag/AgCl QRE, respectively (**Figure IV–3** and **Table IV–2**), corresponding to the published value for unsubstituted copper-salen[199-200] with slight increase of the reduction potential due to the introduction of thiophene groups in our case. In comparison between the cyclic voltammograms of **CuS-1T** and **CuS-CC-1T**, the results indicated that the insertion of the carbon-carbon triple bond between the thienyl units and the salen core did not significantly influence a reduction process of both target molecules. On the other hand, by comparing the reduction process of **CuS-CC-1T** and that of **CuS-CC-2T**, their cyclic voltammograms suggested that the introduction of the additional thiophene ring seemed to decrease the reduction potential.

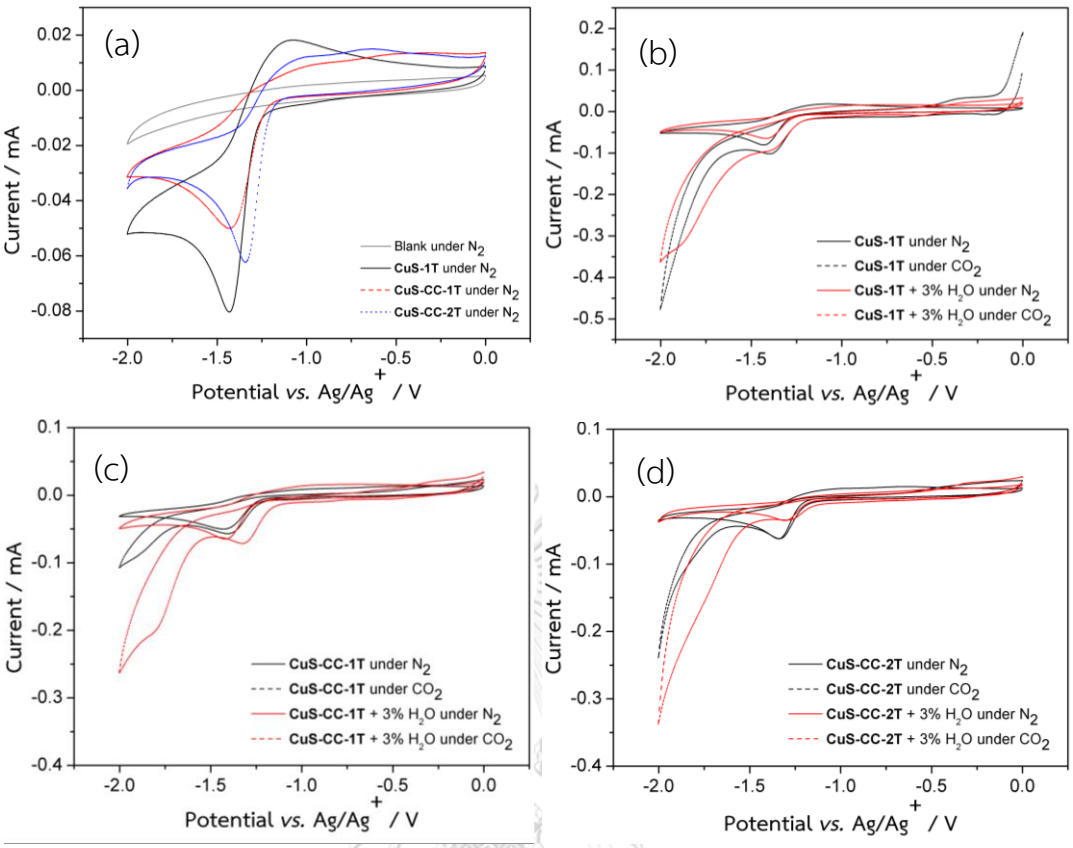

Figure IV–3: Cyclic voltammograms of a 0.1 M nBu$_4$NPF$_6$ solution (grey solid line) containing (a) **CuS-1T** (black solid line), **CuS-CC-1T** (red dashed line) and **CuS-CC-2T** (blue dotted line) under the N_2-saturated condition, (b) the 0.1 M nBu$_4$NPF$_6$ solution containing **CuS-1T** under N_2- (solid line) and CO_2-saturated condition (dashed line) in the absence (black line) and in the presence of H_2O (red line), (c) the 0.1 M nBu$_4$NPF$_6$ solution containing **CuS-CC-1T** under N_2- (solid line) and CO_2-saturated condition (dashed line) in the absence (black line) and in the presence of H_2O (red line) and (d) the 0.1 M nBu$_4$NPF$_6$ solution containing **CuS-CC-2T** under N_2- (solid line) and CO_2-saturated condition (dashed line) in the absence (black line) and in the presence of H_2O (red line). The concentration of each compound was 0.5 mM and the cyclic voltammogrames were collected at the scan rate of 50 mV•s^{-1}.

Table IV–2: Electrochemical data of **CuS-1T**, **CuS-CC-1T** and **CuS-CC-2T**

Compound	Condition		E_{peak} (E_{onset}) / V *vs.* Ag/AgCl	Current at E_{peak} / mA
CuS-1T	Without 3% H_2O	N_2	–1.42 (–1.22)	0.086
		CO_2	–1.42 (–1.22) N.A.[a] (-1.67)	0.102 0.478[b]
	With 3% H_2O	N_2	–1.41 (–1.23)	0.064
		CO_2	–1.39 (–1.20) –1.88 (–1.60)	0.095 0.322
CuS-CC-1T	Without 3% H_2O	N_2	–1.42 (–1.23)	0.051
		CO_2	–1.42 (–1.22) –1.89 (–1.73)	0.059 0.100
	With 3% H_2O	N_2	–1.35 (–1.18)	0.056
		CO_2	–1.33 (–1.15) –1.81 (–1.55)	0.071 0.204
CuS-CC-2T	Without 3% H_2O	N_2	–1.35 (–1.15)	0.057
		CO_2	–1.35 (–1.15) –1.83 (–1.63)	0.063 0.130
	With 3% H_2O	N_2	–1.31 (–1.14)	0.035
		CO_2	–1.29 (–1.12) –1.73 (–1.50)	0.035 0.145

[a] E_{peak} could not be determined.

[b] The current value at the potential of –2.0 V was reported.

Under the CO_2 saturation in the absence of H_2O, the cyclic voltammogram of **CuS-1T** (**Figure IV–3b**) showed its first reduction process occurred at the same potential (–1.42 V *vs.* Ag/AgCl QRE) as that observed in the N_2 atmosphere in the absence of H_2O with slight increase in current from 0.086 to 0.102 mA. After that potential, current was continuously increased to 0.478 mA when potential reached –2.0 V. This observation indicated that **CuS-1T** could promote in the ECR of CO_2. Under the N_2 atmosphere in the presence of 3% H_2O, the first reduction of **CuS-1T** was observed at –1.41 V *vs.* Ag/AgCl QRE (**Figure IV–3b**), indicating that H_2O did not significantly affect the reduction process of this compound. However, under the CO_2-saturated condition in the presence of 3% H_2O, the reduction process occurred at –1.39 V and –1.88 V *vs.* Ag/AgCl QRE with the current of 0.095 and 0.322 mA, respectively (**Figure IV–3b**). Since the first reduction peak appears at the similar potential as that observed in the anhydrous CO_2-saturated condition with slight decrease in current from 0.102 to 0.095 mA, it can be concluded that the first reduction of **CuS-1T** did not significantly related to the ECR of CO_2. Nevertheless, the appearance of the second reduction peak with the peak current of 0.322 mA when 3% H_2O was added, suggested that the second reduction of **CuS-1T** and H_2O should involve in the ECR of CO_2.

In case of **CuS-CC-1T**, the cyclic voltammogram obtained from the anhydrous CO_2-saturated condition showed that the reduction process of **CuS-CC-1T** occurred at the same peak potential (–1.42 V *vs.* Ag/AgCl QRE) as that observed in the anhydrous N_2-saturated one with negligible increase in current from 0.051 to 0.059 mA (black dashed line, **Figure IV–3c**). Furthermore, an additional reduction peak was found at –1.89 V *vs.* Ag/AgCl QRE with the current of 0.100 mA. This observation indicated that the first reduction process of **CuS-CC-1T** did not significantly related to the ECR of CO_2, its the second reduction may involve in the ECR of CO_2. Under the N_2 atmosphere in the presence of 3% H_2O, the cyclic voltammogram of **CuS-CC-1T** exhibited a reduction peak at –1.35 V *vs.* Ag/AgCl QRE without significant peak current increase, compared with those observed under the anhydrous N_2-saturated condition (red solid line, **Figure IV–3c**). This suggested that the addition of H_2O slightly facilitate the reduction process of the target monomers. Under the CO_2 atmosphere in the presence of 3% H_2O, the cyclic voltammogram of **CuS-CC-1T** exhibited the reduction peaks at **–**1.33 V and

–1.81 V *vs.* Ag/AgCl QRE with the current of 0.071 and 0.204 mA, respectively, (red dashed line, **Figure IV–3c**). The very small change in the peak potential and current of the first reduction observed under this condition, compared with those found under the anhydrous CO_2-saturated one, suggested that the first reduction of **CuS-CC-1T** may not involve in the ECR of CO_2. On the contrary, the second reduction at the similar potential with significant current increase suggested that the second reduction of **CuS-CC-1T** and H_2O should involve in the ECR of CO_2. In comparison between the electrochemical behavior of **CuS-1T** and that of **CuS-CC-1T** in the above-mentioned conditions, it can be concluded that the insertion of the carbon-carbon triple bond between the thienyl units and the salen core brought about significant decrease in the reduction potential of the ECR of CO_2 in the presence of H_2O with, however, smaller reduction currents both in the absence and presence of H_2O.

As regards **CuS-CC-2T**, under the CO_2 saturation in the absence of H_2O (black dashed line, **Figure IV–3d**), its reduction process of **CuS-CC-2T** occurred at the same peak potential (–1.35 V *vs.* Ag/AgCl QRE) as that observed in the anhydrous N_2 atmosphere (black solid line, **Figure IV–3d**) with negligible increase in the peak current. Moreover, an additional reduction peak was found at –1.83 V *vs.* Ag/AgCl with the current of 0.130 mA. This observation indicated that the first reduction process of **CuS-CC-2T** did not significantly related to the ECR of CO_2, whereas its second reduction was likely to participate the ECR of CO_2. Under the N_2 atmosphere in the presence of 3% H_2O, the reduction of **CuS-CC-2T** was observed at a slightly lower potential **–**1.31 V *vs.* Ag/AgCl QRE (red solid line, **Figure IV–3d**), compared with those found in the anhydrous CO_2-saturated one, suggesting the negligible effect of the addition of H_2O on the reduction process of **CuS-CC-2T**. Under the CO_2 atmosphere in presence of 3% H_2O, two reduction processes of **CuS-CC-2T** were observed at –1.29 V and –1.73 V *vs.* Ag/AgCl QRE with the peak currents of 0.035 and 0.145 mA, respectively, (red dashed line, **Figure IV–3d**). The very small change in the peak potential and current of the first reduction observed in this condition, compared with those found in the anhydrous CO_2-saturated one, suggested that the first reduction of **CuS-CC-2T** may not involve in the ECR of CO_2. Conversely, the appearrance of the second reduction peak with the significant current increase to 0.145 mA suggested that the second

reduction of **CuS-CC-2T** and H_2O should involve in the ECR of CO_2. In comparison between the electrochemical behavior of **CuS-CC-1T** and that of **CuS-CC-2T** in the above-mentioned conditions, it can be summerized that the addition of thiophene ring in **CuS-CC-2T** led to significant decrease in the reduction potential of the ECR of CO_2 both in the absence and presence of H_2O. However, the addition of H_2O did not significantly affected the reduction process under the N_2-saturated conditon, but it obviously increased the peak current under the CO_2-saturated condition, indicating the possible role of H_2O as the proton source for the ECR of CO_2. To comfirm the role of H_2O in the ECR of CO_2, further investigation of the products from the ECR of CO_2 with and without H_2O by, for example, bulk electrolysis still has to be performed.

Under the anhydrous N_2-saturated condition, the cyclic voltammograms of **NiS-1T**, **NiS-CC-1T** and **NiS-CC-2T** showed reversible reduction peaks at −1.78 V, −1.72 V and −1.69 V *vs.* Ag/AgCl QRE, respectively (**Figure IV–4a** and **Table IV–3**), corresponding to redox processes of the nickel-salen complexes from Ni(II) to Ni(I)[201-202]. In a similar manner observed for the copper-derivatives, the comparison between the cyclic voltammograms of **NiS-1T** and those of **NiS-CC-1T** indicated that the insertion of the carbon-carbon triple bond between the thienyl units and the salen core did not significantly influence a reduction process of both target molecules. Furthermore, the comparison between the electrochemical behavior of **NiS-CC-1T** and that of **NiS-CC-2T** suggested that the introduction of the additional thiophene ring seemed to decrease the reduction potential.

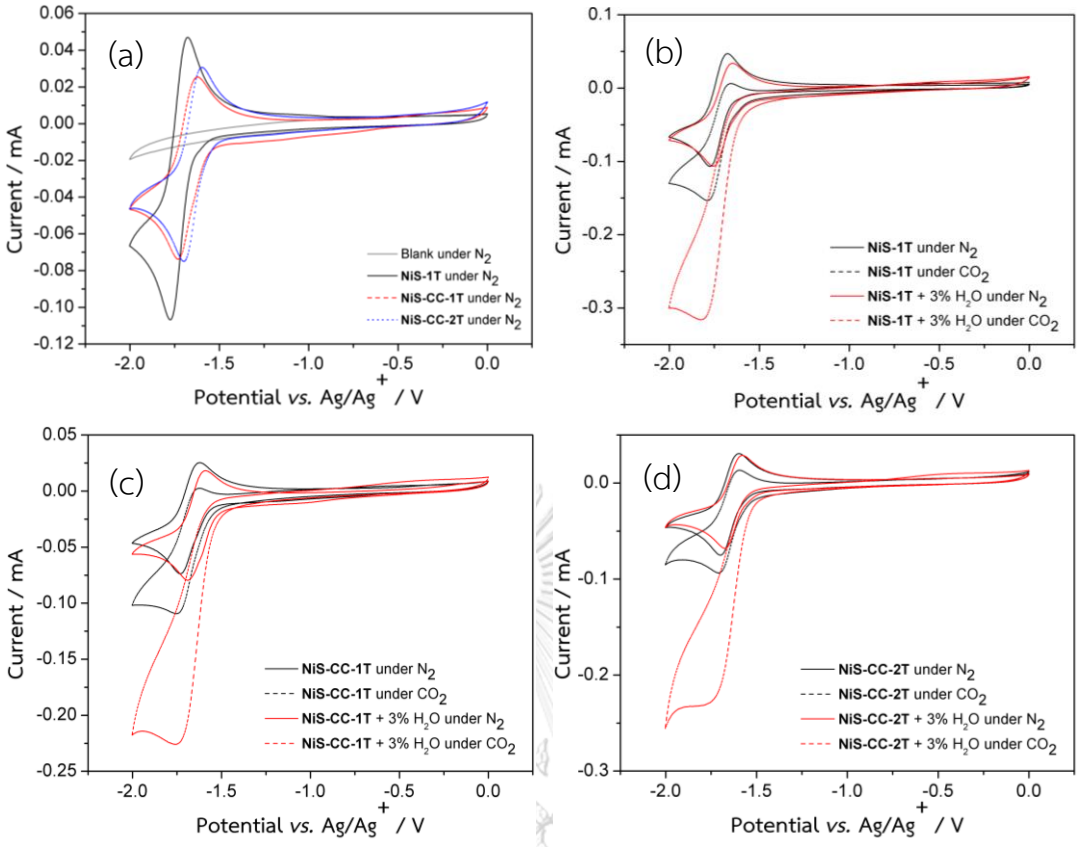

Figure IV–4: Cyclic voltammograms of a 0.1 M nBu$_4$NPF$_6$ solution (grey solid line) containing (a) **NiS-1T** (black solid line), **NiS-CC-1T** (red dashed line) and **NiS-CC-2T** (blue dotted line) under the N_2-saturated condition, (b) the 0.1 M nBu$_4$NPF$_6$ solution containing **NiS-1T** under N_2- (solid line) and CO_2-saturated condition (dashed line) in the absence (black line) and in the presence of H_2O (red line), (c) the 0.1 M nBu$_4$NPF$_6$ solution containing **NiS-CC-1T** under N_2- (solid line) and CO_2-saturated condition (dashed line) in the absence (black line) and in the presence of H_2O (red line) and (d) the 0.1 M nBu$_4$NPF$_6$ solution containing **NiS-CC-2T** under N_2- (solid line) and CO_2-saturated condition (dashed line) in the absence (black line) and in the presence of H_2O (red line). The concentration of each compound was 0.5 mM and the cyclic voltammogrames were collected at the scan rate of 50 mV$\cdot$s^{-1}.

Table IV–3: Electrochemical data of **NiS-1T**, **NiS-CC-1T** and **NiS-CC-2T**

Compound	**Condition**		E_{peak} (E_{onset}) / V *vs.* Ag/AgCl	**Current at E_{peak} / mA**
NiS-1T	Without 3% H_2O	N_2	–1.78 (–1.60)	0.119
		CO_2	–1.79 (–1.60)	0.146
	With 3% H_2O	N_2	–1.75 (–1.55)	0.106
		CO_2	–1.80 (–1.62)	0.306
NiS-CC-1T	Without 3% H_2O	N_2	–1.72 (–1.52)	0.051
		CO_2	–1.74 (–1.52)	0.111
	With 3% H_2O	N_2	–1.69 (–1.49)	0.079
		CO_2	–1.76 (–1.54)	0.226
NiS-CC-2T	Without 3% H_2O	N_2	–1.69 (–1.51)	0.069
		CO_2	–1.72 (–1.52)	0.099
	With 3% H_2O	N_2	–1.67 (–1.49)	0.069
		CO_2	–1.75 (–1.50)	0.231

Under the anhydrous CO_2-saturated condition, results in **Figure IV–4b** showed that the reduction process of **NiS-1T** (black dashed line) occurred at the similar potential (–1.79 V *vs.* Ag/AgCl QRE) as that observed under the anhydrous N_2-saturated one (black solid line, **Figure IV–4b**) with significant current increase from 0.119 to 0.146 mA. This observation indicated that **NiS-1T** might play a role in the ECR of CO_2. Under the N_2 atmosphere in the presence of 3% H_2O, the reduction potential of **NiS-1T** was observed a similar potential as that observed under the anhydrous condition (**–**1.75 V *vs.* Ag/AgCl QRE) with a current of 0.106 mA (red solid line, **Figure IV–4b**). When this analyte solution was saturated with CO_2, the reduction process was found to occurr at –1.80 V *vs.* Ag/AgCl QRE with the current increase to 0.306 mA (red dashed line, **Figure IV–4b**). The large increase in current from 0.146 to 0.306 mA indicated that H_2O significantly affected the reduction process of this compound.

The cyclic voltammogram of **NiS-CC-1T** under the anhydrous CO_2-saturated condition (black dashed line, **Figure IV–4c**) showed that the reduction process of **NiS-CC-1T** occurred at the similar peak potential (**–**1.74 V *vs.* Ag/AgCl QRE) as that observed in the anhydrous N_2-saturated one (black solid line, **Figure IV–4c**) with the current increase from 0.051 to 0.111 mA. This observation indicated that **NiS-CC-1T** might participate the ECR of CO_2. Under the N_2 atmosphere in the presence of 3% H_2O, the cyclic voltammogram of **NiS-CC-1T** exhibited a reduction peak at the comparable potential as that observed under the anhydrous condition (–1.69 V *vs.* Ag/AgCl QRE, red solid line, **Figure IV–4c**) with a current of 0.079 mA. Under the CO_2 atmosphere in presence of 3% H_2O, the reduction process of **NiS-CC-1T** occurred at –1.76 V *vs.* Ag/AgCl QRE with the current of 0.226 mA (red dashed line, **Figure IV–4c**). The current increase from 0.111 to 0.226 mA indicated the significant catalytic activity of **NiS-CC-1T** in the ECR of CO_2. In comparison between the electrochemical behavior of **NiS-1T** and that of **NiS-CC-1T**, the similar effect of the insertion of the carbon-carbon triple bond between the thienyl units and the salen core on the increase in the reduction potential of the ECR of CO_2 as observed for the copper series was also detected.

As regards **NiS-CC-2T**, under the CO_2 saturation in the absence of H_2O (black dashed line, **Figure IV–4d**), its reduction process occurred at the same peak potential (–1.72 V *vs.* Ag/AgCl QRE) as that observed in the anhydrous N_2-saturated one (black

solid line, **Figure IV–4d**) with the current increase from 0.069 to 0.099 mA. This observation indicated that **NiS-CC-2T** might participate the ECR of CO_2. Under the N_2 atmosphere in the presence of 3% H_2O (red solid line, **Figure IV–4d**), the cyclic voltammogram of **NiS-CC-2T** exhibited a reduction peak at the comparable potential (–1.67 V *vs.* Ag/AgCl QRE) as that observed under the anhydrous N_2-condition (black solid line, **Figure IV–4d**). Under the CO_2 atmosphere in presence of 3% H_2O (red dashed line, **Figure IV–4d**), the reduction process of **NiS-CC-2T** occurred at –1.75 V *vs.* Ag/AgCl QRE with the current of 0.231 mA. This reduction peak was observed at a similar potential with that observed under the anhydrous CO_2-saturated condition with current increase from 0.099 to 0.231 mA, indicating the significant catalytic activity of **NiS-CC-2T** in the ECR of CO_2. In contrast to the case of the copper-derivatives, the comparison between the electrochemical behavior of **NiS-CC-1T** and that of **NiS-CC-2T** indicated that the introduction of the addition thiophene unit did not bring about significant change of the reduction potential of the ECR of CO_2. In comparison between the copper- and the nickel-salen monomers, the first reduction of the copper-salen monomers, which occurred in a range between –1.29 V and –1.42 V *vs.* Ag/AgCl QRE, seem not to significantly involve in the ECR of CO_2, but the electrochemical catalytic activity of these compounds become significant at the potential higher than –1.50 V *vs.* Ag/AgCl QRE. On the other hand, there was only one reduction peak observed in a range between –1.67 V and –1.80 V *vs.* Ag/AgCl QRE for the nickel-salen monomers, and these processes also involved in the ECR of CO_2. Furthermore, the addition of H_2O significantly affected the reduction process for the ECR of CO_2 in both series. Considering the current increase, the results suggested that the **MS-nT** monomers gave the larger current increase than the **MS-CC-nT** ones. Moreover, in term of the reduction potential, the results suggested that the **MS-CC-nT** monomers gave the lower reduction potential than the **MS-nT** ones. However, the bulk electrolysis should be performed for more realistic comparison. This experiment will be done and its results will be described elsewhere.

4.2.2 Electrochemical polymerization of target monomers

In order to prepare stable films of the target metallosalen for using as heterogeneous electrocatalysts for the ERC of CO_2, their electropolymerization was performed in this study. Although the target metallosalen could be greatly dissolved in DMF, the potential window in the DMF system is quite narrow for oxidative polymerization. Therefore, the electropolymerization was performed in CH_2Cl_2 having the wider potential range than DMF. From the solubilities of the target metallosalens reported in CH_2Cl_2 in **Table IV–1**, it can be seen that to perform the electropolymerization of each monomer series, *i.e.* **MS-1T**, **MS-2T**, **MS-CC-1T** and **MS-CC-2T**, the concentration of choice had to be approximately the maximum solubilities of the Ni-chelated derivatives. Therefore, the electropolymerization of **MS-1T**, **MS-2T**, **MS-CC-1T** and **MS-CC-2T** series was performed at the concentration of 0.50, 0.03, 0.25 and 0.10 mM, respectively. A cyclic voltammogram of the 0.1 M nBu$_4$NPF$_6$ solution in CH_2Cl_2 is shown in **Figure IV–5**, indicating that a suitable potential range for the oxidative polymerization was between –0.2 V and 1.6 V *vs.* Ag/AgCl QRE.

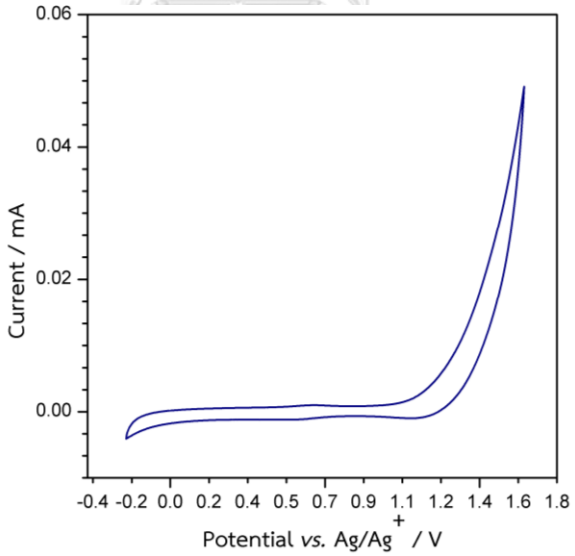

Figure IV–5: Cyclic voltammogram of a 0.1 M nBu$_4$NPF$_6$ solution in CH_2Cl_2 measured by using ITO-coated glass and Pt-plate as the WE and CE, respectively, against Ag/AgCl QRE at a scan rate of 100 mV•s^{-1}.

According to a previous study,[188] a chromium salen complex containing the thienyl groups was successfully electrochemically polymerized under oxidative polymerization at the applied voltage between –0.20 V and +1.60 V *vs* Ag/AgCl QRE with a scan rate of 100 $mV \cdot s^{-1}$, leading to formation of the polymer film that fully covered on the WE. By using the similar condition, the oxidative polymerization of **CuS-1T** and **NiS-1T** was carried out on the ITO-coated glass at the potential between –0.20 V and +1.30 V *vs* Ag/AgCl QRE. The cyclic voltammograms had significant increase in current from the first to the tenth cycles with small positive shift of E_{pa}, indicating the progress of the polymerization of the thienyl unit (**Figure IV–6**) with a increased film. As a result, the polymers of **CuS-1T** (**poly-CuS-1T**) and **NiS-1T** (**poly-NiS-1T**) were obtained as a dark green and yellowish green films, respectively, which were stable under the ambient atmosphere.

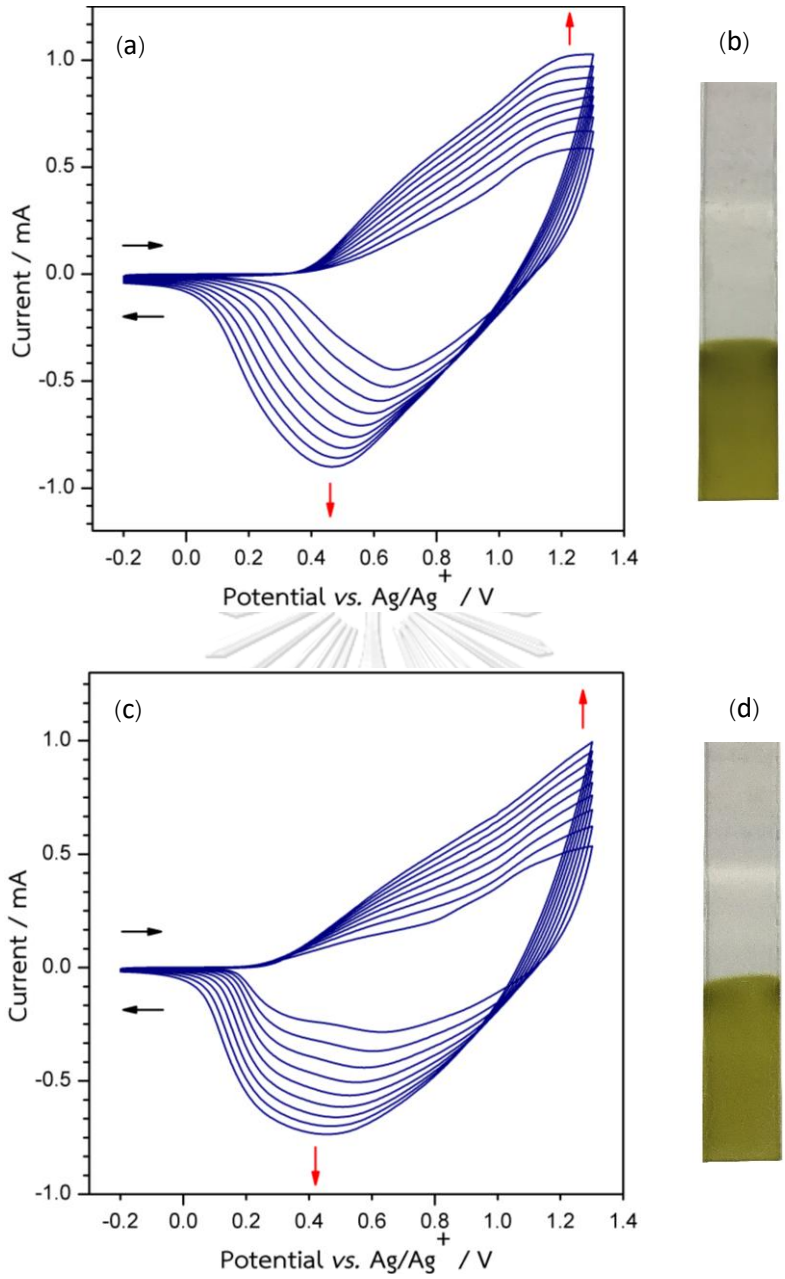

Figure IV–6: Cyclic voltammograms of oxidative polymerization of a 0.1 M nBu$_4$NPF$_6$ in CH_2Cl_2 containing (a) 0.50 mM **CuS-1T** to give (b) the resulting **poly-CuS-1T** film on the ITO-coated glass, and (c) 0.50 mM **NiS-1T** to give (d) the resulting **poly-NiS-1T** film on the ITO-coated glass. The oxidative polymerization was performed at a scan rate of 100 mV·s^{-1} for up to 10 cycles.

In case of **CuS-2T** and **NiS-2T** monomers, the oxidative polymerization was performed at the potential between 0.0 V and +1.50 V *vs* Ag/AgCl QRE with a scan rate of 100 $mV \cdot s^{-1}$. Upon the increase in the number of scanning cycle up to 10 cycles, the increase in the anodic current at +0.90 V, and +1.49 V, and the cathodic current at +0.80 V and +0.35 V *vs* Ag/AgCl QRE was observed for **CuS-2T** (**Figure IV–7a**), while the anodic current increase was not detected for **NiS-2T** (**Figure IV–7c**). However, the resulting film from the polymerization of **CuS-2T** was found to be very thin (**Figure IV–7b**), whereas the polymerization of **NiS-2T** failed to give a visible film, although the number of the scanning cycle was increased up to 50 cycles in both cases. This is attributed to low solubility of both compounds. In comparison between the polymerization of **MS-1T** and that of **MS-2T** series, the required potential for the polymerization of **MS-2T** (approximately +0.90 V *vs* Ag/AgCl QRE) is slightly lower than that of **MS-1T** (+1.15 V *vs* Ag/AgCl QRE). The former value was consistent with the potential reported for the oxidative polymerization of a thienyl-substituted chromium-salen in a previous study.[203] It can be concluded that the introduction of the additional thiophene ring in **MS-2T** brought about significant decrease in the required potential for the oxidative polymerization.

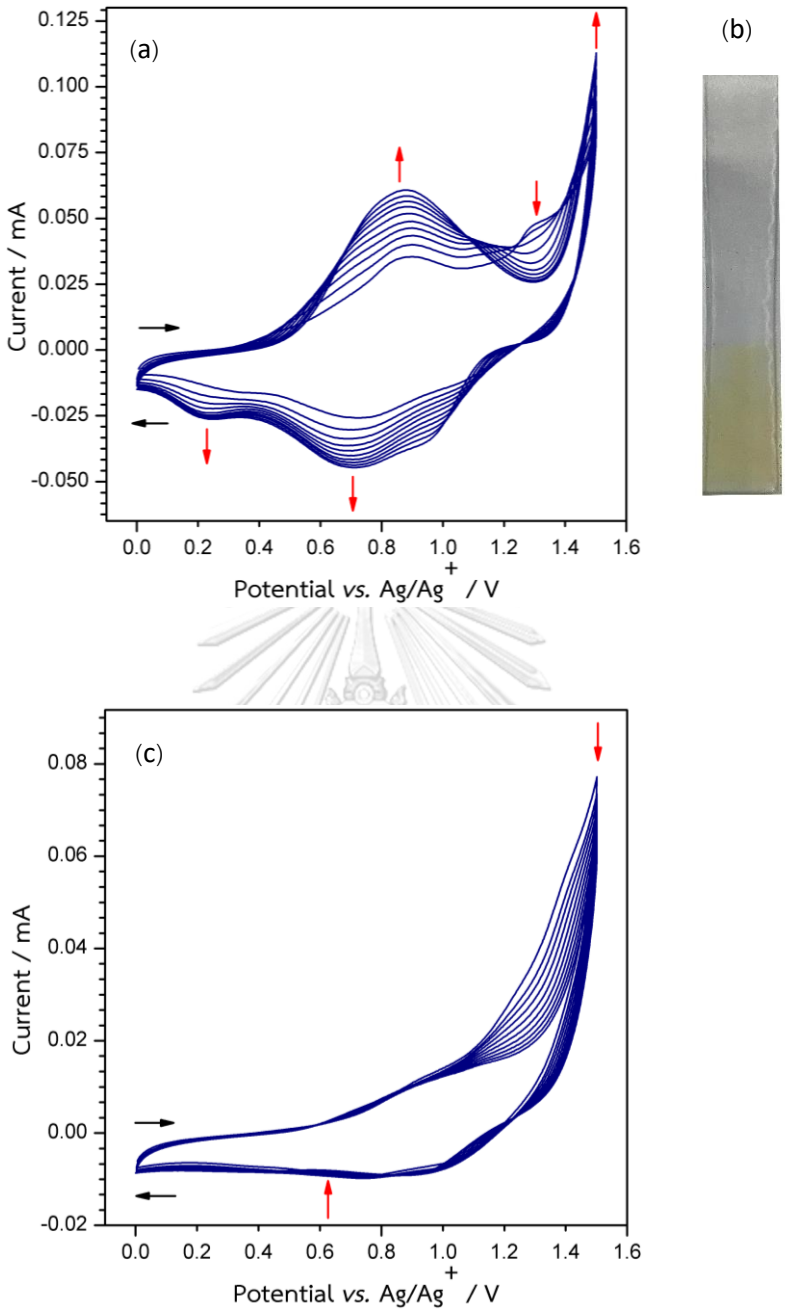

Figure IV–7: Cyclic voltammograms of oxidative polymerization of a 0.1 M nBu$_4$NPF$_6$ in CH_2Cl_2 containing (a) 0.03 mM **CuS-2T** to give (b) the resulting **poly-CuS-2T** film on the ITO-coated glass, and (c) 0.03 mM **NiS-1T**. The oxidative polymerization was performed at a scan rate of 100 mV•s^{-1} for up to 10 cycles.

In a similar manner, the oxidative polymerization of **CuS-CC-1T** and **NiS-CC-1T** was carried out at the potential between 0.0 V and +1.50 V and between 0.0 V and +1.60 V *vs* Ag/AgCl QRE, respectively, with a scan rate of 100 $mV \cdot s^{-1}$. Upon continuous scanning from the first to the tenth cycles, the anodic and cathodic current in both cases was found to decrease as shown in **Figure IV–8**. This is attributed to the increase of the resistivity of the resulting film, which suppresses the progress of the electrochemical polymerization.[204-207] Consequently, the light browish green and light brown films of polymers of **CuS-CC-1T** (**poly-CuS-CC-1T**) and **NiS-CC-1T** (**poly-NiS-CC-1T**), respectively, were obtained (**Figure IV–8b** and **Figure IV–8d**, respectively) and found to be stable under ambient atmosphere. Compared with the **MS-1T** series, the **MS-CC-1T** series required more positive potential for electropolymerization, possible due to the stronger electronic communication between the salen and thiophene units via linear carbon-carbon triple bonds that creates electron-withdrawing effect at the polymerizable α-position of the thiophene rings or, in other words, causes the peripheral thienyl unit less reactive to the electrochemical oxidative polymerization.[208-210]

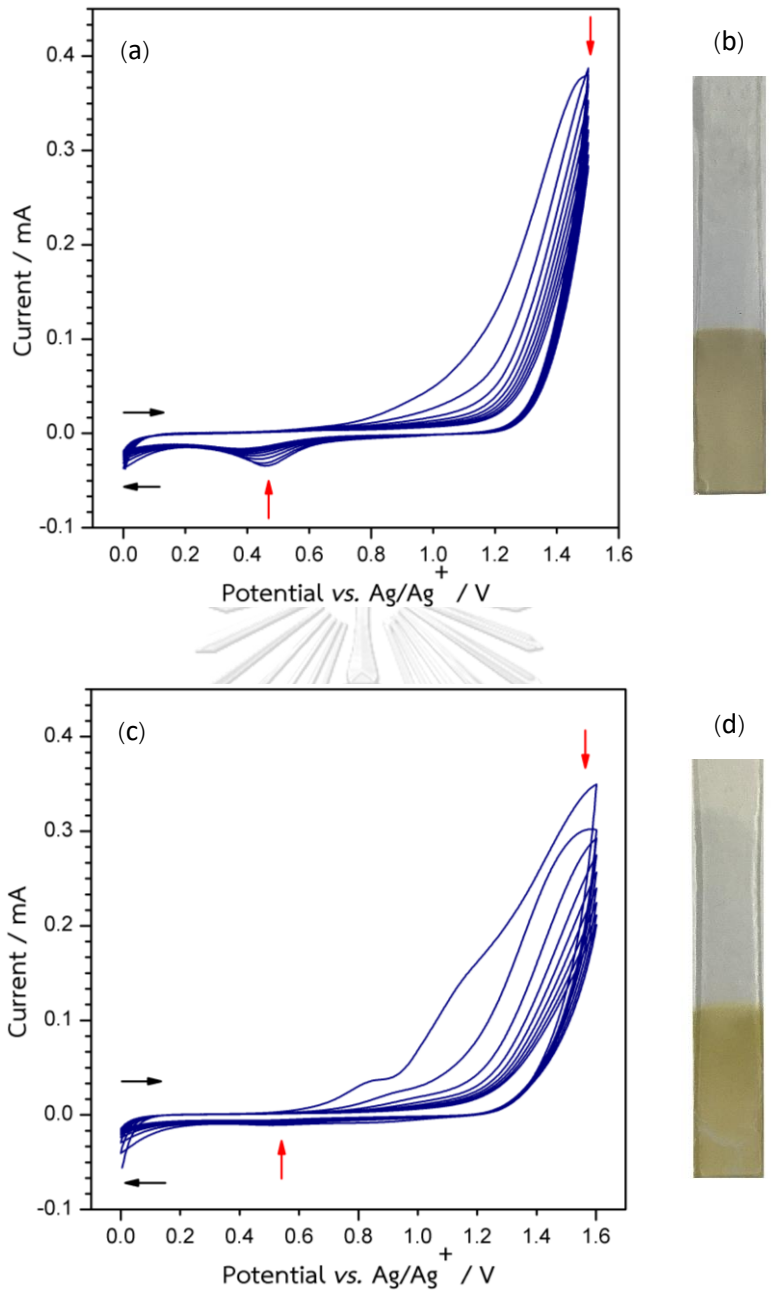

Figure IV–8: Cyclic voltammograms of oxidative polymerization of a 0.1 M nBu$_4$NPF$_6$ in CH_2Cl_2 containing (a) 0.25 mM **CuS-CC-1T** to give (b) the resulting **poly-CuS-CC-1T** film on the ITO-coated glass, and (c) 0.25 mM **NiS-CC-1T** to give (d) the resulting **poly-NiS-CC-1T** film on the ITO-coated glass. The oxidative polymerization was performed at a scan rate of 100 mV•s^{-1} for up to 10 cycles.

In case of **CuS-CC-2T** and **NiS-CC-2T** monomers, the oxidative polymerization was performed at the potential between –0.20 V and +1.50 V and between –0.20 V and +1.55 V *vs* Ag/AgCl QRE, respectively, with a scan rate of 100 $mV \cdot s^{-1}$. The increase in the anodic current at +0.95 V and +1.48 V, and the cathodic current at +0.89 V and +0.36 V *vs* Ag/AgCl QRE was observed for **CuS-CC-2T** and the increase in the anodic current at +0.92 V and +1.52 V, and the cathodic current at +0.88 V and +0.35 V *vs* Ag/AgCl QRE was observed for **NiS-CC-2T** (**Figure IV–9**). In both cases, the cyclic voltammograms exhibited significant increase in current from the first to the tenth cycles with slight positive shift of E_{pa} and negative shift of E_{pc}. As a result, polymers of **CuS-CC-2T** (**poly-CuS-CC-2T**) and **NiS-CC-2T** (**poly-NiS-CC-2T**) were obtained as a stable yellowish brown and light yellow films as shown in **Figure IV–9b** and **Figure IV–9d**, respectively. In comparison between the polymerization of **MS-CC-1T** and that of **MS-CC-2T** series, the result showed that the polymerization of **MS-CC-2T** required less potential than that of **MS-CC-1T**, possibly due to higher susceptibility of the bithiophenyl unit to the electrochemical polymerization, compared with that of the thienyl one as described in previous studies.[186, 203, 211] However, the comparison between the polymerization of **MS-CC-2T** and that of **MS-2T** series indicated the stronger electronic communication between the salen and bithiophene units that creates electron-withdrawing effect at the polymerizable α-position on the bithiophene rings in **MS-CC-2T** led to require more positive potential than **MS-2T** for the electrochemical oxidative polymerization.

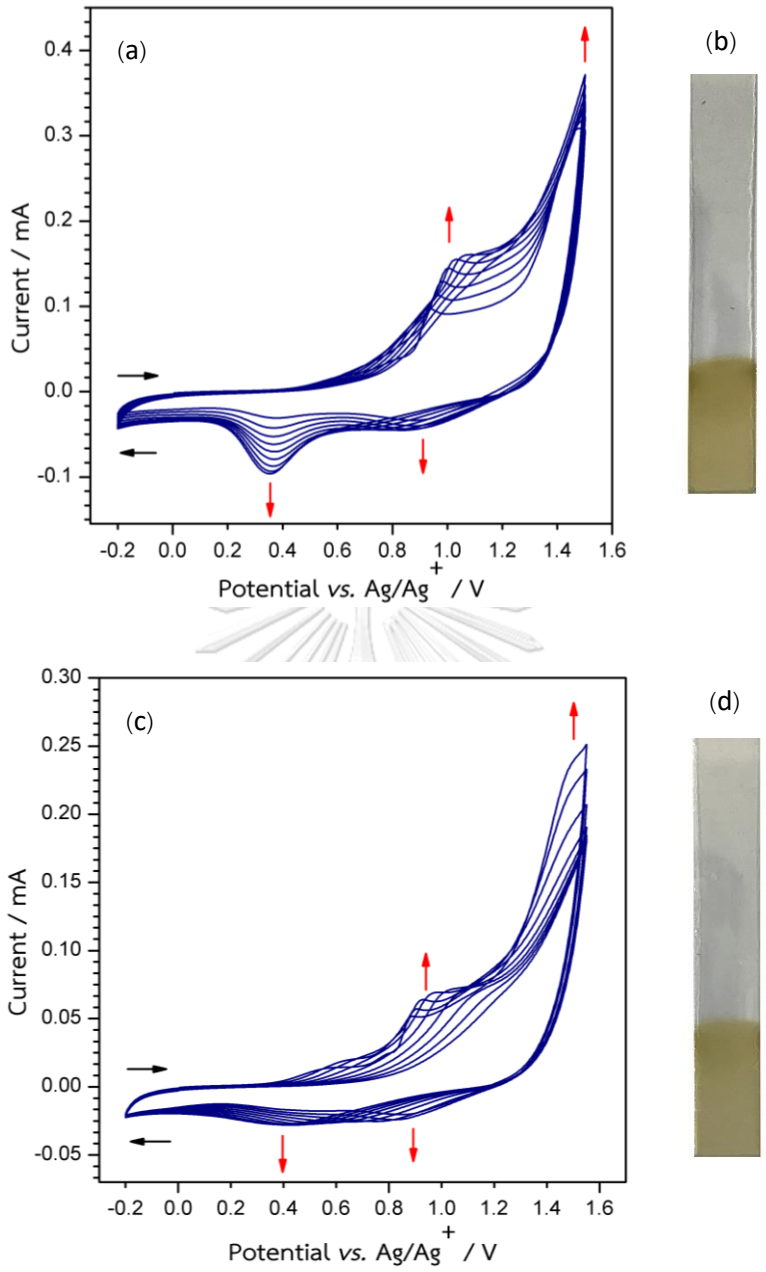

Figure IV–9: Cyclic voltammograms of oxidative polymerization of a 0.1 M nBu$_4$NPF$_6$ in CH_2Cl_2 containing (a) 0.10 mM **CuS-CC-2T** to give (b) the resulting **poly-CuS-CC-2T** film on the ITO-coated glass, and (c) 0.10 mM **NiS-CC-2T** to give (d) the resulting **poly-NiS-CC-2T** film on the ITO-coated glass. The oxidative polymerization was performed at a scan rate of 100 mV•s^{-1} for up to 10 cycles.

4.2.3 Electrochemical reduction of CO_2 of target polymers

The ECR of CO_2 of **poly-CuS-1T**, **poly-CuS-CC-1T**, **poly-CuS-CC-2T**, **poly-NiS-1T**, **poly-NiS-CC-1T** and **poly-NiS-CC-2T** was studied by using the same cyclic voltammetry setup as that described for their monomers in Section 4.2.1, except that the WE in this case was the polymer films on the ITO-coated glass and the electrolyte solution contained no salen monomer. The electrochemical window was determined by the cyclic voltammograms of a 0.1 M nBu$_4$NPF$_6$ solution using a clean ITO-coated glass as the WE. The results in **Figure IV–10** showed that although the current under the N_2 atmosphere did not significantly change upto –2.0 V *vs* Ag/AgCl QRE, that under the CO_2 atmosphere drastically increased at the potential higher than –1.7 V *vs* Ag/AgCl QRE. Therefore, the potential range chosen for the heterogeneous ECR of CO_2 was between 0.0 V and –1.7 V *vs* Ag/AgCl QRE.

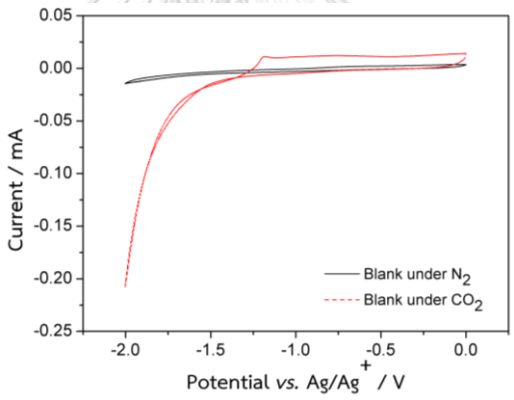

Figure IV–10: Cyclic voltammograms of a 0.1 M nBu$_4$NPF$_6$ solution in DMF under the N_2- (solid line) and CO_2-saturated condition (dashed line).

When the polymer films on the ITO-coated glasses were used on the WE, it is surprising that the electrochemical features of the films under the N_2 atmosphere were not consistent with those observed for their corresponding monomers (**Figure IV–11**). Moreover, under the CO_2 atmosphere, these polymer films gave no significant current enhancement. This observation was confirmed by using the freshly made polymer films under the same conditions and setup. This unexpected result may be explained by high resistance of the films due to possible aggregation of the repeating units in the polymer chains or unfavorable morphology of the polymer films. To investigate the detailed cause of this, further optimization of the polymerization condition and in-

depth film studies have to be performed. Therefore, the ECR of CO_2 of these films was not continued in this work.

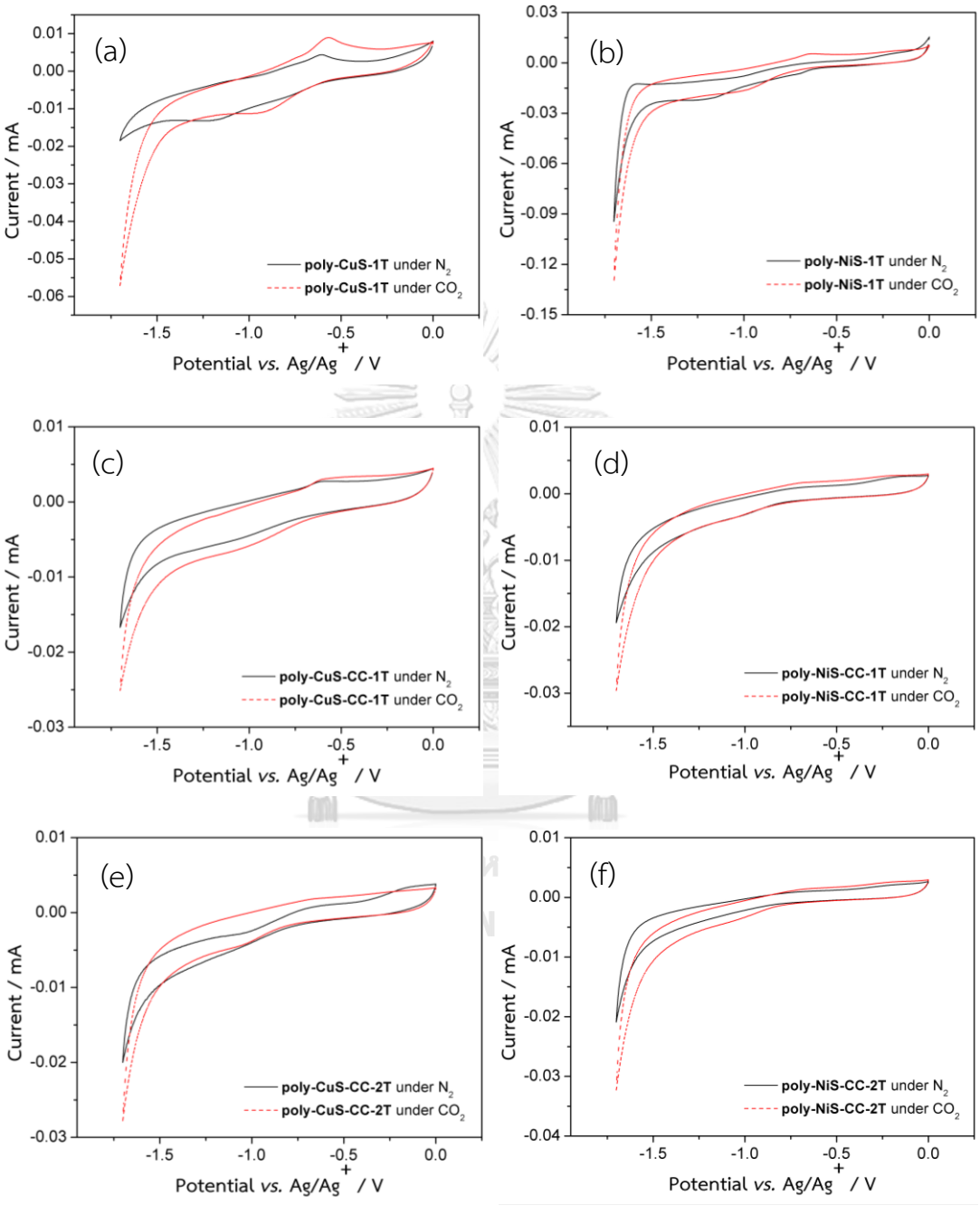

Figure IV–11: Cyclic voltammograms of (a) **poly-CuS-1T**, (b) **poly-NiS-1T**, (c) **poly-CuS-CC-1T**, (d) **poly-NiS-CC-1T**, (e) **poly-CuS-CC-2T** and (f) **poly-NiS-CC-2T** under N_2- (black solid line) and CO_2-saturated condition (red dashed line). The cyclic voltammograms were recorded in a 0.1 M nBu$_4$NPF$_6$ solution in DMF at the scan rate of 50 mV·s^{-1}.

CHAPTER V
CONCLUSION

A series of the novel asymmetric copper- and nickel-salens bearing the thienyl and bithiophenyl units attached on their phenoxyl rings directly and via the carbon-carbon triple-bond spacer was successfully synthesized. The characterization of the target compounds was carried out by ^{1}H-NMR and ^{13}C-NMR spectroscopy and mass spectrometry. The solubilities of the target compounds were found to vary in a range of 0.03–0.90, 0.01–0.05 and 0.04–2.74 mM in CH_2Cl_2, CH_3CN and DMF, respectively. Their electrocatalytic activities for the homogeneous ECR of CO_2 in DMF were determined by cyclic voltammetry. Under the CO_2-saturated condition, results revealed that both copper- and nickel-salens should be able to work as catalysts for the ECR of CO_2 by showing the current increase of the reduction peaks compared with those observed under the N_2 atmosphere. Moreover, the results showed that the insertion of the carbon-carbon triple bond between the thienyl units and the salen core led to the decrease in the required reduction potential. Furthermore, the introduction of the thienyl rings also encouraged the current increase in reduction process of both in copper- and nickel-salen, while the additional thiophene rings did not play a significant role in this aspect. In addition, the water gave significant contribution in the reduction of CO_2 by increasing the peak current in most cases. The oxidative polymerization of all target monomers, except the ones bearing the bithiophenyl groups directly linked to the salen core that exhibited low solubilities, gave stable thin films of the corresponding polymers. The results indicated that the monomers having the carbon-carbon triple-bond spacer required higher potential for the polymerization, compared to the ones having the thiophene-based groups directly linked to the salen core. Additionally, the monomers containing the bithiophenyl groups required lower potential to proceed the polymerization than those bearing the thienyl rings. Due to unexpected electrochemical behavior of the resulting polymers, the electrocatalytic activities of these polymers for the ECR of CO_2 could not be yet investigated, and will be further described elsewhere. Possible future work is to

analyte the products from the homogeneous ECR of CO_2 by the bulk electrolysis for more realistic comparison of the catalytic efficiency of each monomer. Furthermore, the further optimization of the polymerization condition should be performed to obtain the efficient polymeric catalyst for the heterogeneous ECR of CO_2, as well as the determination of products from this process in a similar manner to the homogeneous one.

REFERENCES

1. National Research, C., *Advancing the Science of Climate Change*. The National Academies Press: Washington, DC, 2010.

2. O'Neill, B. C.; Oppenheimer, M.; Warren, R.; Hallegatte, S.; Kopp, R. E.; Portner, H. O.; Scholes, R.; Birkmann, J.; Foden, W.; Licker, R.; Mach, K. J.; Marbaix, P.; Mastrandrea, M. D.; Price, J.; Takahashi, K.; van Ypersele, J.-P.; Yohe, G., IPCC reasons for concern regarding climate change risks. *Nature Clim. Change* **2017,** *7* (1), 28–37.

3. Sumaila, U. R.; Cheung, W. W. L.; Lam, V. W. Y.; Pauly, D.; Herrick, S., Climate change impacts on the biophysics and economics of world fisheries. *Nature Clim. Change* **2011,** *1* (9), 449–456.

4. Bachelet, D.; Neilson, R. P.; Lenihan, J. M.; Drapek, R. J., Climate change effects on vegetation distribution and carbon budget in the United States. *Ecosystems* **2001,** *4* (3), 164–185.

5. Brown, C. J.; Fulton, E. A.; Hobday, A. J.; Matear, R. J.; Possingham, H. P.; Bulman, C.; Christensen, V.; Forrest, R. E.; Gehrke, P. C.; Gribble, N. A.; Griffiths, S. P.; Lozano-Montes, H.; Martin, J. M.; Metcalf, S.; Okey, T. A.; Watson, R.; Richardson, A. J., Effects of climate-driven primary production change on marine food webs: implications for fisheries and conservation. *Glob. Change Biol.* **2010,** *16* (4), 1194–1212.

6. Benson, E. E.; Kubiak, C. P.; Sathrum, A. J.; Smieja, J. M., Electrocatalytic and homogeneous approaches to conversion of CO_2 to liquid fuels. *Chem. Soc. Rev.* **2009,** *38* (1), 89–99.

7. Centi, G.; Perathoner, S., Opportunities and prospects in the chemical recycling of carbon dioxide to fuels. *Catal. Today* **2009,** *148* (3–4), 191–205.

8. Spinner, N. S.; Vega, J. A.; Mustain, W. E., Recent progress in the electrochemical conversion and utilization of CO_2. *Catal. Sci. Technol.* **2012,** *2* (1), 19–28.

9. Costentin, C.; Robert, M.; Saveant, J.-M., Catalysis of the electrochemical reduction of carbon dioxide. *Chem. Soc. Rev.* **2013,** *42* (6), 2423–2436.

10. Kuhl, K. P.; Cave, E. R.; Abram, D. N.; Jaramillo, T. F., New insights into the electrochemical reduction of carbon dioxide on metallic copper surfaces. *Energ. Environ. Sci.* **2012,** *5* (5), 7050–7059.

11. Summers, D. P.; Leach, S.; Frese, K. W., The electrochemical reduction of aqueous carbon dioxide to methanol at molybdenum electrodes with low overpotentials. *J. Electroanal. Chem. Interfacial Electrochem.* **1986,** *205* (1), 219–232.

12. García, M.; Aguirre, M. J.; Canzi, G.; Kubiak, C. P.; Ohlbaum, M.; Isaacs, M., Electro and photoelectrochemical reduction of carbon dioxide on multimetallic porphyrins/polyoxotungstate modified electrodes. *Electrochim. Acta* **2014,** *115*, 146–154.

13. Furuya, N.; Matsui, K., Electroreduction of carbon dioxide on gas-diffusion electrodes modified by metal phthalocyanines. *J. Electroanal. Chem. Interfacial Electrochem.* **1989,** *271* (1), 181–191.

14. Magdesieva, T. V.; Zhukov, I. V.; Kravchuk, D. N.; Semenikhin, O. A.; Tomilova, L. G.; Butin, K. P., Electrocatalytic CO_2 reduction in methanol catalyzed by mono-, di-, and electropolymerized phthalocyanine complexes. *Russ. Chem. Bull.* **2002,** *51* (5), 805–812.

15. Finn, C.; Schnittger, S.; Yellowlees, L. J.; Love, J. B., Molecular approaches to the electrochemical reduction of carbon dioxide. *Chem. Commun.* **2012,** *48* (10), 1392–1399.

16. Singh, S.; Phukan, B.; Mukherjee, C.; Verma, A., Salen ligand complexes as electrocatalysts for direct electrochemical reduction of gaseous carbon dioxide to value added products. *RSC Adv.* **2015,** *5* (5), 3581–3589.

17. Hori, Y.; Kikuchi, K.; Murata, A.; Suzuki, S., Production of methane and ethylene in electrochemical reduction of carbon dioxide at copper electrode in aqueous hydrogencarbonate solution. *Chem. Lett.* **1986,** *15* (6), 897–898.

18. Hori, Y.; Murata, A.; Takahashi, R., Formation of hydrocarbons in the electrochemical reduction of carbon dioxide at a copper electrode in aqueous solution. *J. Chem. Soc., Faraday Trans. 1.* **1989,** *85* (8), 2309–2326.

19. Hori, Y.; Wakebe, H.; Tsukamoto, T.; Koga, O., Electrocatalytic process of CO selectivity in electrochemical reduction of CO_2 at metal electrodes in aqueous media. *Electrochim. Acta* **1994,** *39* (11), 1833-1839.

20. Heeger, A. J., Nobel lecture: semiconducting and metallic polymers: the fourth generation of polymeric materials. *Rev. Mod. Phys.* **2001,** *73* (3), 681–700.

21. Perepichka, I. F.; Perepichka, D. F.; Meng, H.; Wudl, F., Light-emitting polythiophenes. *Adv. Mater. (Weinheim, Ger.)* **2005,** *17* (19), 2281–2305.

22. Yutaka, O.; Masao, U.; Keiro, M.; Katsumi, Y., Visible-light electroluminescent diodes utilizing poly(3-alkylthiophene). *Jpn. J. Appl. Phys.* **1991,** *30* (11B), L1938.

23. Yutaka, O.; Masao, U.; Keiro, M.; Katsumi, Y., Effects of | alkyl chain length and carrier confinement layer | on characteristics of poly(3-alkylthiophene) electroluminescent diodes. *Solid State Commun.* **1991,** *80* (8), 605–608.

24. Braun, D.; Gustafsson, G.; McBranch, D.; Heeger, A. J., Electroluminescence and electrical transport in poly(3-octylthiophene) diodes. *J. Appl. Phys.* **1992,** *72* (2), 564–568.

25. Ohshita, J.; Tada, Y.; Kunai, A.; Harima, Y.; Kunugi, Y., Hole-injection properties of annealed polythiophene films to replace PEDOT–PSS in multilayered OLED systems. *Synth. Met.* **2009,** *159* (3), 214–217.

26. Cook, J. H.; Al-Attar, H. A.; Monkman, A. P., Effect of PEDOT–PSS resistivity and work function on PLED performance. *Org. Electron.* **2014,** *15* (1), 245–250.

27. Zamoshchik, N.; Bendikov, M., Doped conductive polymers: modeling of polythiophene with explicitly used counterions. *Adv. Funct. Mater.* **2008,** *18* (21), 3377–3385.

28. Padinger, F.; Rittberger, R. S.; Sariciftci, N. S., Effects of postproduction treatment on plastic solar cells. *Adv. Funct. Mater.* **2003,** *13* (1), 85–88.

29. Li, G.; Zhu, R.; Yang, Y., Polymer solar cells. *Nat Photon* **2012,** *6* (3), 153–161.

30. Yan, W.; Li, Y.; Sun, W.; Peng, H.; Ye, S.; Liu, Z.; Bian, Z.; Huang, C., High-performance hybrid perovskite solar cells with polythiophene as hole-transporting layer via electrochemical polymerization. *RSC Adv.* **2014,** *4* (62), 33039–33046.

31. Yanagida, S.; Senadeera, G. K. R.; Nakamura, K.; Kitamura, T.; Wada, Y., Polythiophene-sensitized TiO_2 solar cells. *J. Photochem. Photobiol. A: Chem.* **2004,** *166* (1), 75-80.

32. Beek, W. J. E.; Wienk, M. M.; Janssen, R. A. J., Hybrid solar cells from regioregular polythiophene and ZnO nanoparticles. *Adv. Funct. Mater.* **2006,** *16* (8), 1112–1116.

33. Hayakawa, A.; Yoshikawa, O.; Fujieda, T.; Uehara, K.; Yoshikawa, S., High performance polythiophene/fullerene bulk-heterojunction solar cell with a TiO_x hole blocking layer. *Appl. Phys. Lett.* **2007,** *90* (16), 163517.

34. Shit, A.; Nandi, A. K., Interface engineering of hybrid perovskite solar cells with poly(3-thiophene acetic acid) under ambient conditions. *Phys. Chem. Chem. Phys.* **2016,** *18* (15), 10182–10190.

35. Turkoglu, G.; Cinar, M. E.; Ozturk, T., Thiophene-based organic semiconductors. *Top. Curr. Chem.* **2017,** *375* (6), 84.

36. Chang, J. B.; Liu, V.; Subramanian, V.; Sivula, K.; Luscombe, C.; Murphy, A.; Liu, J.; Frechet, J. M. J., Printable polythiophene gas sensor array for low-cost electronic noses. *J. Appl. Phys.* **2006,** *100* (1), 014506/1–014506/7.

37. Si, P.; Mortensen, J.; Komolov, A.; Denborg, J.; Møller, P. J., Polymer coated quartz crystal microbalance sensors for detection of volatile organic compounds in gas mixtures. *Anal. Chim. Acta* **2007,** *597* (2), 223–230.

38. Tawfik, S. M.; Shim, J.; Biechele-Speziale, D.; Sharipov, M.; Lee, Y.-I., Novel “turn off-on” sensors for highly selective and sensitive detection of spermine based on heparin-quenching of fluorescence CdTe quantum dots-coated amphiphilic thiophene copolymers. *Sens. Actuators B: Chem.* **2018,** *257* (Supplement C), 734–744.

39. Wang, X.; Zheng, Y.; Xu, L., An electrochemical adenine sensor employing enhanced three-dimensional conductivity and molecularly imprinted sites of Au NPs bridged poly(3-thiophene acetic acid). *Sens. Actuators B: Chem.* **2018,** *255* (Part 3), 2952–2958.

40. Gautier, C.; Cougnon, C.; Pilard, J.-F.; Casse, N., Label-free detection of DNA hybridization based on EIS investigation of conducting properties of functionalized polythiophene matrix. *J. Electroanal. Chem.* **2006,** *587* (2), 276–283.

41. Kingsborough, R. P.; Swager, T. M., Electroactivity enhancement by redox matching in cobalt salen-based conducting polymers. *Adv. Mater. (Weinheim, Ger.)* **1998,** *10* (14), 1100–1104.

42. Kingsborough, R. P.; Swager, T. M., Polythiophene hybrids of transition-metal bis(salicylidenimine)s: correlation between structure and electronic properties. *J. Am. Chem. Soc.* **1999,** *121* (38), 8825–8834.

43. Kingsborough, R. P.; Swager, T. M., Electrocatalytic conducting polymers: oxygen reduction by a polythiophene-cobalt salen hybrid. *Chem. Mater.* **2000,** *12* (4), 872–874.

44. Canali, L.; C. Sherrington, D., Utilisation of homogeneous and supported chiral metal(salen) complexes in asymmetric catalysis. *Chem. Soc. Rev.* **1999,** *28* (2), 85–93.

45. Katsuki, T., Chiral metallosalen complexes: structures and catalyst tuning for asymmetric epoxidation and cyclopropanation. *Adv. Synth. Catal.* **2002,** *344* (2), 131–147.

46. Larrow, J. F.; Jacobsen, E. N., Asymmetric processes catalyzed by chiral(salen) metal complex. *Top. Organomet Chem.* **2004,** *6*, 123–152.

47. Cozzi, P. G., Metal-salen schiff base complexes in catalysis: practical aspects. *Chem. Soc. Rev.* **2004,** *33* (7), 410–421.

48. McGarrigle, E. M.; Gilheany, D. G., Chromium– and manganese–salen promoted epoxidation of alkenes. *Chem. Rev.* **2005,** *105* (5), 1563–1602.

49. Takahashi, I.; Koga, O.; Hoshi, N.; Hori, Y., Electrochemical reduction of CO_2 at copper single crystal Cu(S)-[n(111)×(111)] and Cu(S)-[n(110)×(100)] electrodes. *J. Electroanal. Chem.* **2002,** *533* (1–2), 135–143.

50. Yano, H.; Shirai, F.; Nakayama, M.; Ogura, K., Electrochemical reduction of CO_2 at three-phase (gas | liquid | solid) and two-phase (liquid | solid) interfaces on Ag electrodes. *J. Electroanal. Chem.* **2002,** *533* (1–2), 113–118.

51. Kedzierzawski, P.; Augustynski, J., Poisoning and activation of the gold cathode during electroreduction of CO_2. *J. Electrochem. Soc.* **1994,** *141* (5), L58–L60.

52. Ogura, K.; Endo, N., Electrochemical reduction of CO_2 with a functional gas-diffusion electrode in aqueous solutions with and without propylene carbonate. *J. Electrochem. Soc.* **1999,** *146* (10), 3736–3740.

53. Gattrell, M.; Gupta, N.; Co, A., A review of the aqueous electrochemical reduction of CO_2 to hydrocarbons at copper. *J. Electroanal. Chem.* **2006,** *594* (1), 1–19.

54. Hori, Y., Electrochemical CO_2 reduction on metal electrodes. In *Mod. Aspect. Electroc.*, Vayenas, C. G.; White, R. E.; Gamboa-Aldeco, M. E., Eds. Springer New York: New York, NY, **2008**; pp 89–189.

55. Whipple, D. T.; Kenis, P. J. A., Prospects of CO_2 utilization via direct heterogeneous electrochemical reduction. *J. Phys. Chem. Lett.* **2010,** *1* (24), 3451–3458.

56. Miedaner, A.; Curtis, C. J.; Barkley, R. M.; DuBois, D. L., Electrochemical reduction of CO_2 catalyzed by small organophosphine dendrimers containing palladium. *Inorg. Chem.* **1994,** *33* (24), 5482–5490.

57. Aresta, M., Carbon dioxide reduction and uses as a chemical feedstock. In *Activation of Small Molecules*, Wiley-VCH Verlag GmbH & Co. KGaA: **2006**; pp 1–41.

58. Kumar, B.; Llorente, M.; Froehlich, J.; Dang, T.; Sathrum, A.; Kubiak, C. P., Photochemical and photoelectrochemical reduction of CO_2. *Annu. Rev. Phys. Chem.* **2012,** *63* (1), 541–569.

59. Dry, M. E., The Fischer–Tropsch process: 1950–2000. *Catal. Today* **2002,** *71* (3–4), 227–241.

60. Rakowski Dubois, M.; Dubois, D. L., Development of molecular electrocatalysts for CO_2 reduction and H_2 production/oxidation. *Acc. Chem. Res.* **2009,** *42* (12), 1974–1982.

61. Costamagna, J. A.; Isaacs, M.; Aguirre, M. J.; Ramírez, G.; Azocar, I., Electroreduction of CO_2 catalyzed by metallomacrocyclics. In *N4-Macrocyclic Metal Complexes*, Zagal, J. H.; Bedioui, F.; Dodelet, J.-P., Eds. Springer New York: New York, NY, **2006**; pp 191–254.

62. Lin, S.; Diercks, C. S.; Zhang, Y.-B.; Kornienko, N.; Nichols, E. M.; Zhao, Y.; Paris, A. R.; Kim, D.; Yang, P.; Yaghi, O. M.; Chang, C. J., Covalent organic frameworks comprising cobalt porphyrins for catalytic CO_2 reduction in water. *Science* **2015,** *349* (6253), 1208.

63. Hammouche, M.; Lexa, D.; Momenteau, M.; Saveant, J. M., Chemical catalysis of electrochemical reactions. Homogeneous catalysis of the electrochemical reduction

of carbon dioxide by iron("0") porphyrins. Role of the addition of magnesium cations. *J. Am. Chem. Soc.* **1991,** *113* (22), 8455–8466.

64. Bhugun, I.; Lexa, D.; Savéant, J.-M., Catalysis of the electrochemical reduction of carbon dioxide by iron(0) Porphyrins: synergystic effect of weak Brönsted acids. *J. Am. Chem. Soc.* **1996,** *118* (7), 1769–1776.

65. Tripkovic, V.; Vanin, M.; Karamad, M.; Björketun, M. E.; Jacobsen, K. W.; Thygesen, K. S.; Rossmeisl, J., Electrochemical CO_2 and CO reduction on metal-functionalized porphyrin-like graphene. *J. Phys. Chem. C* **2013,** *117* (18), 9187–9195.

66. Mondal, B.; Rana, A.; Sen, P.; Dey, A., Intermediates involved in the $2e^-/2H^+$ reduction of CO_2 to CO by iron(0) Porphyrin. *J. Am. Chem. Soc.* **2015,** *137* (35), 11214–11217.

67. Choi, J.; Benedetti, T. M.; Jalili, R.; Walker, A.; Wallace, G. G.; Officer, D. L., High performance Fe porphyrin/ionic liquid Co-catalyst for electrochemical CO_2 reduction. *Chem.–Eur. J.* **2016,** *22* (40), 14158–14161.

68. Fukatsu, A.; Kondo, M.; Okabe, Y.; Masaoka, S., Electrochemical analysis of iron-porphyrin-catalyzed CO_2 reduction under photoirradiation. *J. Photochem Photobiol. A: Chem.* **2015,** *313* (Supplement C), 143–148.

69. Bonin, J.; Chaussemier, M.; Robert, M.; Routier, M., Homogeneous photocatalytic reduction of CO_2 to CO using iron(0) porphyrin catalysts: mechanism and intrinsic limitations. *ChemCatChem* **2014,** *6* (11), 3200–3207.

70. Meshitsuka, S.; Ichikawa, M.; Tamaru, K., Electrocatalysis by metal phthalocyanines in the reduction of carbon dioxide. *J. Chem. Soc., Chem. Commun.* **1974,** (5), 158–159.

71. Zhang, X.; Wu, Z.; Zhang, X.; Li, L.; Li, Y.; Xu, H.; Li, X.; Yu, X.; Zhang, Z.; Liang, Y.; Wang, H., Highly selective and active CO_2 reduction electrocatalysts based on cobalt phthalocyanine/carbon nanotube hybrid structures. *Nat. Commun.* **2017,** *8*, 14675.

72. Kramer, W. W.; McCrory, C. C. L., Polymer coordination promotes selective CO_2 reduction by cobalt phthalocyanine. *Chem. Sci.* **2016,** *7* (4), 2506–2515.

73. Morlanés, N.; Takanabe, K.; Rodionov, V., Simultaneous reduction of CO_2 and splitting of H_2O by a single immobilized cobalt phthalocyanine electrocatalyst. *ACS Catal.* **2016,** *6* (5), 3092–3095.

74. Lieber, C. M.; Lewis, N. S., Catalytic reduction of carbon dioxide at carbon electrodes modified with cobalt phthalocyanine. *J. Am. Chem. Soc.* **1984,** *106* (17), 5033–5034.

75. Kapusta, S.; Hackerman, N., Carbon dioxide reduction at a metal phthalocyanine catalyzed carbon electrode. *J. Electrochem. Soc.* **1984,** *131* (7), 1511–1514.

76. Yamanaka, I.; Tabata, K.; Mino, W.; Furusawa, T., Electroreduction of carbon dioxide to carbon monoxide by Co-phthalocyanine electrocatalyst under ambient conditions. *ISIJ International* **2015,** *55* (2), 399–403.

77. Beley, M.; Collin, J.-P.; Ruppert, R.; Sauvage, J.-P., Nickel(II)-cyclam: an extremely selective electrocatalyst for reduction of CO_2 in water. *J. Chem. Soc., Chem. Commun.* **1984,** (19), 1315–1316.

78. Scibioh, M. A.; Ragini, P. V.; Rani, S.; Vijayaraghavan, V. R.; Viswanathan, B., Reduction of CO_2 by nickel (II) macrocycle catalyst at HMDE. *J. Chem. Sci.* **2001,** *113* (4), 343–350.

79. Rudolph, M.; Dautz, S.; Jäger, E.-G., Macrocyclic [N42-] coordinated nickel complexes as catalysts for the formation of oxalate by electrochemical reduction of carbon dioxide. *J. Am. Chem. Soc.* **2000,** *122* (44), 10821–10830.

80. Fisher, B. J.; Eisenberg, R., Electrocatalytic reduction of carbon dioxide by using macrocycles of nickel and cobalt. *J. Am. Chem. Soc.* **1980,** *102* (24), 7361–7363.

81. Beley, M.; Collin, J. P.; Ruppert, R.; Sauvage, J. P., Electrocatalytic reduction of carbon dioxide by nickel cyclam^{2+} in water: study of the factors affecting the efficiency and the selectivity of the process. *J. Am. Chem. Soc.* **1986,** *108* (24), 7461–7467.

82. Collin, J. P.; Jouaiti, A.; Sauvage, J. P., Electrocatalytic properties of (tetraazacyclotetradecane)nickel^{2+} and Ni_2(biscyclam)$^{4+}$ with respect to carbon dioxide and water reduction. *Inorg. Chem.* **1988,** *27* (11), 1986–1990.

83. Balazs, G. B.; Anson, F. C., Effects of CO on the electrocatalytic activity of Ni (cyclam)$^{2+}$ toward the reduction of CO_2. *J. Electroanal. Chem.* **1993,** *361* (1), 149–157.

84. Ménard, G.; Gilbert, T. M.; Hatnean, J. A.; Kraft, A.; Krossing, I.; Stephan, D. W., Stoichiometric reduction of CO_2 to CO by phosphine/AlX_3-based frustrated Lewis pairs. *Organometallics* **2013,** *32* (15), 4416–4422.

85. Huang, J.; Chen, J.; Gao, H.; Chen, L., Kinetic aspects for the reduction of CO_2 and CS_2 with mixed-ligand ruthenium(II) hydride complexes containing phosphine and bipyridine. *Inorg. Chem.* **2014,** *53* (18), 9570–9580.

86. Gauthron, I.; Mugnier, Y.; Hierso, K.; D. Harvey, P., Electroreduction of $Pd_2(dppm)_2Cl_2$ and $Pd(dppm)Cl_2$ [dppm=bis(diphenylphosphino)methane] in aprotic medium under carbon dioxide: electrogeneration of $Pd_3(\mu_3\text{-}CO)(\mu\text{-}dppm)_3$. *New J. Chem.* **1998,** *22* (3), 237–246.

87. Zhang, Z.; Chi, M.; Veith, G. M.; Zhang, P.; Lutterman, D. A.; Rosenthal, J.; Overbury, S. H.; Dai, S.; Zhu, H., Rational design of Bi nanoparticles for efficient electrochemical CO_2 reduction: the elucidation of size and surface condition effects. *ACS Catal.* **2016,** *6* (9), 6255–6264.

88. Slater, S.; Wagenknecht, J. H., Electrochemical reduction of carbon dioxide catalyzed by $Rh(diphos)_2Cl$. *J. Am. Chem. Soc.* **1984,** *106* (18), 5367–5368.

89. DuBois, D. L.; Miedaner, A.; Haltiwanger, R. C., Electrochemical reduction of carbon dioxide catalyzed by $[Pd(triphosphine)(solvent)](BF_4)_2$ complexes: synthetic and mechanistic studies. *J. Am. Chem. Soc.* **1991,** *113* (23), 8753–8764.

90. Haines, R. J.; Wittrig, R. E.; Kubiak, C. P., Electrocatalytic reduction of carbon dioxide by the binuclear copper complex $[Cu_2(6\text{-}(diphenylphosphino\text{-}2,2'\text{-}bipyridyl)_2(MeCN)_2][PF_6]_2$. *Inorg. Chem.* **1994,** *33* (21), 4723–4728.

91. Dubois, D. L., Development of transition metal phosphine complexes as electrocatalysts for CO_2 and CO reduction. *Comments Inorg. Chem.* **1997,** *19* (5), 307–325.

92. Simón-Manso, E.; Kubiak, C. P., Dinuclear nickel complexes as catalysts for electrochemical reduction of carbon dioxide. *Organometallics* **2005,** *24* (1), 96–102.

93. Raebiger, J. W.; Turner, J. W.; Noll, B. C.; Curtis, C. J.; Miedaner, A.; Cox, B.; DuBois, D. L., Electrochemical reduction of CO_2 to CO catalyzed by a bimetallic palladium complex. *Organometallics* **2006,** *25* (14), 3345–3351.

94. Portenkirchner, E.; Gasiorowski, J.; Oppelt, K.; Schlager, S.; Schwarzinger, C.; Neugebauer, H.; Knör, G.; Sariciftci, N. S., Electrocatalytic reduction of carbon dioxide

to carbon monoxide by a polymerized film of an alkynyl-substituted rhenium(I) complex. *ChemCatChem* **2013,** *5* (7), 1790–1796.

95. Canales, J.; Ramirez, J.; Estiu, G.; Costamagna, J., Bis-bipyridine hexa-aza-macrocycle complexes of zinc(II) and nickel(II) and the catalytic reduction of carbon dioxide. *Polyhedron* **2000,** *19* (22–23), 2373–2381.

96. Chardon-Noblat, S.; Deronzier, A.; Hartl, F.; van Slageren, J.; Mahabiersing, T., A novel organometallic polymer of osmium(0), $[Os(2,2'\text{-bipyridine})(CO)_2]_n$: its electrosynthesis and electrocatalytic properties towards CO_2 reduction. *Eur. J. Inorg. Chem.* **2001,** *2001* (3), 613–617.

97. Collomb-Dunand-Sauthier, M.-N.; Deronzier, A.; Ziessel, R., Electrocatalytic reduction of CO_2 in water on a polymeric $[\{Ru0(bpy)(CO)_2\}]$(bpy=2,2'-bipyridine) complex immobilized on carbon electrodes. *J. Chem. Soc., Chem. Commun.* **1994,** (2), 189–191.

98. Hawecker, J.; Lehn, J.-M.; Ziessel, R., Electrocatalytic reduction of carbon dioxide mediated by $Re(bipy)(CO)_3Cl$ (bipy=2,2'-bipyridine). *J. Chem. Soc., Chem. Commun.* **1984,** (6), 328–330.

99. Ishida, H.; Tanaka, K.; Tanaka, T., Electrochemical CO_2 reduction catalyzed by ruthenium complexes $[Ru(bpy)_2(CO)_2]^{2+}$ and $[Ru(bpy)_2(CO)Cl]^+$. Effect of pH on the formation of CO and HCOO. *Organometallics* **1987,** *6* (1), 181–186.

100. Bolinger, C. M.; Story, N.; Sullivan, B. P.; Meyer, T. J., Electrocatalytic reduction of carbon dioxide by 2,2'-bipyridine complexes of rhodium and iridium. *Inorg. Chem.* **1988,** *27* (25), 4582–4587.

101. Bruce, M. R. M.; Megehee, E.; Sullivan, B. P.; Thorp, H.; O'Toole, T. R.; Downard, A.; Meyer, T. J., Electrocatalytic reduction of carbon dioxide by associative activation. *Organometallics* **1988,** *7* (1), 238–240.

102. Harnisch, F.; Freguia, S., A basic tutorial on cyclic voltammetry for the investigation of electroactive microbial biofilms. *Chem.–Asian J.* **2012,** *7* (3), 466–475.

103. Reche, I.; Gallardo, I.; Guirado, G., Cyclic voltammetry using silver as cathode material: a simple method for determining electro and chemical features and solubility values of CO_2 in ionic liquids. *Phys. Chem. Chem. Phys.* **2015,** *17* (4), 2339–2343.

104. Chesney, D. J., Laboratory techniques in electroanalytical chemistry, 2nd edition edited by Peter T. Kissinger (Purdue University) and William R. Heineman (University of Cincinnati). Dekker: Monticello, NY. **1996**. xxii + 986 pp. $79. ISBN 0-8247-9445-1. *J. Am. Chem. Soc.* **1996,** *118* (44), 10946–10946.

105. Wang, J., Study of electrode reactions and interfacial properties. In *Anal. Electrochem.*, John Wiley & Sons, Inc.: **2006**; pp 29–66.

106. Marusak, R. A.; Doan, K.; Cummings, S. D., Appendix 2: introduction to cyclic voltammetry1–6. In *Integrated Approach to Coordination Chemistry*, John Wiley & Sons, Inc.: **2007**; pp 235–241.

107. Behar, D.; Dhanasekaran, T.; Neta, P.; Hosten, C. M.; Ejeh, D.; Hambright, P.; Fujita, E., Cobalt porphyrin catalyzed reduction of CO_2. Radiation chemical, photochemical, and electrochemical studies. *J. Phys. Chem. A* **1998,** *102* (17), 2870–2877.

108. Shapoval, G. S.; Gorodyskii, A. V., Electrochemical initiation of polymerization. *Usp. Khim.* **1973,** *42* (5), 854–80.

109. Roncali, J., Conjugated poly(thiophenes): synthesis, functionalization, and applications. *Chem. Rev.* **1992,** *92* (4), 711–738.

110. Mengoli, G.; Tidswell, B. M., Polymeric coatings on steel produced by the electroinitiated polymerization of acrylic monomers. *Polymer* **1975,** *16* (12), 881–888.

111. Abruna, H. D.; Denisevich, P.; Umana, M.; Meyer, T. J.; Murray, R. W., Rectifying interfaces using two-layer films of electrochemically polymerized vinylpyridine and vinylbipyridine complexes of ruthenium and iron on electrodes. *J. Am. Chem. Soc.* **1981,** *103* (1), 1–5.

112. Pistoia, G.; Voso, M. A., Electroinitiated radical polymerizations in acid solutions. *Gazz. Chim. Ital.* **1976,** *106* (3-6), 267–76.

113. Pistoia, G.; Scrosati, B.; Voso, M. A., Electroinitiated polymerization of acrylonitrile in aqueous sulphuric acid. *Eur. Polym. J.* **1976,** *12* (1), 53–57.

114. Mengoli, G.; Musiani, M. M.; Pagura, C.; Paolucci, F., The inhibition of the corrosion of mild steel in aqueous acids by in situ polymerization of unsaturated compounds. *Corros. Sci.* **1991,** *32* (7), 743–753.

115. Zhang, X.; Bell, J. P.; Narkis, M., The electropolymerization of poly(styrene-co-4-carboxyphenyl maleimide) coatings onto steel. *J. Appl. Polym. Sci.* **1996,** *62* (8), 1303–1312.

116. Ling, X. Formation of polymer coatings by electropolymerization. UWSpace, **1998**.

117. Diaz, A. F.; Martinez, A.; Kanazawa, K. K.; Salmón, M., Electrochemistry of some substituted pyrroles. *J. Electroanal. Chem. Interfacial Electrochem.* **1981,** *130* (Supplement C), 181–187.

118. Diaz, A. F.; Castillo, J.; Kanazawa, K. K.; Logan, J. A.; Salmon, M.; Fajardo, O., Conducting poly-*N*-alkylpyrrole polymer films. *J. Electroanal. Chem. and Interfacial Electrochem.* **1982,** *133* (2), 233–239.

119. Diaz, A. F.; Kanazawa, K. K. In *Polypyrrole: an electrochemical approach to conducting polymers*, Plenum: **1983**; pp 417–41.

120. Kaeriyama, K.; Sato, M.; Tanaka, S., Electrochemical preparation of conducting polyalkylthiophene films. *Synth. Met.* **1987,** *18* (1), 233–236.

121. Waltman, R. J.; Diaz, A. F.; Bargon, J., Substituent effects in the electropolymerization of aromatic heterocyclic compounds. *J. Phys. Chem.* **1984,** *88* (19), 4343–6.

122. Tourillon, G.; Garnier, F., New electrochemically generated organic conducting polymers. *J. Electroanal. Chem. Interfacial Electrochem.* **1982,** *135* (1), 173–178.

123. Zein El Abedin, S.; Borissenko, N.; Endres, F., Electropolymerization of benzene in a room temperature ionic liquid. *Electrochem. Commun.* **2004,** *6* (4), 422–426.

124. Le Berre, V.; Angely, L.; Simonet, J.; Mousset, G.; Bellec, M., Electrochemical polymerization of paradialkoxybenzenes: Part I. Anodic oxidation of paradimethoxybenzene in dry acetonitrile. *J. Electroanal. Chem. Interfacial Electrochem.* **1987,** *218* (1), 173–185.

125. Aeiyach, S.; Lacaze, P. C., Electropolymerization of benzene and biphenyl in organic media: influence of different parameters (solvent, water, acidity, salt) on the formation of polyparaphenylene films (PPP). *J. Polym. Sci. Part A: Polym. Chem.* **1989,** *27* (2), 515–526.

126. Shelepin, I. V.; Fedorova, A. I., Initiation of polymerization of methyl methacrylate at potentials of hydrogen-ion reduction. *Zh. Fiz. Khim.* **1964,** *38* (11), 2676–9.

127. Tidswell, B. M.; Mortimer, D. A., Electropolymerization : direct film formation on metal substrates-I: kinetics and mechanism. *Eur. Polym. J.* **1981,** *17* (7), 735–744.

128. Tidswell, B. M.; Mortimer, D. A., Electropoly merization: direct film formation on metal substrates II locus of polymerization. *Eur. Polym. J.* **1981,** *17* (7), 745–754.

129. Atwood, D. A.; Remington, M. P.; Rutherford, D., Use of the salan ligands to form bimetallic aluminum complexes. *Organometallics* **1996,** *15* (22), 4763–4769.

130. Pfeiffer, P.; Breith, E.; Lübbe, E.; Tsumaki, T., Tricyclische orthokondensierte Nebenvalenzringe. *Justus Liebigs Ann. Chem.* **1933,** *503* (1), 84–130.

131. Diehl, H.; Hach, C. C., Bis(*N,N'*-disalicylalethylenediamine)-**μ**-aquodicobalt(II). *Inorg. synth. III* **1950**, 196–201.

132. Cheng, J.; Wei, K.; Ma, X.; Zhou, X.; Xiang, H., Synthesis and photophysical properties of colorful salen-type schiff bases. *J. Phys. Chem. C* **2013,** *117* (32), 16552–16563.

133. Chiang, L.; Allan, L. E. N.; Alcantara, J.; Wang, M. C. P.; Storr, T.; Shaver, M. P., Tuning ligand electronics and peripheral substitution on cobalt salen complexes: structure and polymerisation activity. *Dalton Trans.* **2014,** *43* (11), 4295–4304.

134. Mirkhani, V.; Moghadam, M.; Tangestaninejad, S.; Bahramian, B., Effect of bulky substitution on catalytic activity of a manganese salen complex used in biomimetic alkene epoxidation and alkane hydroxylation with sodium periodate. *J. Iran. Chem. Soc.* **2008,** *5* (3), 375–383.

135. Skljarevski, S.; Peverly, A. A.; Peters, D. G., Cyclic voltammetric and spectrophotometric investigation of the catalytic reduction of 1,1,2-trichloro-1,2,2-trifluoroethane (CFC-113) by electrogenerated cobalt(I) salen in dimethylformamide saturated with carbon dioxide. *J. Electroanal. Chem.* **2011,** *661* (1), 39–43.

136. Darensbourg, D. J.; Mackiewicz, R. M.; Phelps, A. L.; Billodeaux, D. R., Copolymerization of CO_2 and epoxides catalyzed by metal salen complexes. *Acc. Chem. Res.* **2004,** *37* (11), 836–844.

137. Cohen, C. T.; Coates, G. W., Alternating copolymerization of propylene oxide and carbon dioxide with highly efficient and selective (salen)Co(III) catalysts: effect of ligand and cocatalyst variation. *J. Polym. Sci. Part A: Polym. Chem.* **2006,** *44* (17), 5182–5191.

138. Hutson, G. E.; Turkmen, Y. E.; Rawal, V. H., Salen promoted enantioselective Nazarov cyclizations of activated and unactivated dienones. *J. Am. Chem. Soc.* **2013,** *135* (13), 4988–4991.

139. Murakami, M.; Uchida, T.; Saito, B.; Katsuki, T., Ru(salen)-catalyzed asymmetric sulfimidation and subsequent [2,3]sigmatropic rearrangement. *Chirality* **2003,** *15* (2), 116–123.

140. Darensbourg, D. J.; Billodeaux, D. R., Aluminum salen complexes and tetrabutylammonium salts: a binary catalytic system for production of polycarbonates from CO_2 and cyclohexene oxide. *Inorg. Chem.* **2005,** *44* (5), 1433–1442.

141. Nakano, K.; Nakamura, M.; Nozaki, K., Alternating copolymerization of cyclohexene oxide with carbon dioxide catalyzed by (salalen)CrCl complexes. *Macromolecules (Washington, DC, U. S.)* **2009,** *42* (18), 6972–6980.

142. Park, J.; Lang, K.; Abboud, K. A.; Hong, S., Self-assembled dinuclear cobalt(II)-salen catalyst through hydrogen-bonding and its application to enantioselective nitro-aldol (Henry) reaction. *J. Am. Chem. Soc.* **2008,** *130* (49), 16484–16485.

143. Zulauf, A.; Mellah, M.; Schulz, E., New chiral thiophene-salen chromium complexes for the asymmetric Henry reaction. *J. Org. Chem.* **2009,** *74* (5), 2242–2245.

144. Roncali, J., Electrogenerated functional conjugated polymers as advanced electrode materials. *J. Mater. Chem.* **1999,** *9* (9), 1875–1893.

145. Turut, A.; Koleli, F., Semiconductive polymer-based schottky diode. *J. Appl. Phys.* **1992,** *72* (2), 818–19.

146. Zotti, G.; Schiavon, G.; Berlin, A.; Pagani, G., Thiophene oligomers as polythiophene models. 3. Conductive and capacitive behavior of end-capped oligothienyls as thin films. A contribution to the conduction mechanism and to the faradaic-capacitive debate of conducting polymers. *Adv. Mater. (Weinheim, Fed. Repub. Ger.)* **1993,** *5* (7–8), 551–554.

147. Rudge, A.; Davey, J.; Raistrick, I.; Gottesfeld, S.; Ferraris, J. P., Conducting polymers as active materials in electrochemical capacitors. *J. Power Sources* **1994,** *47* (1–2), 89–107.

148. Laforgue, A.; Simon, P.; Sarrazin, C.; Fauvarque, J.-F., Polythiophene-based supercapacitors. *J. Power Sources* **1999,** *80* (1–2), 142–148.

149. Tang, J.; Kong, L.; Zhang, J.; Zhan, L.; Zhan, H.; Zhou, Y.; Zhan, C., Solvent-free, oxidatively prepared polythiophene: high specific capacity as a cathode active material for lithium batteries. *React. Funct. Polym.* **2008,** *68* (9), 1408–1413.

150. Aydin, M.; Esat, B.; Kilic, C.; Koese, M. E.; Ata, A.; Yilmaz, F., A polythiophene derivative bearing TEMPO as a cathode material for rechargeable batteries. *Eur. Polym. J.* **2011,** *47* (12), 2283–2294.

151. Fu, C.; Zhou, H.; Liu, R.; Huang, Z.; Chen, J.; Kuang, Y., Supercapacitor based on electropolymerized polythiophene and multi-walled carbon nanotubes composites. *Mater. Chem. Phys.* **2012,** *132* (2-3), 596–600.

152. Aizawa, M.; Shinohara, H.; Yamada, T.; Akagi, K.; Shirakawa, H., Electrochemical fabrication of a polypyrrole/polythiophene P-N junction diode. *Synth. Met.* **1987,** *18* (1), 711–714.

153. Dyreklev, P.; Berggren, M.; Inganäs, O.; Andersson, M. R.; Wennerström, O.; Hjertberg, T., Polarized electroluminescence from an oriented substituted polythiophene in a light emitting diode. *Adv. Mater.* **1995,** *7* (1), 43–45.

154. Kaminorz, Y.; Smela, E.; Inganäs, O.; Brehmer, L., Sensitivity of polythiophene planar light-emitting diodes to oxygen. *Adv. Mater.* **1998,** *10* (10), 765–769.

155. Ng, S.-C.; Xu, J.-M.; S. O. Chan, H.; Fujii, A.; Yoshino, K., Regioregular poly[3-butyl-2,5-thienylene-alt-1,4-phenylene]: synthesis, preliminary characterization aspects and application in the fabrication of light-emitting diodes. *J. Mater. Chem.* **1999,** *9* (2), 381–385.

156. R. Andersson, M.; Thomas, O.; Mammo, W.; Svensson, M.; Theander, M.; Inganas, O., Substituted polythiophenes designed for optoelectronic devices and conductors. *J. Mater. Chem.* **1999,** *9* (9), 1933–1940.

157. Lere-Porte, J.-P.; Moreau, J. J. E.; Serein-Spirau, F.; Torreilles, C.; Righi, A.; Sauvajol, J.-L.; Brunet, M., Synthesis, orientation and optical properties of thiophene-dialkoxyphenylene copolymers. *J. Mater. Chem.* **2000,** *10* (4), 927–932.

158. Ding, A.-L.; Pei, J.; Lai, Y.-H.; Huang, W., Phenylene-functionalized polythiophene derivatives for light-emitting diodes: their synthesis, characterization and properties. *J. Mater. Chem.* **2001,** *11* (12), 3082–3086.

159. Wang, X. J.; Andersson, M. R.; Thompson, M. E.; Inganäs, O., Electrophosphorescence from polythiophene blends light-emitting diodes. *Synth. Met.* **2003,** *137* (1–3), 1019–1020.

160. Xia, Y.; Luo, J.; Deng, X.; Li, X.; Li, D.; Zhu, X.; Yang, W.; Cao, Y., Novel random low-band-gap fluorene-based copolymers for deep red/near infrared light-emitting diodes and bulk heterojunction photovoltaic cells. *Macromol. Chem. Phys.* **2006,** *207* (5), 511–520.

161. Fehse, K.; Walzer, K.; Leo, K.; Lövenich, W.; Elschner, A., Highly conductive polymer anodes as replacements for inorganic materials in high-efficiency organic light-emitting diodes. *Adv. Mater.* **2007,** *19* (3), 441–444.

162. Tsumura, A.; Koezuka, H.; Ando, T., Macromolecular electronic device: field-effect transistor with a polythiophene thin film. *Appl. Phys. Lett.* **1986,** *49* (18), 1210–12.

163. Koezuka, H.; Tsumura, A.; Ando, T., Field-effect transistor with polythiophene thin film. *Synth. Met.* **1987,** *18* (1-3), 699–704.

164. Tsumura, A.; Koezuka, H.; Ando, T., Polythiophene field-effect transistor: its characteristics and operation mechanism. *Synth. Met.* **1988,** *25* (1), 11–23.

165. Osaka, I.; Sauve, G.; Zhang, R.; Kowalewski, T.; McCullough, R. D., Novel thiophene-thiazolothiazole copolymers for organic field-effect transistors. *Adv. Mater. (Weinheim, Ger.)* **2007,** *19* (23), 4160–4165.

166. Lan, Y.-K.; Yang, C. H.; Yang, H.-C., Theoretical investigations of electronic structure and charge transport properties in polythiophene-based organic field-effect transistors. *Polym. Int.* **2010,** *59* (1), 16–21.

167. Voigt, M. M.; Guite, A.; Chung, D.-Y.; Khan, R. U. A.; Campbell, A. J.; Bradley, D. D. C.; Meng, F.; Steinke, J. H. G.; Tierney, S.; McCulloch, I.; Penxten, H.; Lutsen, L.;

Douheret, O.; Manca, J.; Brokmann, U.; Soennichsen, K.; Huelsenberg, D.; Bock, W.; Barron, C.; Blanckaert, N.; Springer, S.; Grupp, J.; Mosley, A., Polymer field-effect transistors fabricated by the sequential gravure printing of polythiophene, two insulator layers, and a metal ink gate. *Adv. Funct. Mater.* **2010,** *20* (2), 239–246.

168. Yoshino, K.; Kaneto, K., Application of insulator-metal transition of conducting polymers. *Mol. Cryst. Liq. Cryst.* **1985,** *121*, 247–254.

169. Garnier, F.; Horowitz, G., Organic semiconducting polymers as molecular material for electronic devices. *Synth. Met.* **1987,** *18* (1), 693–698.

170. Smestad, G. P.; Spiekermann, S.; Kowalik, J.; Grant, C. D.; Schwartzberg, A. M.; Zhang, J.; Tolbert, L. M.; Moons, E., A technique to compare polythiophene solid-state dye sensitized TiO_2 solar cells to liquid junction devices. *Sol. Energy Mater. Sol. Cells* **2003,** *76* (1), 85–105.

171. Colladet, K.; Fourier, S.; Cleij, T. J.; Lutsen, L.; Gelan, J.; Vanderzande, D.; Huong Nguyen, L.; Neugebauer, H.; Sariciftci, S.; Aguirre, A.; Janssen, G.; Goovaerts, E., Low band gap donor–acceptor conjugated polymers toward organic solar cells applications. *Macromolecules* **2007,** *40* (1), 65–72.

172. Tan, Z. a.; Hou, J.; He, Y.; Zhou, E.; Yang, C.; Li, Y., Synthesis and photovoltaic properties of a donor–acceptor double-cable polythiophene with high content of C_{60} pendant. *Macromolecules* **2007,** *40* (6), 1868–1873.

173. Woo, C. H.; Holcombe, T. W.; Unruh, D. A.; Sellinger, A.; Fréchet, J. M. J., Phenyl vs alkyl polythiophene: a solar cell comparison using a vinazene derivative as acceptor. *Chem. Mater.* **2010,** *22* (5), 1673–1679.

174. Oosterhout, S. D.; Koster, L. J. A.; van Bavel, S. S.; Loos, J.; Stenzel, O.; Thiedmann, R.; Schmidt, V.; Campo, B.; Cleij, T. J.; Lutzen, L.; Vanderzande, D.; Wienk, M. M.; Janssen, R. A. J., Controlling the morphology and efficiency of hybrid ZnO:polythiophene solar cells via side chain functionalization. *Adv. Energy Mater.* **2011,** *1* (1), 90–96.

175. Hu, H.; Jiang, K.; Yang, G.; Liu, J.; Li, Z.; Lin, H.; Liu, Y.; Zhao, J.; Zhang, J.; Huang, F.; Qu, Y.; Ma, W.; Yan, H., Terthiophene-based D–A polymer with an asymmetric arrangement of alkyl chains that enables efficient polymer solar cells. *J. Am. Chem. Soc.* **2015,** *137* (44), 14149–14157.

176. Garnier, F.; Tourillon, G.; Gazard, M.; Dubois, J. C., Organic conducting polymers derived from substituted thiophenes as electrochromic material. *J. Electroanal. Chem. Interfacial Electrochem.* **1983,** *148* (2), 299–303.

177. Kumar, A.; Welsh, D. M.; Morvant, M. C.; Piroux, F.; Abboud, K. A.; Reynolds, J. R., Conducting poly(3,4-alkylenedioxythiophene) derivatives as fast electrochromics with high-contrast ratios. *Chem. Mater.* **1998,** *10* (3), 896–902.

178. Lu, W.; Fadeev, A. G.; Qi, B.; Smela, E.; Mattes, B. R.; Ding, J.; Spinks, G. M.; Mazurkiewicz, J.; Zhou, D.; Wallace, G. G.; MacFarlane, D. R.; Forsyth, S. A.; Forsyth, M., Use of ionic liquids for π-conjugated polymer electrochemical devices. *Science (Washington, DC, U. S.)* **2002,** *297* (5583), 983–987.

179. Meng, H.; Tucker, D.; Chaffins, S.; Chen, Y.; Helgeson, R.; Dunn, B.; Wudl, F., An unusual electrochromic device based on a new low-bandgap conjugated polymer. *Adv. Mater. (Weinheim, Ger.)* **2003,** *15* (2), 146–149.

180. Nicho, M. E.; Hu, H.; Lopez-Mata, C.; Escalante, J., Synthesis of derivatives of polythiophene and their application in an electrochromic device. *Sol. Energy Mater. Sol. Cells* **2004,** *82* (1-2), 105–118.

181. Thompson, B. C.; Kim, Y.-G.; McCarley, T. D.; Reynolds, J. R., Soluble narrow band gap and blue propylenedioxythiophene-cyanovinylene polymers as multifunctional materials for photovoltaic and electrochromic applications. *J. Am. Chem. Soc.* **2006,** *128* (39), 12714–12725.

182. Beaujuge, P. M.; Ellinger, S.; Reynolds, J. R., The donor-acceptor approach allows a black-to-transmissive switching polymeric electrochrome. *Nat. Mater.* **2008,** *7* (10), 795–799.

183. Zhang, X.; Steckler, T. T.; Dasari, R. R.; Ohira, S.; Potscavage, W. J., Jr.; Tiwari, S. P.; Coppee, S.; Ellinger, S.; Barlow, S.; Bredas, J.-L.; Kippelen, B.; Reynolds, J. R.; Marder, S. R., Dithienopyrrole-based donor-acceptor copolymers: low band-gap materials for charge transport, photovoltaics and electrochromism. *J. Mater. Chem.* **2010,** *20* (1), 123–134.

184. Chen, T.-A.; Wu, X.; Rieke, R. D., Regiocontrolled synthesis of poly(3-alkylthiophenes) mediated by Rieke zinc: their characterization and solid-state properties. *J. Am. Chem. Soc.* **1995,** *117* (1), 233–244.

185. Loewe, R. S.; Khersonsky, S. M.; McCullough, R. D., A simple method to prepare head-to-tail coupled, regioregular poly(3-alkylthiophenes) using Grignard metathesis. *Adv. Mater.* **1999,** *11* (3), 250–253.

186. Blanchard, P.; Cravino, A.; Levillain, E., Electrochemistry of oligothiophenes and polythiophenes. In *Handbook of Thiophene-Based Materials*, John Wiley & Sons, Ltd: **2009**; pp 419–453.

187. Sellner, H.; Karjalainen, J. K.; Seebach, D., Preparation of dendritic and non-dendritic styryl-substituted salens for cross-linking suspension copolymerization with styrene and multiple use of the corresponding Mn and Cr complexes in enantioselective epoxidations and hetero-Diels–Alder reactions. *Chem.–Eur. J.* **2001,** *7* (13), 2873–2887.

188. Voituriez, A.; Mellah, M.; Schulz, E., Design and electropolymerization of new chiral thiophene-salen complexes. *Synth. Met.* **2006,** *156* (2–4), 166–175.

189. Kim, G. J.; Shin, J. H., Application of new unsymmetrical chiral Mn(III), Co(II,III) and Ti(IV) salen complexes in enantioselective catalytic reactions. *Catal. Lett.* **1999,** *63* (1), 83–90.

190. Renehan, M. F.; Schanz, H.-J.; McGarrigle, E. M.; Dalton, C. T.; Daly, A. M.; Gilheany, D. G., Unsymmetrical chiral salen schiff base ligands: synthesis and use in metal-based asymmetric epoxidation reactions. *J. Mol. Catal. A: Chem.* **2005,** *231* (1–2), 205–220.

191. Holbach, M.; Zheng, X.; Burd, C.; Jones, C. W.; Weck, M., A practical one-pot synthesis of enantiopure unsymmetrical salen ligands. *J. Org. Chem.* **2006,** *71* (7), 2903–2906.

192. Martínez, R. F.; Ávalos, M.; Babiano, R.; Cintas, P.; Jiménez, J. L.; Light, M. E.; Palacios, J. C., Schiff bases from TRIS and ortho-hydroxyarenecarbaldehydes: structures and tautomeric equilibria in the solid state and in solution. *Eur. J. Org. Chem.* **2011,** *2011* (17), 3137–3145.

193. Müller, S.; Liepold, B.; Roth, G. J.; Bestmann, H. J., An improved one-pot procedure for the synthesis of alkynes from aldehydes. *Synlett* **1996,** *6*, 521–522.

194. Glaser, C., Beiträge zur Kenntniss des Acetenylbenzols. *Ber. dtsch. chem. Ges.* **1869,** *2* (1), 422–424.

195. Glaser, C., Untersuchungen über einige Derivate der Zimmtsäure. *Justus Liebigs Ann. Chem.* **1870,** *154* (2), 137–171.

196. Chinchilla, R.; Nájera, C., The Sonogashira reaction: a booming methodology in synthetic organic chemistry. *Chem. Rev.* **2007,** *107* (3), 874–922.

197. Polyansky, D. E., Electrocatalysts for carbon dioxide reduction. In *Encyclopedia of Applied Electrochemistry*, Kreysa, G.; Ota, K.-i.; Savinell, R. F., Eds. Springer New York: New York, NY, **2014**; pp 431–437.

198. Willner, I.; Maidan, R.; Mandler, D.; Duerr, H.; Doerr, G.; Zengerle, K., Photosensitized reduction of carbon dioxide to methane and hydrogen evolution in the presence of ruthenium and osmium colloids: strategies to design selectivity of products distribution. *J. Am. Chem. Soc.* **1987,** *109* (20), 6080–6086.

199. Deunf, E.; Zaborova, E.; Guieu, S.; Blériot, Y.; Verpeaux, J.-N.; Buriez, O.; Sollogoub, M.; Amatore, C., Synthesis and electrochemical study of an original copper(II)-capped salen–cyclodextrin complex. *Eur. J. Inorg. Chem.* **2010,** *2010* (29), 4720–4727.

200. Zolezzi, S.; Spodine, E.; Decinti, A., Electrochemical studies of copper(II) complexes with schiff-base ligands. *Polyhedron* **2002,** *21* (1), 55–59.

201. Yates, J. M.; Fell, J. S.; Miranda, J. A.; Gherman, B. F., Metal-salens as catalysts in electroreductive cyclization and electrohydrocyclization: computational and experimental studies. *ECS Trans.* **2013,** *50* (29), 5–15.

202. Tomczyk, D.; Nowak, L.; Bukowski, W.; Bester, K.; Urbaniak, P.; Andrijewski, G.; Olejniczak, B., Reductive and oxidative electrochemical study and spectroscopic properties of nickel(II) complexes with N_2O_2 schiff bases derived from (±)-trans-*N,N*'-bis(salicylidene)-1,2-cyclohexanediamine. *Electrochim. Acta* **2014,** *121* (Supplement C), 64–77.

203. Zulauf, A.; Hong, X.; Brisset, F.; Schulz, E.; Mellah, M., Electropolymerization of chiral chromium-salen complexes: new materials for heterogeneous asymmetric catalysis. *New J. Chem.* **2012,** *36* (6), 1399–1407.

204. Asswadi, F. A.; Yousef, U. S.; Hathoot, A. S.; Abdel Azzem, M.; Galal, A., Electropolymerization of diaminofluorene and its electrochemical properties. *Ara. J. Chem.* **2015,** *8* (4), 433–441.

205. Damaceanu, M.-D.; Marin, L., Structure-property relationship in fluorene-based polymer films obtained by electropolymerization of 4,4'-(9-fluorenylidene)-dianiline. *RSC Adv.* **2015,** *5* (117), 97016–97026.

206. Tarajko, A.; Cybulski, H.; Chmielewski, M. J.; Bukowska, J.; Skompska, M., Electrochemical and spectroscopic characterization of poly(1,8-diaminocarbazole): part I. Electropolymerization and determination of the polymer structure by FTIR studies and DFT calculations. *Electrochim. Acta* **2009,** *54* (21), 4743–4750.

207. Lakard, B.; Herlem, G.; Lakard, S.; Fahys, B., Ab initio study of the polymerization mechanism of poly(*p*-phenylenediamine). *J. Mol. Struct.: THEOCHEM* **2003,** *638* (1), 177–187.

208. Waltman, R. J.; Diaz, A. F.; Bargon, J., Substituent effects in the electropolymerization of aromatic heterocyclic compounds. *J. Phys. Chem.* **1984,** *88* (19), 4343–4346.

209. Waltman, R. J.; Bargon, J., Electrically conducting polymers: a review of the electropolymerization reaction, of the effects of chemical structure on polymer film properties, and of applications towards technology. *Can. J. Chem.* **1986,** *64* (1), 76–95.

210. Turbiez, M.; Frère, P.; Allain, M.; Gallego-Planas, N.; Roncali, J., Effect of structural factor on the electropolymerization of bithiophenic precursors containing a 3,4-ethylenedisulfanylthiophene unit. *Macromolecules* **2005,** *38* (16), 6806–6812.

211. Shimidzu, T.; Segawa, H.; Wu, F.; Nakayama, N., Approaches to conducting polymer devices with nanostructures: photoelectrochemical function of one-dimensional and two-dimensional porphyrin polymers with oligothienyl molecular wire. *J. Photochem. Photobiol. A: Chem.* **1995,** *92* (1), 121–127.

APPENDIX

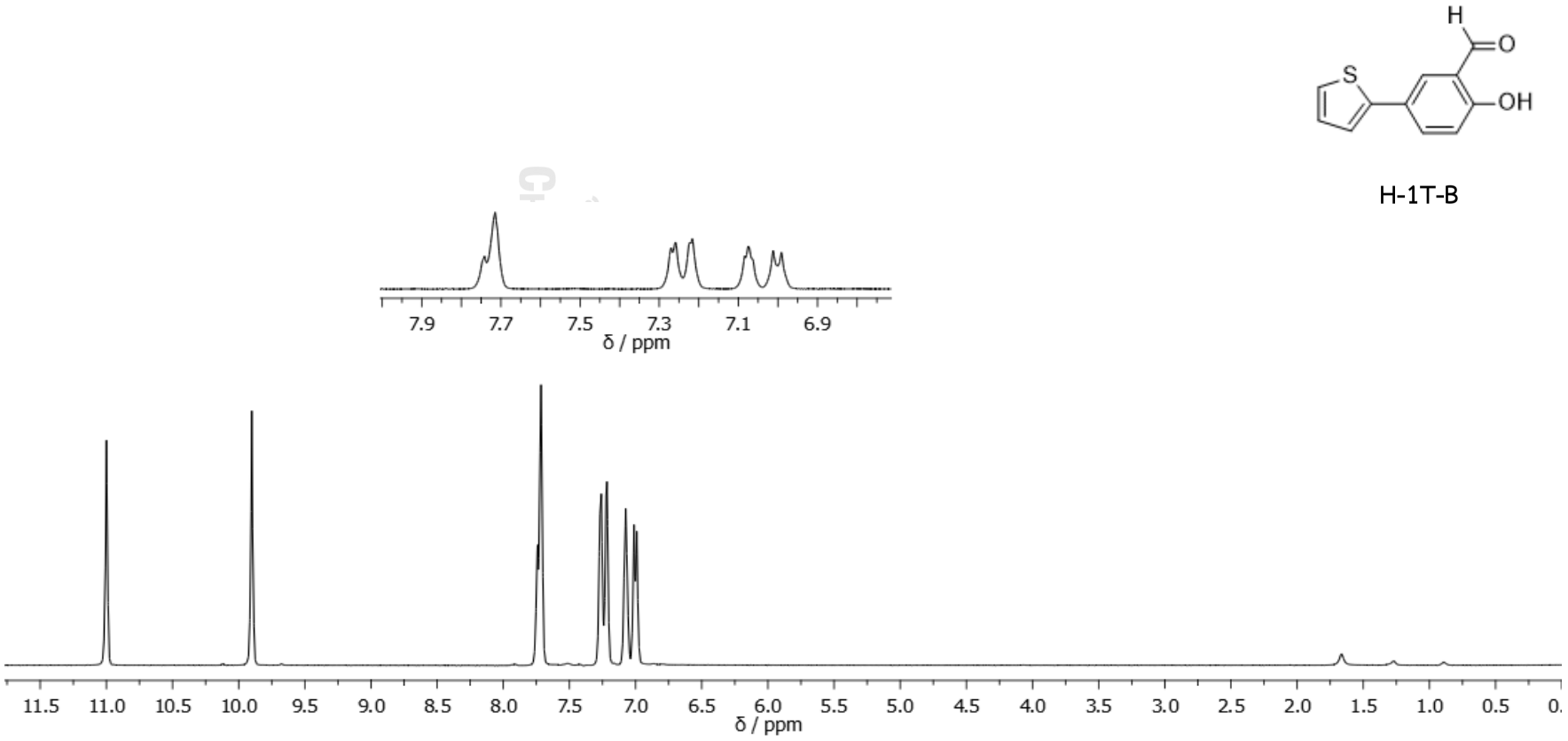

Figure A–1: ^{1}H-NMR spectrum of compound **H-1T-B**

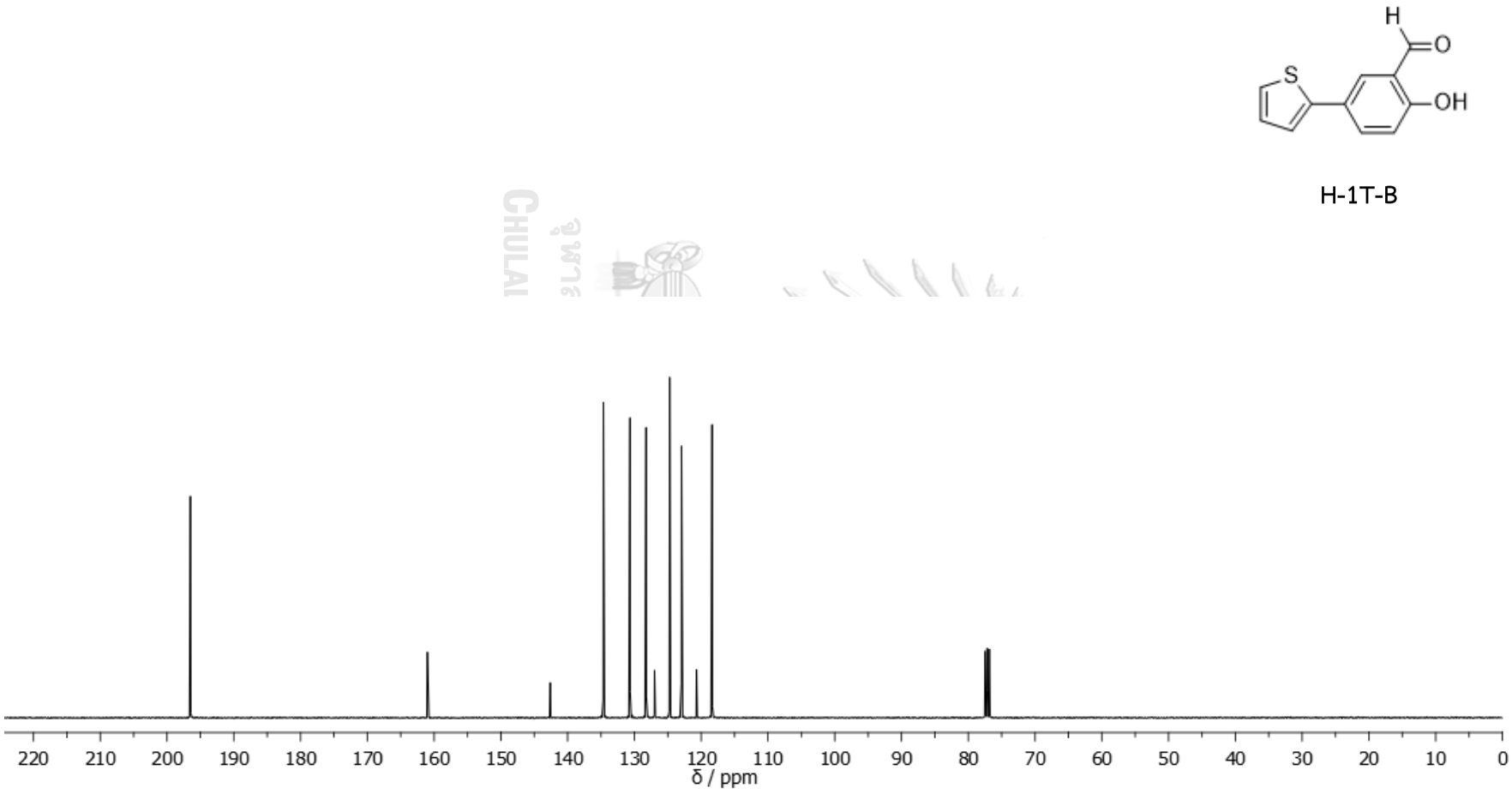

Figure A–2: ^{13}C-NMR spectrum of compound **H-1T-B**

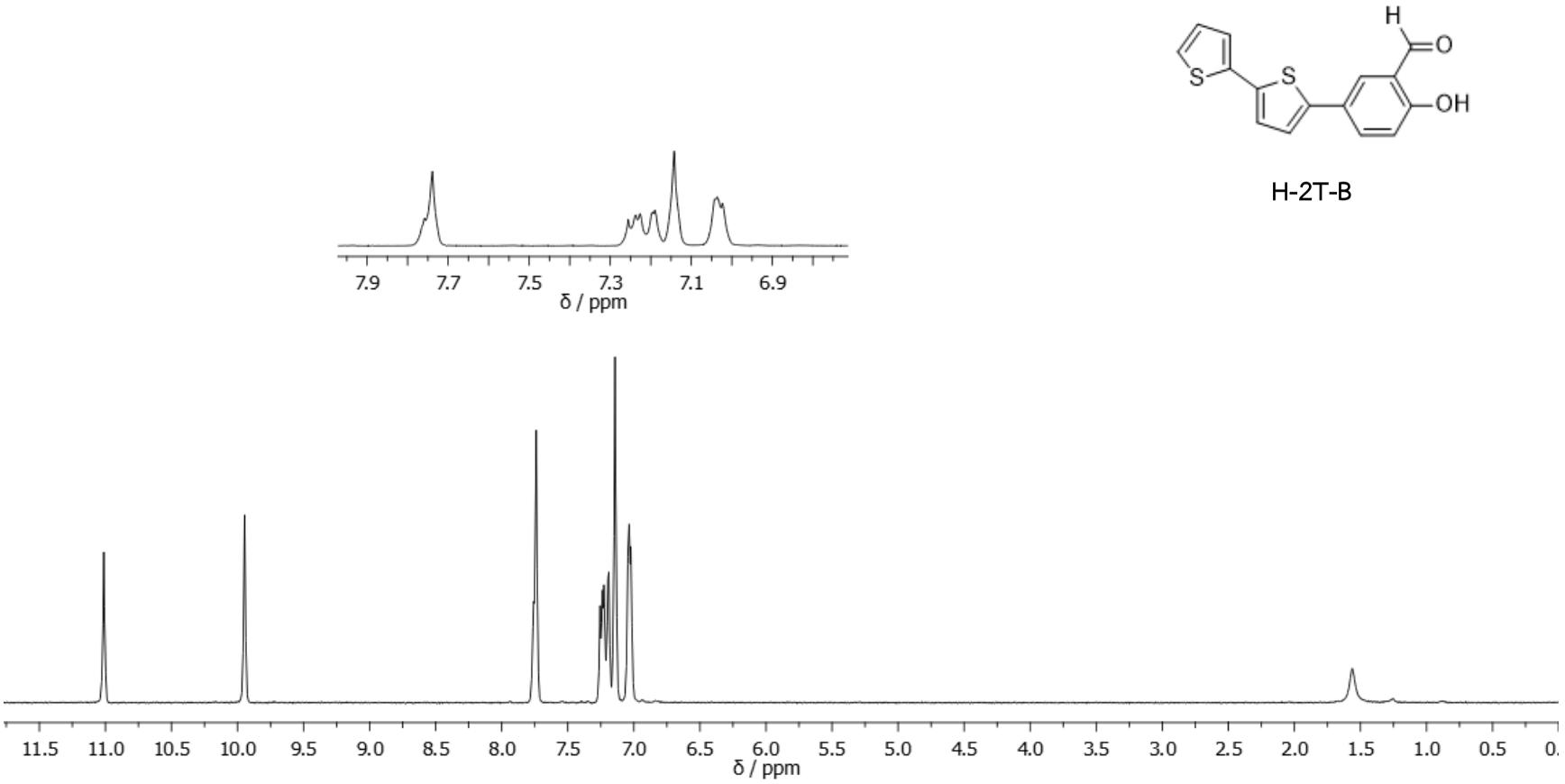

Figure A–3: ^{1}H-NMR spectrum of compound **H-2T-B**

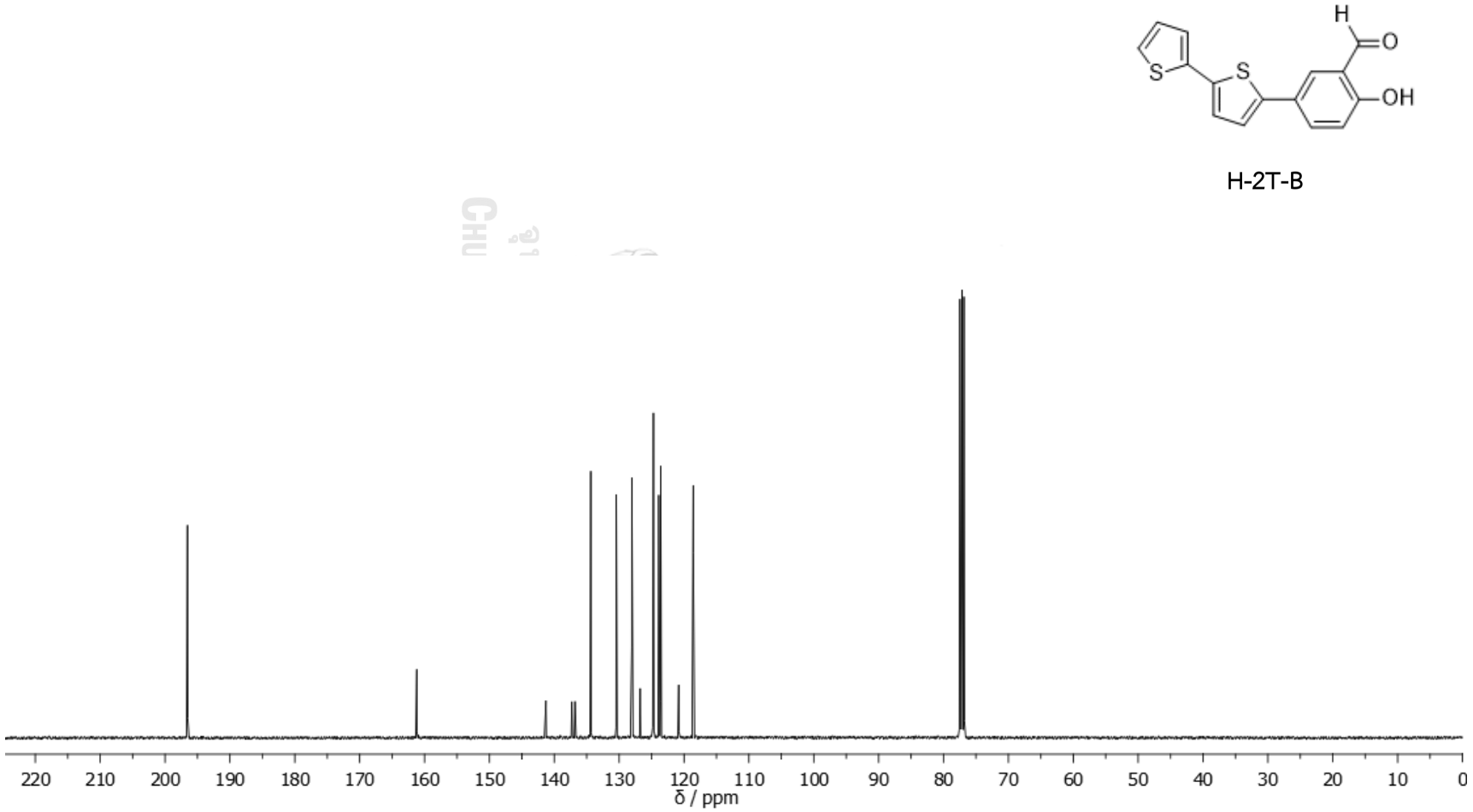

Figure A–4: ^{13}C-NMR spectrum of compound **H-2T-B**

Mass Spectrum List Report

Analysis Info

Analysis Name	OSCK20170905001_1.d	Acquisition Date	9/5/2017 1:45:42 PM
Method	Tune_low_POS_Natee20130403.m	Operator	Administrator
Sample Name	H-2Th-B	Instrument	micrOTOF 72
	H-2Th-B		

Acquisition Parameter

Source Type	ESI	Ion Polarity	Positive	Set Corrector Fill	50 V
Scan Range	n/a	Capillary Exit	180.0 V	Set Pulsar Pull	337 V
Scan Begin	50 m/z	Hexapole RF	150.0 V	Set Pulsar Push	337 V
Scan End	3000 m/z	Skimmer 1	45.0 V	Set Reflector	1300 V
		Hexapole 1	24.3 V	Set Flight Tube	9000 V
				Set Detector TOF	2295 V

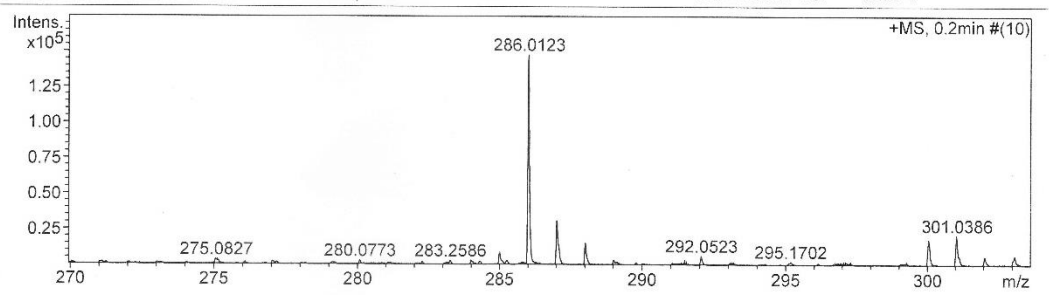

#	m/z	I	I %	S/N	FWHM	Res.
1	271.0954	1785	1.2	4.3	0.1355	2000
2	272.0288	1225	0.8	3.6	0.1000	2720
3	273.0334	1260	0.9	3.7	0.1134	2408
4	275.0827	3021	2.1	8.8	0.1008	2729
5	276.0695	1539	1.0	4.5	0.0597	4622
6	278.1881	364	0.2	1.1	0.0689	4040
7	280.0773	2502	1.7	7.3	0.0567	4938
8	282.0620	542	0.4	1.6	0.0773	3649
9	282.2740	1798	1.2	5.2	0.0587	4808
10	283.2586	2593	1.8	7.5	0.0676	4192
11	284.3046	2094	1.4	6.0	0.0848	3352
12	286.0123	147358	100.0	424.8	0.0608	4707
13	287.0192	30776	20.9	88.6	0.0732	3919
14	288.0116	15492	10.5	44.6	0.0646	4456
15	289.0167	3160	2.1	9.1	0.0655	4414
16	291.0543	1298	0.9	3.7	0.0577	5047
17	292.0523	6082	4.1	17.4	0.0625	4674
18	293.1511	1133	0.8	3.2	0.1129	2597
19	295.1702	1812	1.2	5.2	0.1112	2655
20	296.1299	1185	0.8	3.4	0.0655	4518
21	297.1196	1499	1.0	4.3	0.1274	2332
22	298.1189	334	0.2	0.9	0.0481	6197
23	299.2557	2038	1.4	5.8	0.0630	4750
24	300.0421	17831	12.1	50.6	0.0870	3450
25	301.0386	21064	14.3	59.7	0.0717	4201

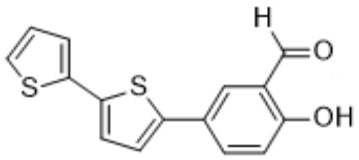

H-2T-B

Chemical Formula: $C_{15}H_{10}O_2S_2$

Exact Mass: 286.0122

$[(M+H)^+]$: 287.0195

Figure A–5: HR-ESI spectrum of compound **H-2T-B**

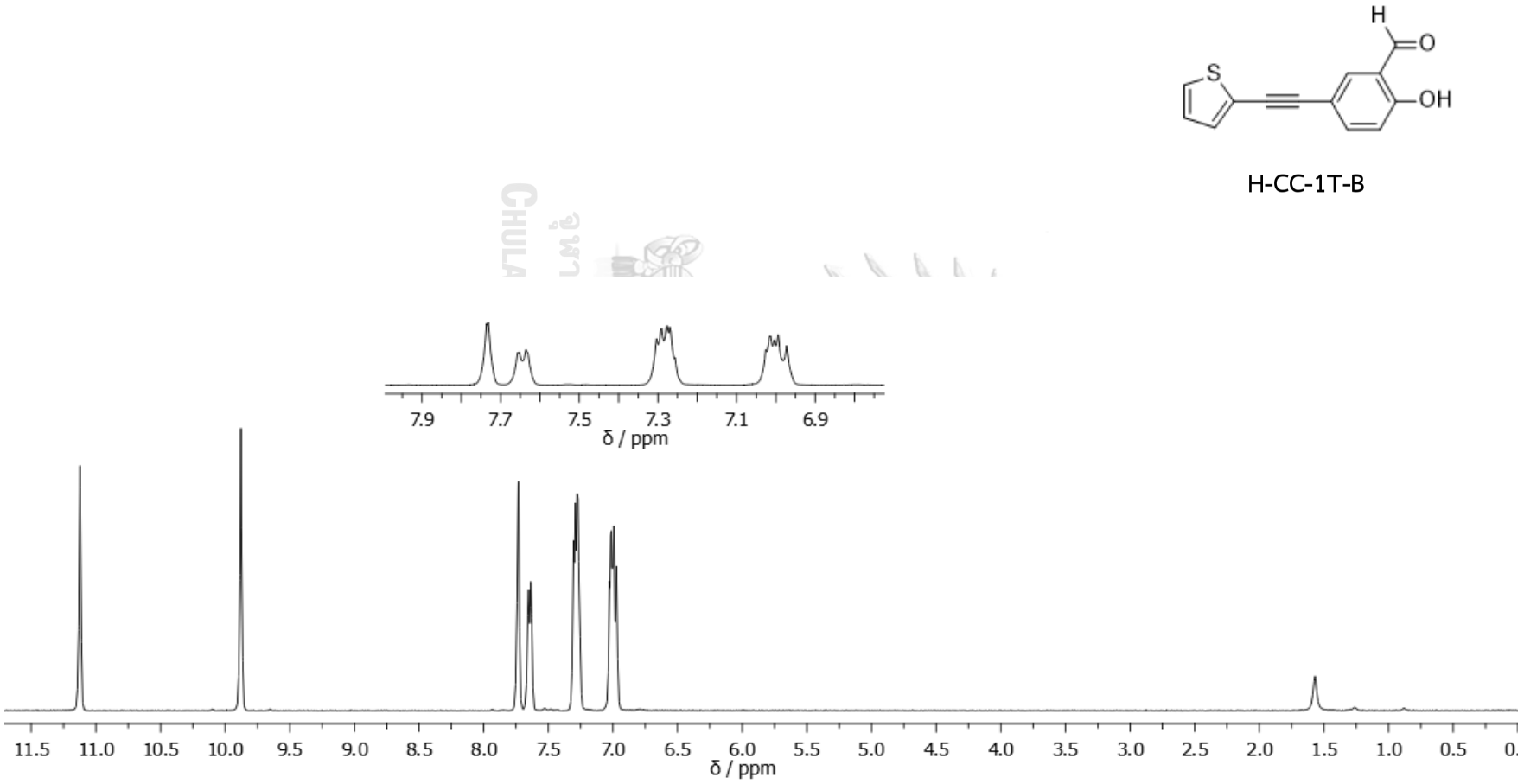

Figure A–6: ^{1}H-NMR spectrum of compound **H-CC-1T-B**

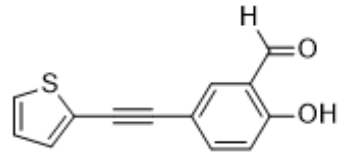

H-CC-1T-B

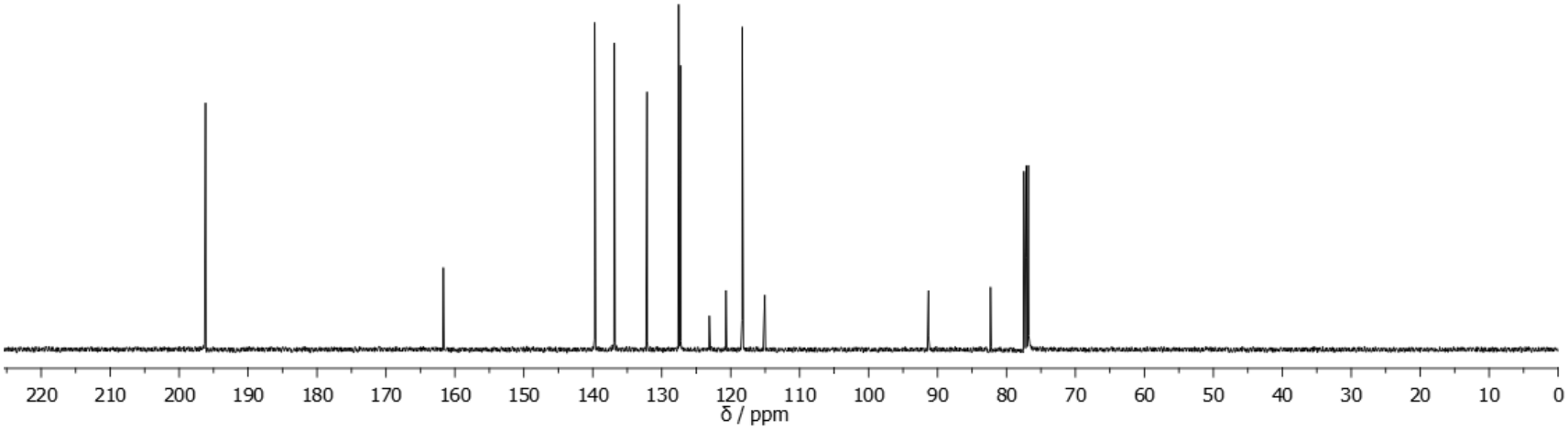

Figure A–7: ^{13}C-NMR spectrum of compound **H-CC-1T-B**

Mass Spectrum List Report

Analysis Info

Analysis Name	OSCK20170905002.d	Acquisition Date	9/5/2017 1:48:32 PM
Method	Tune_low_POS_Natee20130403.m	Operator	Administrator
Sample Name	H-CC-1Th-B H-CC-1Th-B	Instrument	micrOTOF 72

Acquisition Parameter

Source Type	ESI	Ion Polarity	Positive	Set Corrector Fill	50 V
Scan Range	n/a	Capillary Exit	180.0 V	Set Pulsar Pull	337 V
Scan Begin	50 m/z	Hexapole RF	150.0 V	Set Pulsar Push	337 V
Scan End	3000 m/z	Skimmer 1	45.0 V	Set Reflector	1300 V
		Hexapole 1	24.3 V	Set Flight Tube	9000 V
				Set Detector TOF	2295 V

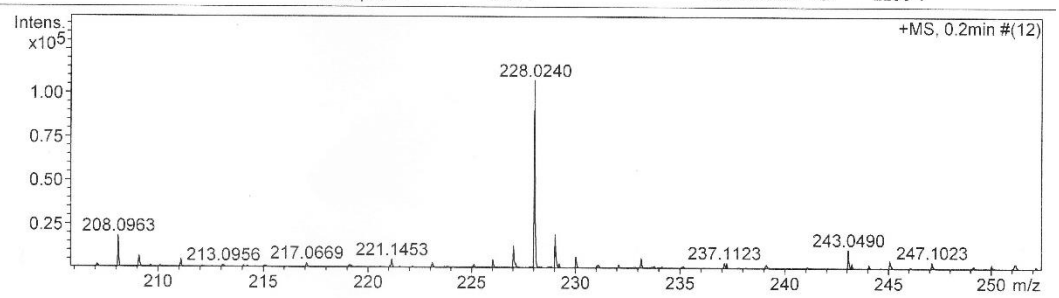

#	m/z	I	I %	S/N	FWHM	Res.
1	208.0963	18023	16.8	52.1	0.0453	4592
2	213.0956	1525	1.4	4.4	0.0754	2827
3	214.0602	1290	1.2	3.7	0.0353	6066
4	215.0490	1327	1.2	3.8	0.1353	1589
5	217.0669	2521	2.3	7.2	0.0908	2390
6	218.0775	376	0.4	1.1	0.1021	2136
7	220.5986	798	0.7	2.3	0.0086	25790
8	221.1453	4872	4.5	13.9	0.0676	3269
9	222.1455	812	0.8	2.3	0.1037	2141
10	224.0990	835	0.8	2.4	0.0992	2259
11	226.0134	4932	4.6	14.0	0.0603	3747
12	227.0180	12757	11.9	36.0	0.0549	4133
13	228.0240	107297	100.0	302.7	0.0485	4700
14	229.0284	19392	18.1	54.6	0.0513	4463
15	230.0250	6734	6.3	19.0	0.0553	4157
16	231.0903	2073	1.9	5.8	0.1197	1931
17	232.0845	2186	2.0	6.1	0.0565	4105
18	233.1497	5862	5.5	16.4	0.0562	4148
19	233.7698	663	0.6	1.9	0.0200	11689
20	235.1339	1469	1.4	4.1	0.1205	1952
21	237.1123	3348	3.1	9.3	0.0774	3063
22	238.1269	861	0.8	2.4	0.0686	3473
23	240.0971	637	0.6	1.8	0.0725	3313
24	243.0490	10947	10.2	30.3	0.0548	4437
25	244.0506	2514	2.3	7.0	0.0570	4279
26	246.0688	958	0.9	2.6	0.0998	2465
27	247.1023	3870	3.6	10.7	0.0703	3514
28	249.1234	1580	1.5	4.3	0.1174	2122
29	250.0092	2418	2.3	6.6	0.0603	4143
30	251.1318	2923	2.7	8.0	0.1398	1797

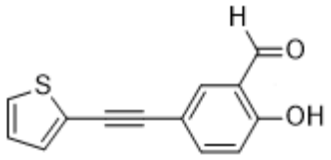

H-CC-1T-B

Chemical Formula: $C_{13}H_8O_2S$

Exact Mass: 228.0245

$[(M+H)^+]$: 229.0318

Figure A–8: HR-ESI spectrum of compound **H-CC-1T-B**

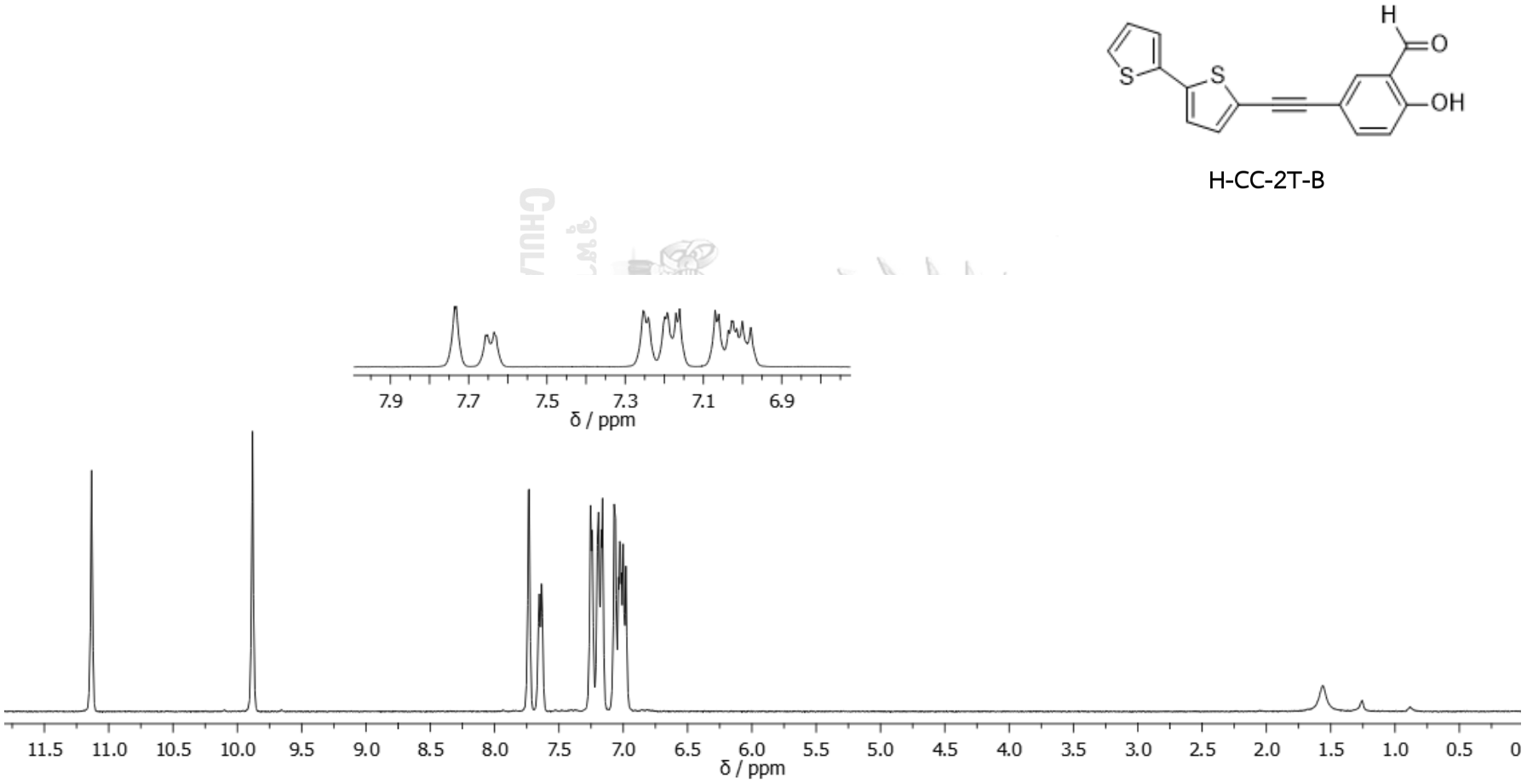

Figure A–9: ^{1}H-NMR spectrum of compound H-CC-2T-B

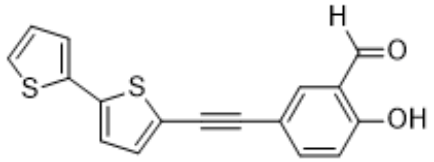

H-CC-2T-B

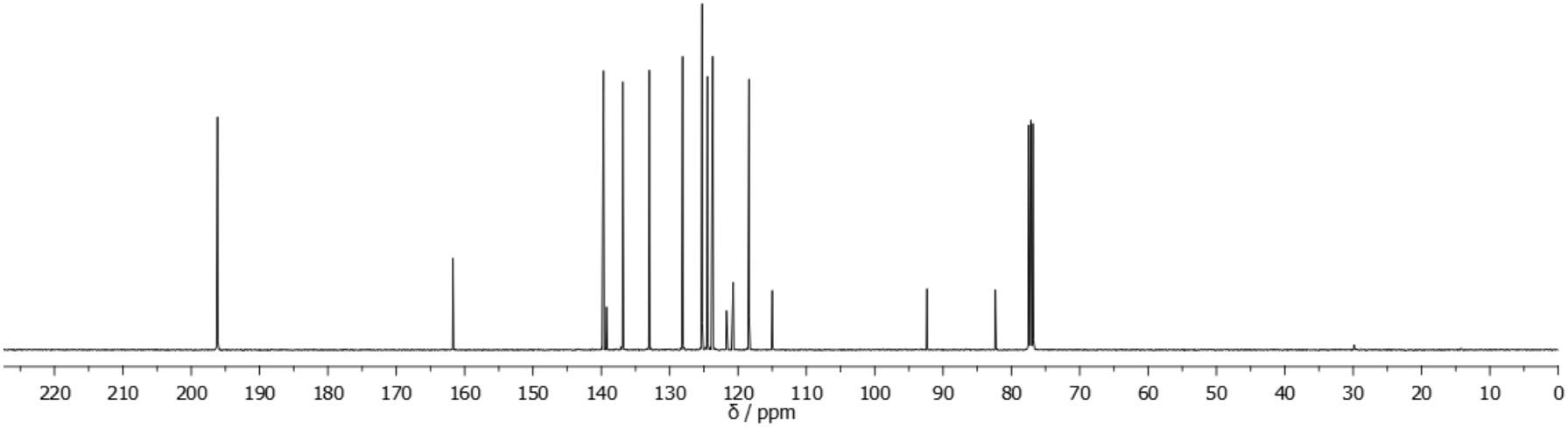

Figure A–10: ^{13}C-NMR spectrum of compound **H-CC-2T-B**

Mass Spectrum List Report

Analysis Info

Analysis Name	OSCK20170905003.d	Acquisition Date	9/5/2017 1:51:27 PM
Method	Tune_low_POS_Natee20130403.m	Operator	Administrator
Sample Name	H-CC-2Th-B	Instrument	micrOTOF 72
	H-CC-2Th-B		

Acquisition Parameter

Source Type	ESI	Ion Polarity	Positive	Set Corrector Fill	50 V
Scan Range	n/a	Capillary Exit	180.0 V	Set Pulsar Pull	337 V
Scan Begin	50 m/z	Hexapole RF	150.0 V	Set Pulsar Push	337 V
Scan End	3000 m/z	Skimmer 1	45.0 V	Set Reflector	1300 V
		Hexapole 1	24.3 V	Set Flight Tube	9000 V
				Set Detector TOF	2295 V

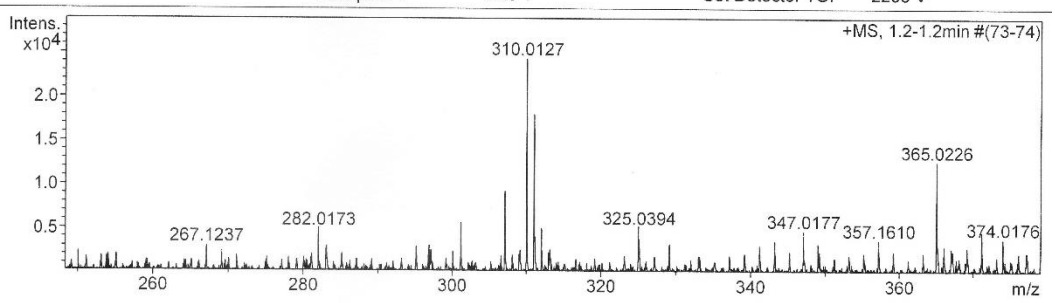

#	m/z	I	I %	S/N	FWHM	Res.
1	249.1182	1161	4.8	3.3	0.1072	2323
2	259.1013	1222	5.1	4.0	0.0261	9927
3	267.1237	2698	11.2	8.7	0.0817	3271
4	275.0959	1238	5.1	4.0	0.1024	2686
5	278.0401	1499	6.2	4.8	0.0550	5059
6	282.0173	4849	20.1	15.6	0.0557	5061
7	295.1431	2747	11.4	8.8	0.1123	2627
8	296.8407	2847	11.8	9.1	0.0148	20026
9	301.1375	5434	22.6	17.3	0.0671	4488
10	307.0833	8805	36.6	28.0	0.0737	4166
11	308.0859	1799	7.5	5.7	0.0688	4480
12	309.1513	2124	8.8	6.7	0.1576	1962
13	310.0127	24073	100.0	76.4	0.0655	4736
14	311.0185	17778	73.8	56.4	0.0644	4827
15	312.0177	4781	19.9	15.2	0.0693	4504
16	313.1698	2395	10.0	7.6	0.1100	2848
17	316.6566	1322	5.5	4.2	0.0180	17613
18	323.1629	1706	7.1	5.4	0.1205	2681
19	325.0394	5058	21.0	15.9	0.0733	4435
20	329.1572	3054	12.7	9.6	0.0825	3988
21	337.1710	1516	6.3	4.8	0.1322	2550
22	341.1625	2919	12.1	9.1	0.0871	3916
23	347.0177	4480	18.6	14.1	0.0644	5387
24	351.1861	1414	5.9	4.5	0.1349	2603
25	355.1733	1984	8.2	6.3	0.1245	2852
26	357.1610	3450	14.3	10.9	0.1086	3287
27	365.0226	12397	51.5	39.5	0.0924	3952
28	369.1772	2626	10.9	8.4	0.1104	3344
29	374.0176	3633	15.1	11.7	0.0597	6269
30	387.1813	1495	6.2	4.8	0.1447	2676

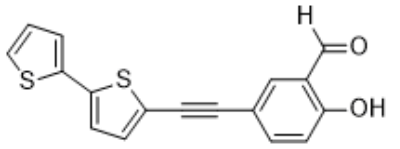

H-CC-2T-B

Chemical Formula: $C_{17}H_{10}O_2S_2$

Exact Mass: 310.0122

$[(M+H)^+]$: 311.0195

Figure A–11: HR-ESI spectrum of compound **H-CC-2T-B**

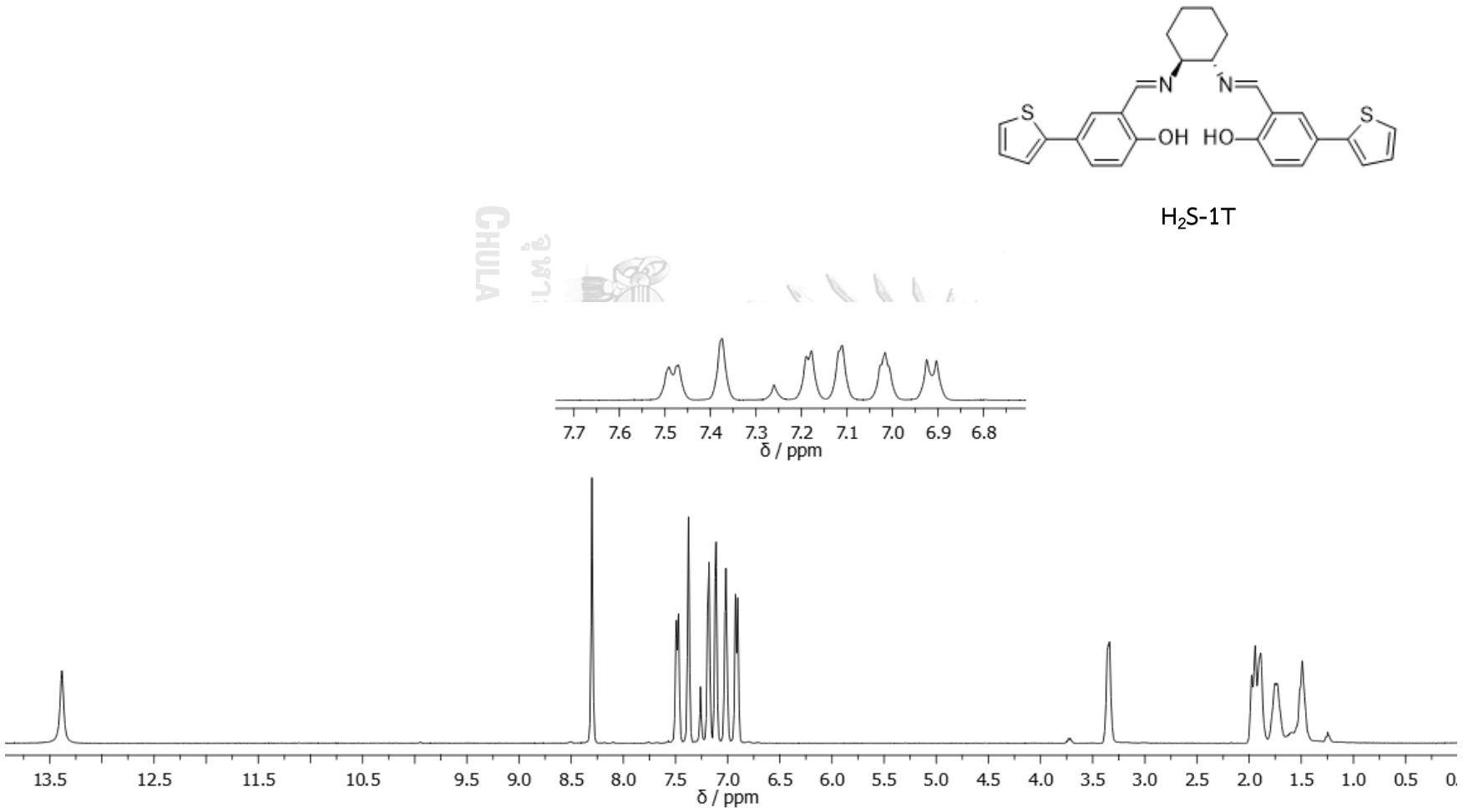

Figure A–12: ^{1}H-NMR spectrum of compound **H_2S-1T**

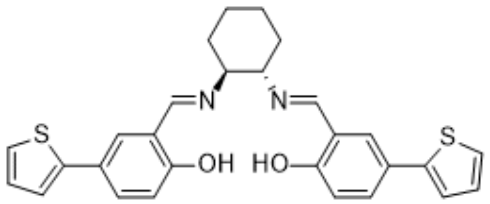

H_2S-1T

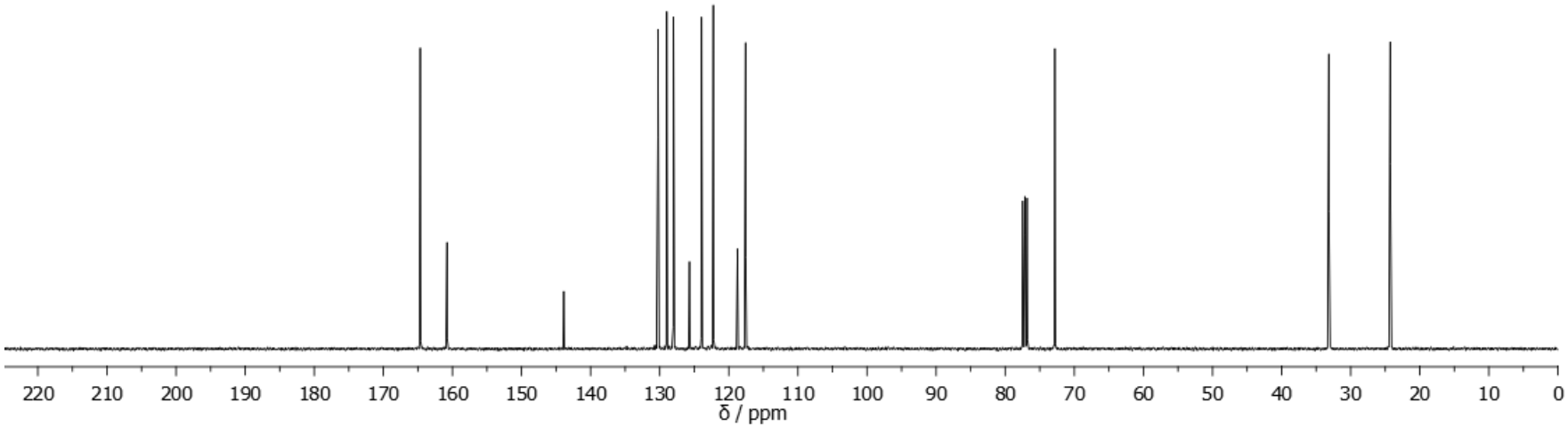

Figure A–13: ^{13}C-NMR spectrum of compound **H_2S-1T**

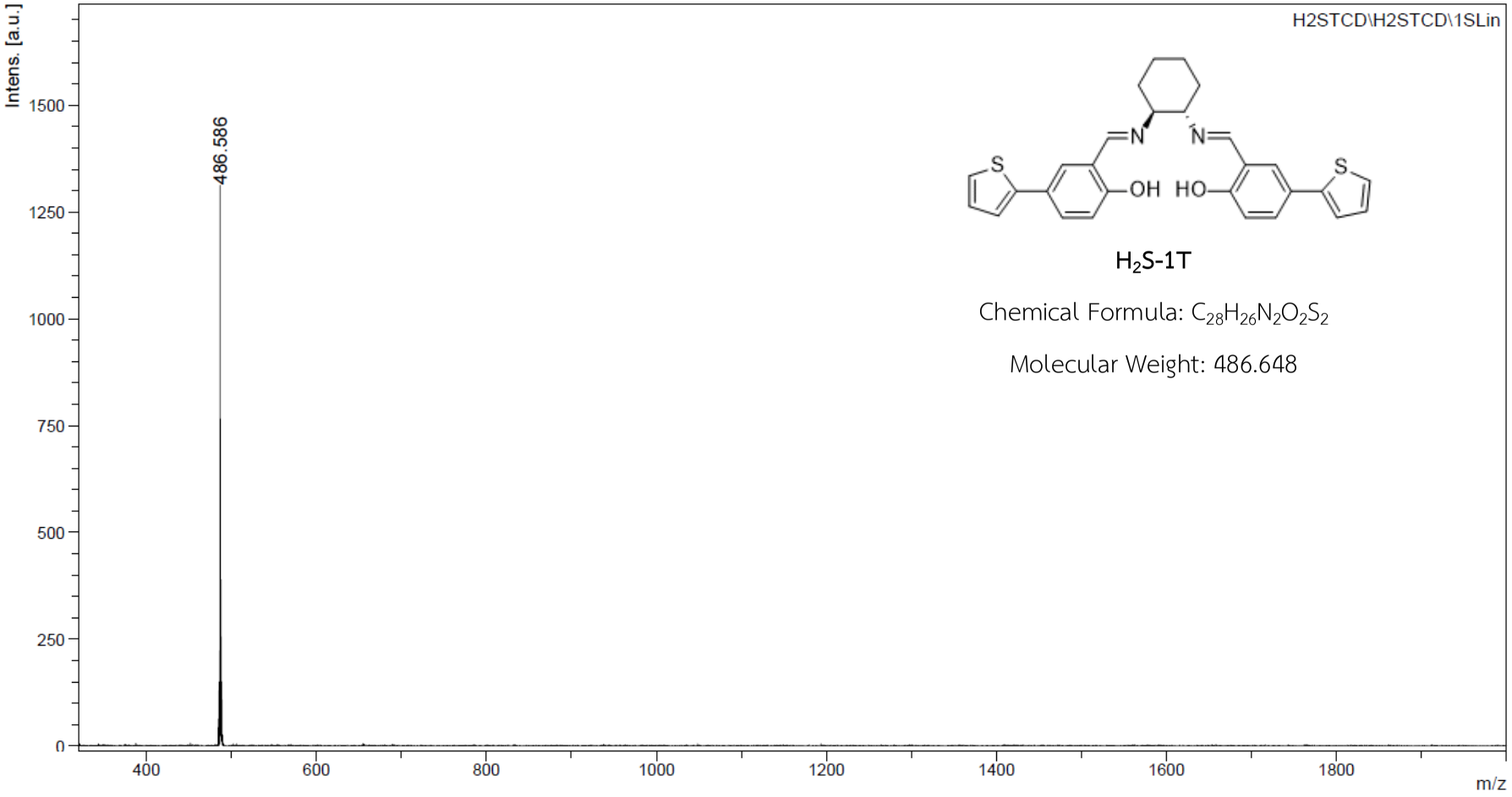

Figure A–14: MALDI-TOF spectrum of compound **H_2S-1T**

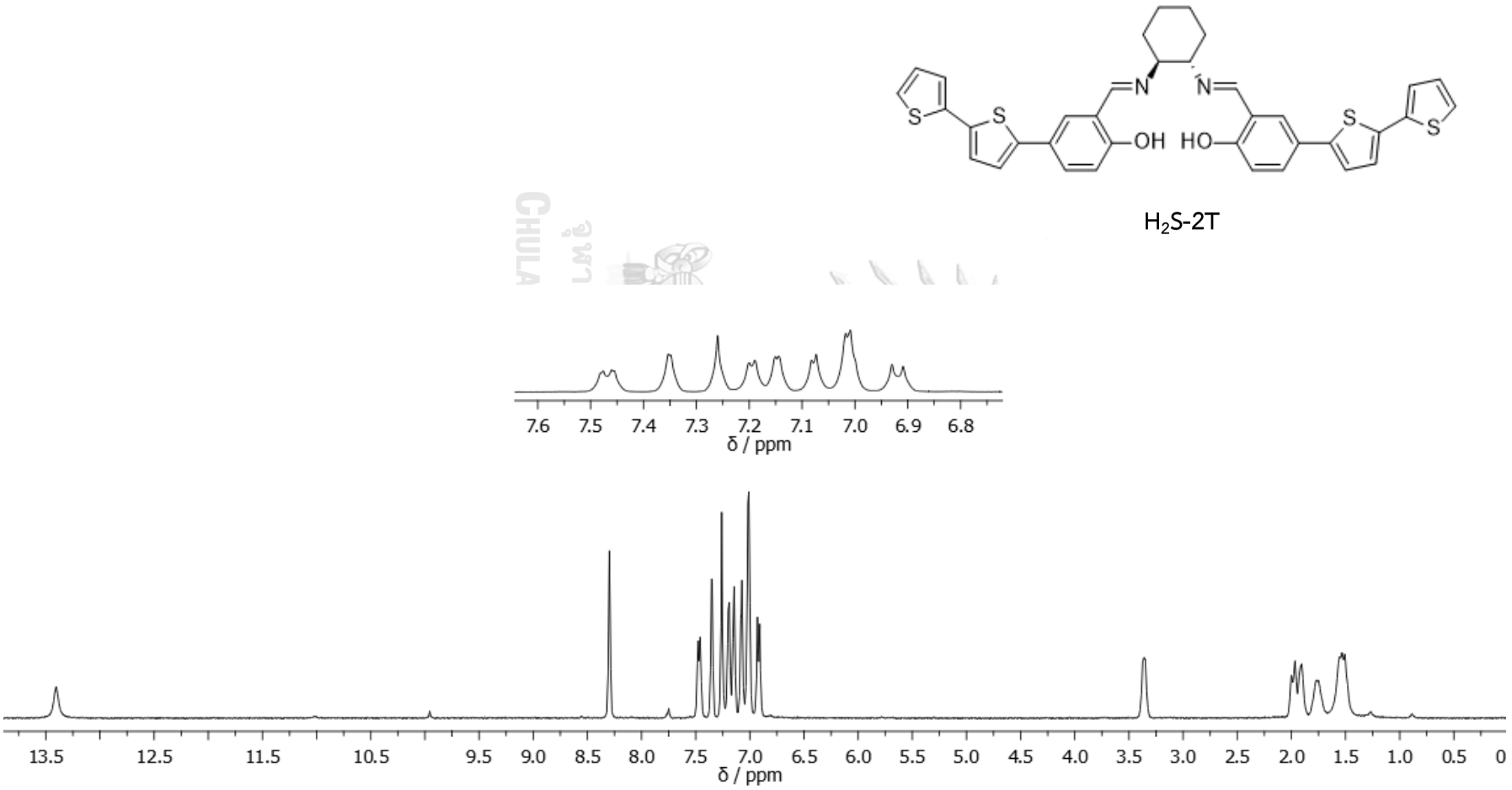

Figure A–15: ^{1}H-NMR spectrum of compound **H_2S-2T**

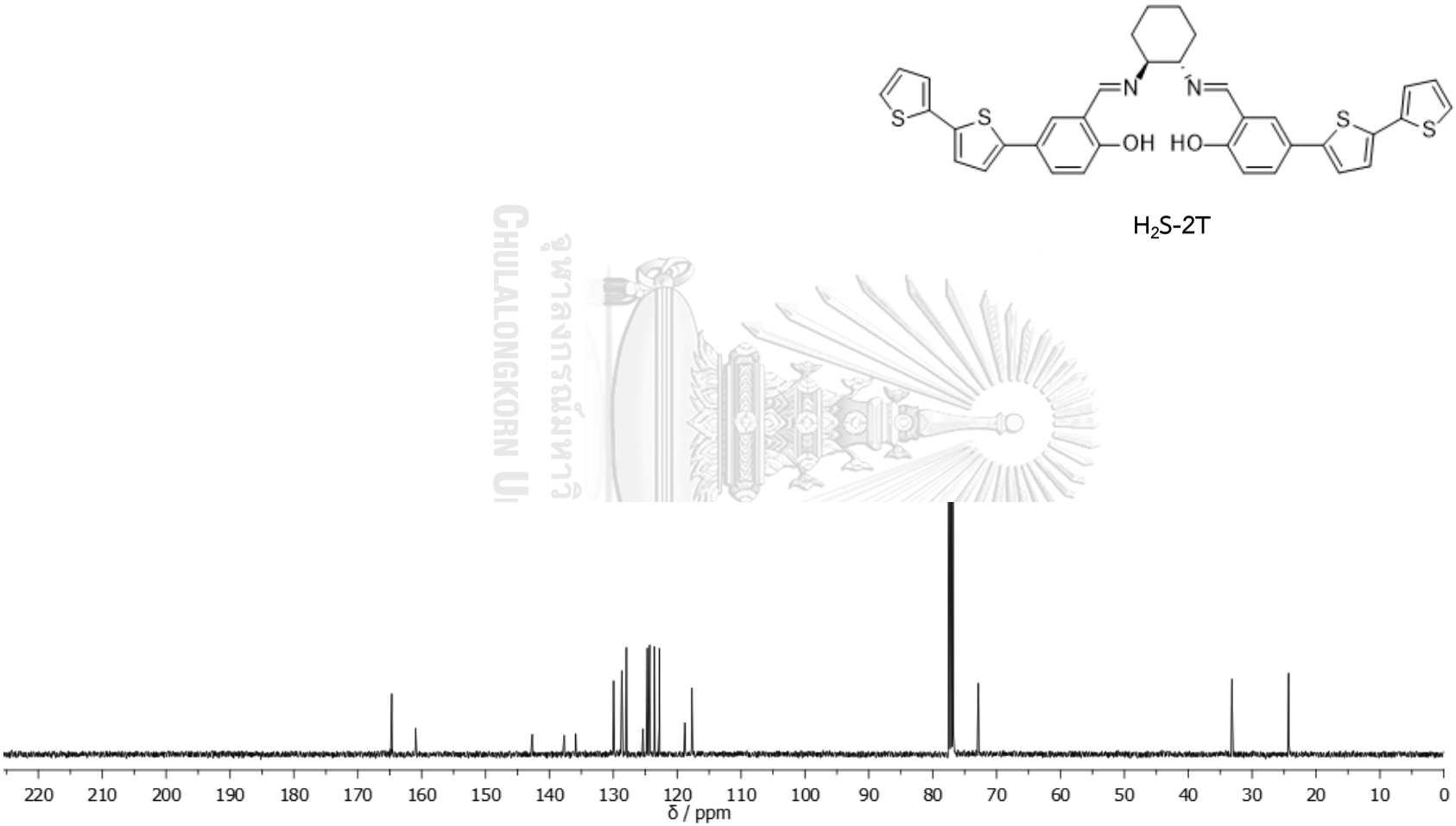

H_2S-2T

Figure A–16: ^{13}C-NMR spectrum of compound **H_2S-2T**

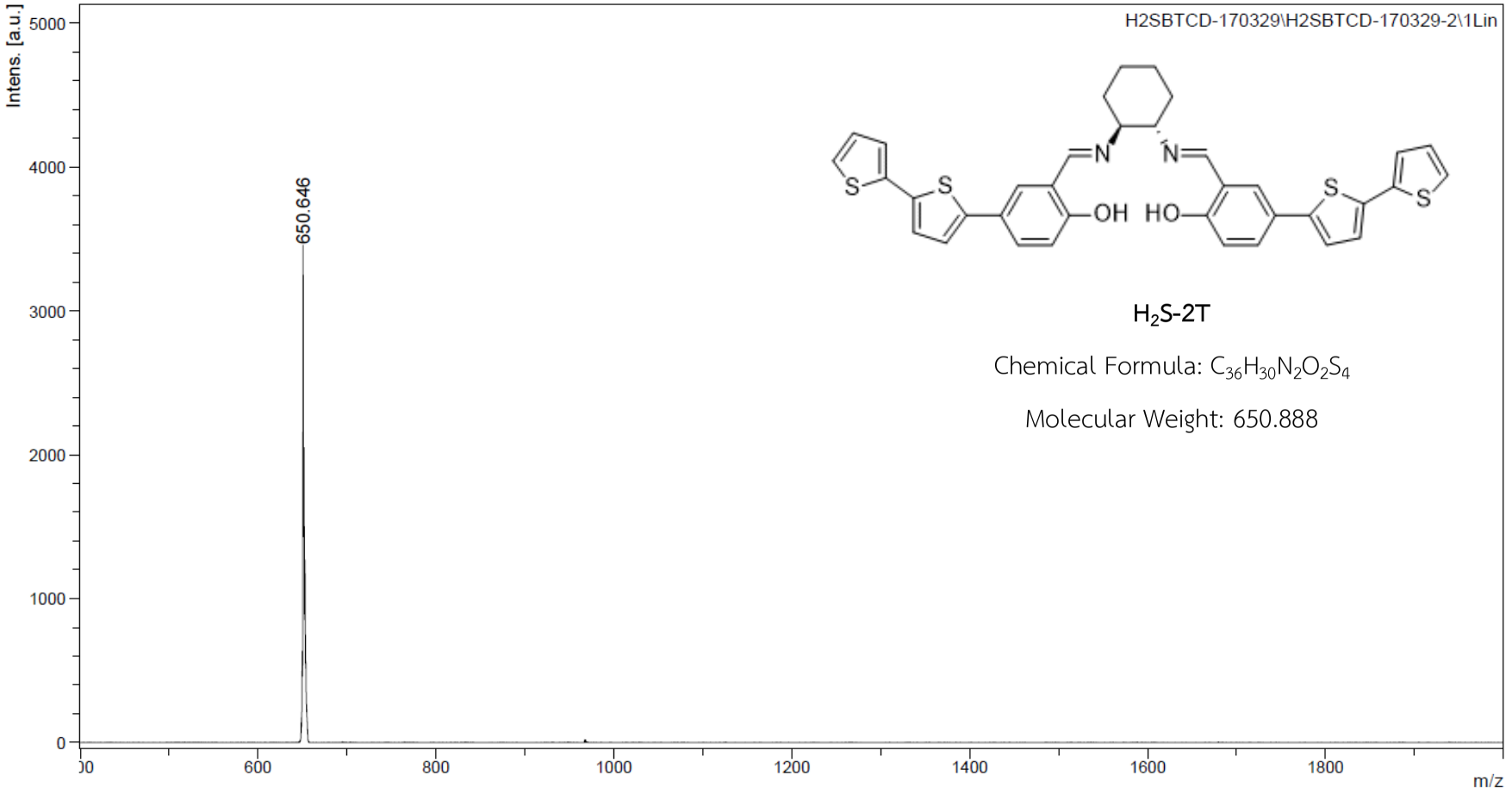

Figure A–17: MALDI-TOF spectrum of compound **H_2S-2T**

Mass Spectrum List Report

Analysis Info

Analysis Name	OSCK00531001.d	Acquisition Date	6/2/2017 9:35:39 AM
Method	Tune_wide_POS_Natee20130403.m	Operator	Administrator
Sample Name	H2S-2th	Instrument	micrOTOF 72
	H2S-2th		

Acquisition Parameter

Source Type	ESI	Ion Polarity	Positive	Set Corrector Fill	50 V
Scan Range	n/a	Capillary Exit	200.0 V	Set Pulsar Pull	337 V
Scan Begin	50 m/z	Hexapole RF	600.0 V	Set Pulsar Push	337 V
Scan End	3000 m/z	Skimmer 1	70.0 V	Set Reflector	1300 V
		Hexapole 1	25.0 V	Set Flight Tube	9000 V
				Set Detector TOF	2295 V

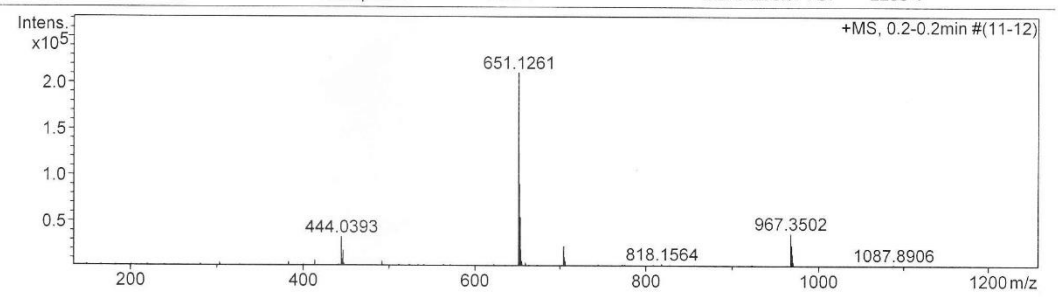

#	m/z	I	I %	S/N	FWHM	Res.
1	303.1948	4786	2.3	12.4	0.0127	23953
2	303.3006	4128	2.0	10.7	0.0246	12305
3	383.1237	5612	2.7	14.9	0.0737	5200
4	413.2688	7759	3.7	20.3	0.0906	4560
5	444.0393	33203	15.7	87.6	0.0899	4938
6	445.0451	8767	4.2	22.5	0.0867	5130
7	446.0365	18610	8.8	48.7	0.0891	5006
8	447.0396	4533	2.1	11.2	0.1108	4035
9	491.2802	6437	3.1	15.7	0.1129	4350
10	651.1261	210887	100.0	541.7	0.1243	5236
11	652.1276	90768	43.0	232.4	0.1213	5376
12	653.1249	54580	25.9	139.2	0.1253	5214
13	654.1244	19316	9.2	48.4	0.1226	5336
14	655.1237	6778	3.2	16.0	0.1148	5709
15	659.4279	5334	2.5	12.3	0.0318	20742
16	704.0356	23394	11.1	59.8	0.1234	5704
17	705.0402	11253	5.3	28.0	0.1270	5551
18	706.0363	7168	3.4	17.3	0.1244	5674
19	818.1564	4332	2.1	10.5	0.1676	4880
20	967.3502	37595	17.8	109.9	0.1792	5397
21	968.3541	24493	11.6	71.2	0.1783	5431
22	969.3503	14661	7.0	42.2	0.1754	5526
23	970.3480	6408	3.0	17.8	0.1807	5370
24	1354.1517	5864	2.8	16.3	0.2700	5016
25	1355.1528	5454	2.6	15.1	0.2328	5820
26	1356.1565	4736	2.2	13.0	0.2278	5952
27	1879.9709	4178	2.0	12.4	0.0340	55222
28	1880.2279	4246	2.0	12.7	0.0350	53744
29	2356.8700	5958	2.8	17.8	0.0347	67882
30	2357.0893	4705	2.2	13.9	0.0635	37111

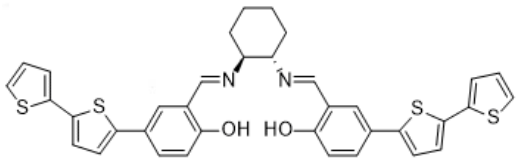

H_2S-2T

Chemical Formula: $C_{36}H_{30}N_2O_2S_4$

Exact Mass: 650.1190

$[(M+H)^+]$: 651.1263

Figure A–18: HR-ESI spectrum of compound **H_2S-2T**

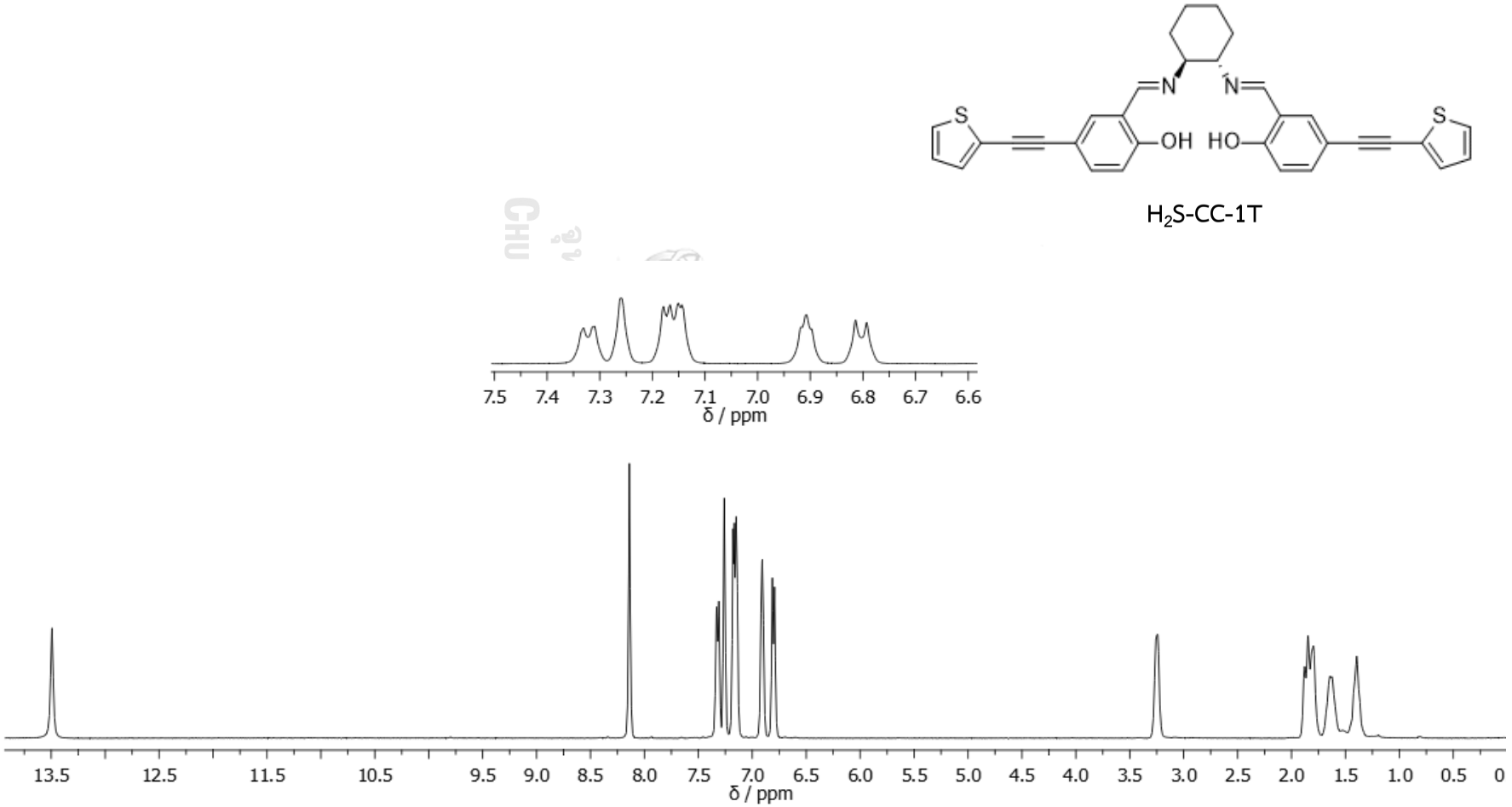

Figure A–19: ^{1}H-NMR spectrum of compound **H_2S-CC-1T**

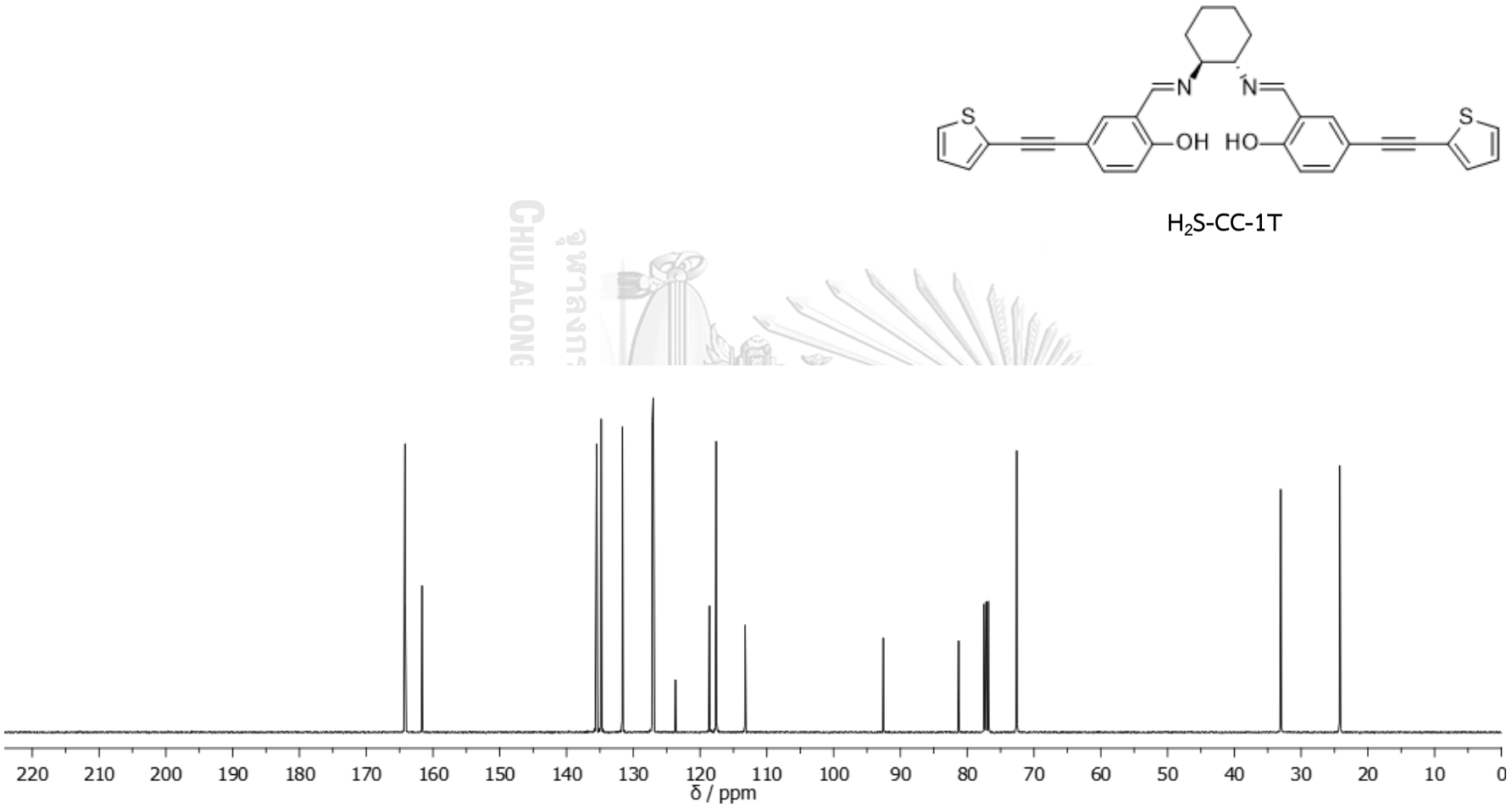

H_2S-CC-1T

Figure A–20: ^{13}C-NMR spectrum of compound **H_2S-CC-1T**

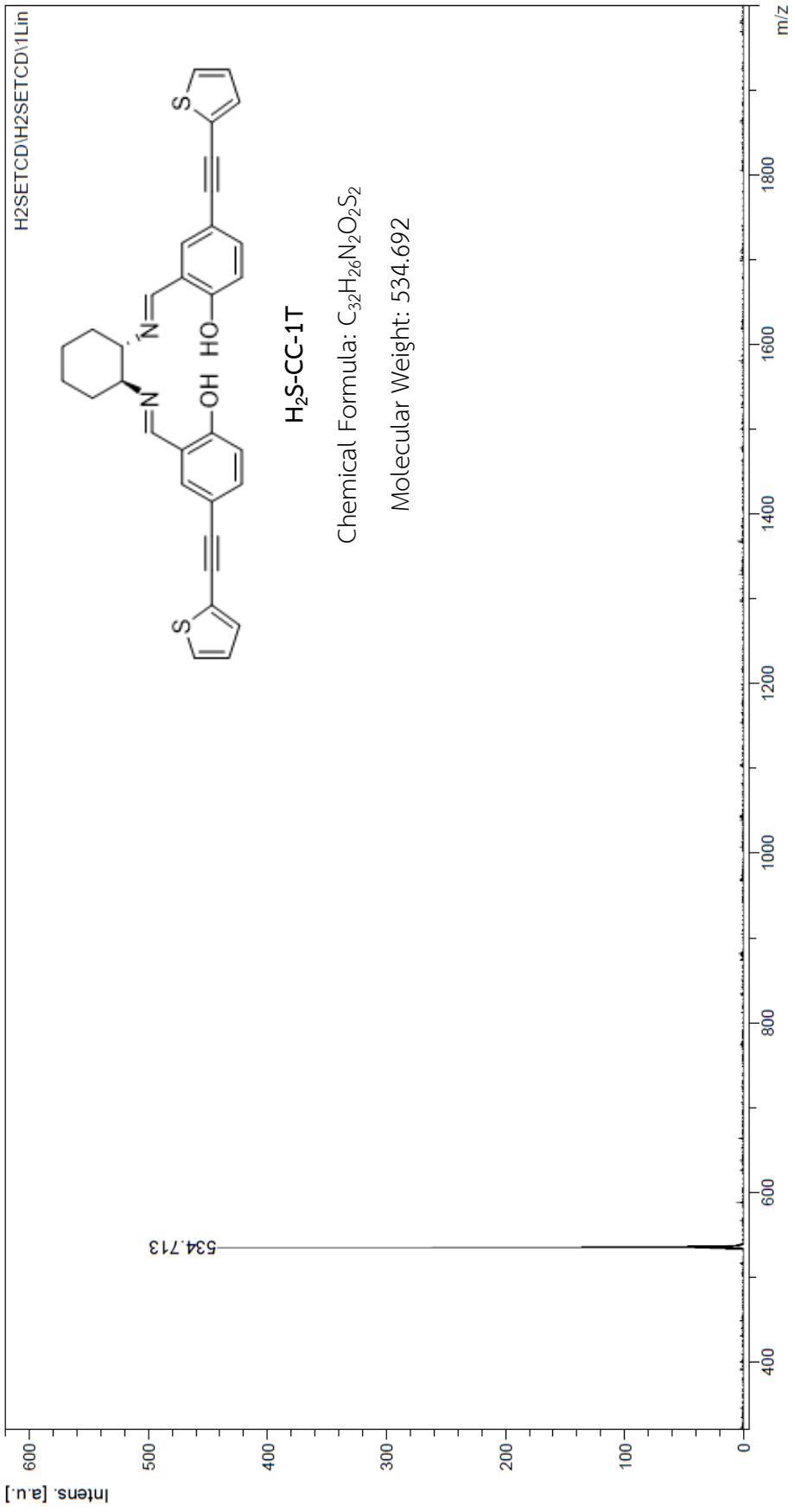

Figure A–21: MALDI-TOF spectrum of compound **H_2S-CC-1T**

Mass Spectrum List Report

Analysis Info

Analysis Name	OSCK00531002_1.d	Acquisition Date	6/2/2017 9:41:36 AM
Method	Tune_wide_POS_Tawatchai_05Feb2016.m	Operator	Administrator
Sample Name	H2S-CC-1TH	Instrument	micrOTOF 72
	H2S-CC-1TH		

Acquisition Parameter

Source Type	ESI	Ion Polarity	Positive	Set Corrector Fill	50 V
Scan Range	n/a	Capillary Exit	180.0 V	Set Pulsar Pull	337 V
Scan Begin	50 m/z	Hexapole RF	400.0 V	Set Pulsar Push	337 V
Scan End	3000 m/z	Skimmer 1	70.0 V	Set Reflector	1300 V
		Hexapole 1	25.0 V	Set Flight Tube	9000 V
				Set Detector TOF	2295 V

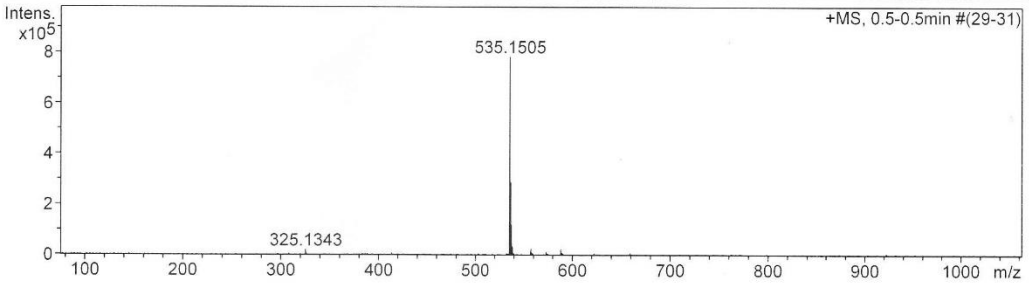

#	m/z	I	I %	S/N	FWHM	Res.
1	325.1343	19470	2.5	48.9	0.0727	4473
2	386.0515	5959	0.8	14.4	0.0918	4208
3	413.2665	7422	0.9	18.0	0.1018	4060
4	534.7955	5657	0.7	13.0	0.4733	1130
5	535.1505	782740	100.0	1973.9	0.1150	4655
6	535.7162	7571	1.0	17.8	0.3693	1451
7	536.1530	287207	36.7	723.4	0.1137	4715
8	537.1495	119103	15.2	299.2	0.1113	4827
9	538.1502	30926	4.0	76.7	0.1172	4591
10	539.1544	7519	1.0	17.7	0.1353	3986
11	557.1307	24758	3.2	61.4	0.1134	4912
12	558.1343	9545	1.2	22.9	0.1169	4774
13	559.1274	5951	0.8	13.8	0.1368	4088
14	573.1041	10782	1.4	26.1	0.1160	4942
15	588.0609	21776	2.8	54.3	0.1162	5063
16	589.0636	8567	1.1	20.6	0.1226	4806
17	659.2495	6557	0.8	15.8	0.1199	5501
18	922.0089	6543	0.8	16.2	0.1740	5300
19	1069.2918	44701	5.7	114.1	0.2018	5298
20	1070.2937	33605	4.3	85.5	0.2012	5319
21	1071.2904	20814	2.7	52.5	0.2108	5081
22	1072.2973	9311	1.2	22.8	0.2159	4967
23	1091.2697	10300	1.3	25.3	0.2143	5093
24	1092.2717	8257	1.1	20.0	0.1986	5501
25	1093.2687	7391	0.9	17.8	0.1980	5522
26	1122.1994	22389	2.9	56.0	0.2159	5198
27	1123.2067	17267	2.2	42.9	0.2079	5403
28	1124.2029	11071	1.4	27.1	0.2054	5472
29	1604.4308	5621	0.7	14.2	0.2868	5595
30	2339.1677	5958	0.8	15.1	0.0354	66158

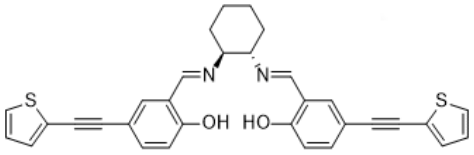

H_2S-CC-1T

Chemical Formula: $C_{32}H_{26}N_2O_2S_2$

Exact Mass: 534.1436

$[(M+H)^+]$: 535.1508

Figure A–22: HR-ESI spectrum of compound **H_2S-CC-1T**

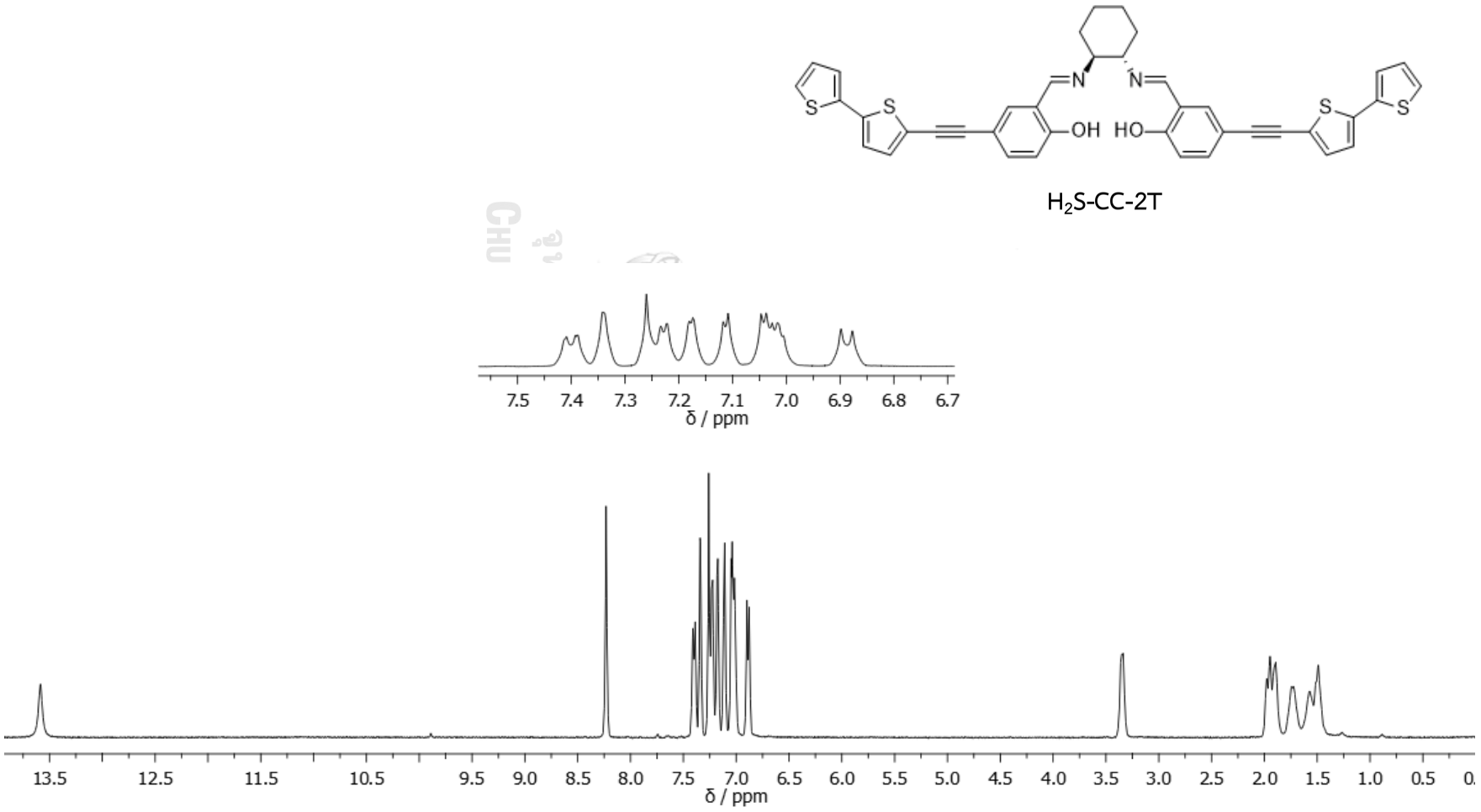

Figure A–23: ^{1}H-NMR spectrum of compound **H_2S-CC-2T**

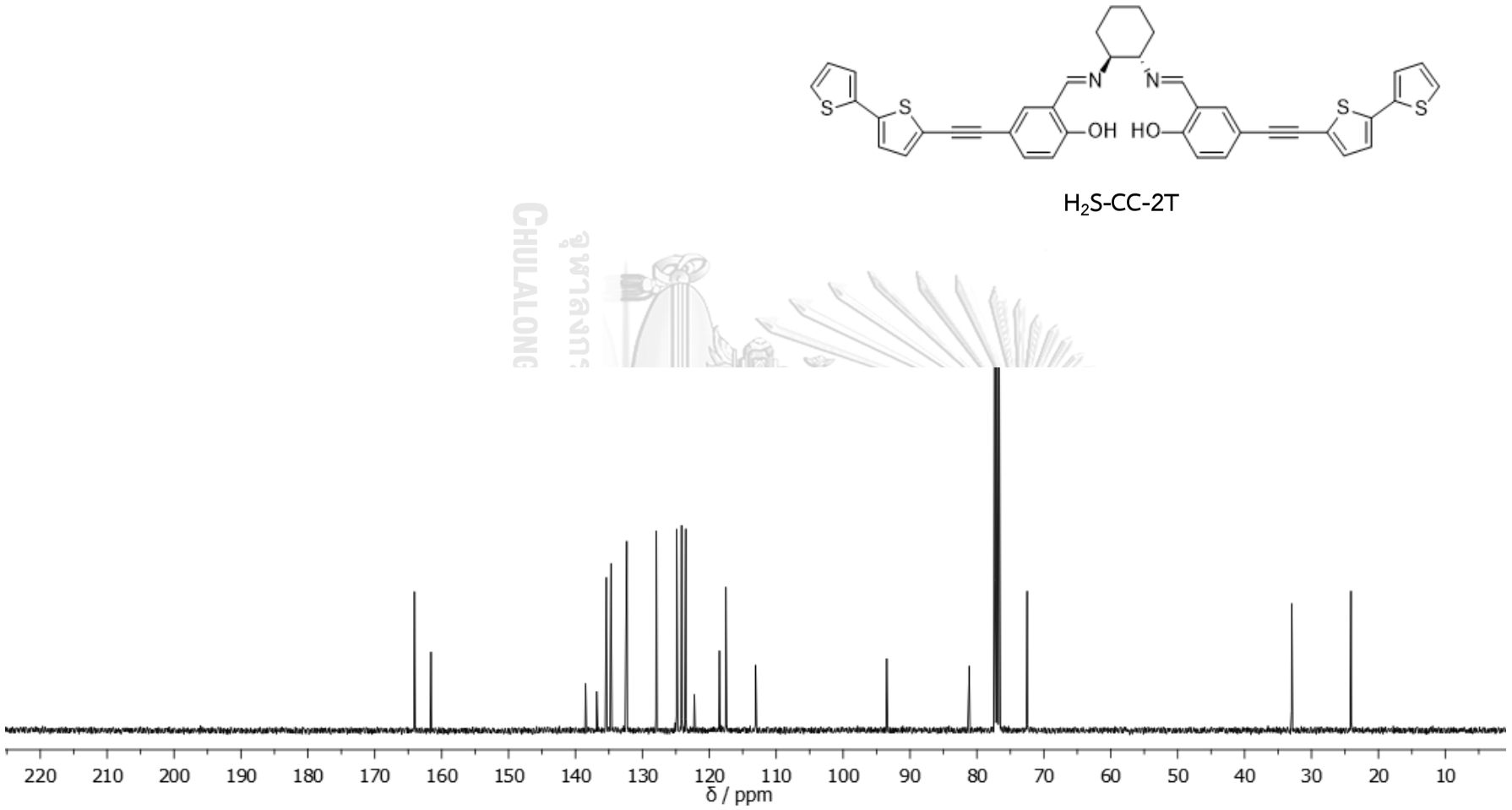

Figure A–24: ^{13}C-NMR spectrum of compound **H_2S-CC-2T**

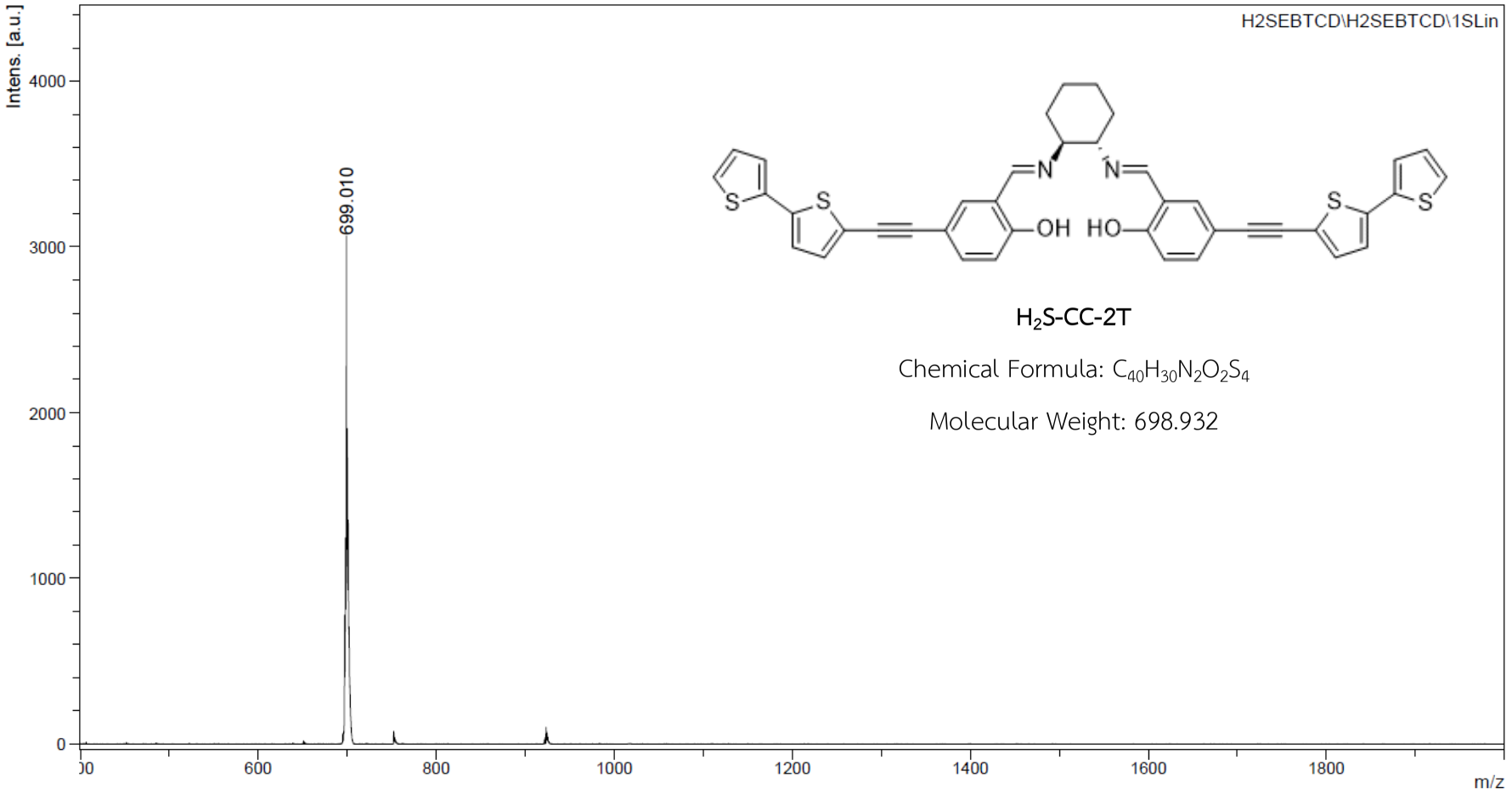

Figure A–25: MALDI-TOF spectrum of compound **H_2S-CC-2T**

Mass Spectrum List Report

Analysis Info

Analysis Name	OSCK00531003.d	Acquisition Date	6/2/2017 9:44:18 AM
Method	Tune_wide_POS_Tawatchai_05Feb2016.m	Operator	Administrator
Sample Name	H2S-CC-2TH	Instrument	micrOTOF 72
	H2S-CC-2TH		

Acquisition Parameter

Source Type	ESI	Ion Polarity	Positive	Set Corrector Fill	50 V
Scan Range	n/a	Capillary Exit	200.0 V	Set Pulsar Pull	337 V
Scan Begin	50 m/z	Hexapole RF	400.0 V	Set Pulsar Push	337 V
Scan End	3000 m/z	Skimmer 1	70.0 V	Set Reflector	1300 V
		Hexapole 1	25.0 V	Set Flight Tube	9000 V
				Set Detector TOF	2295 V

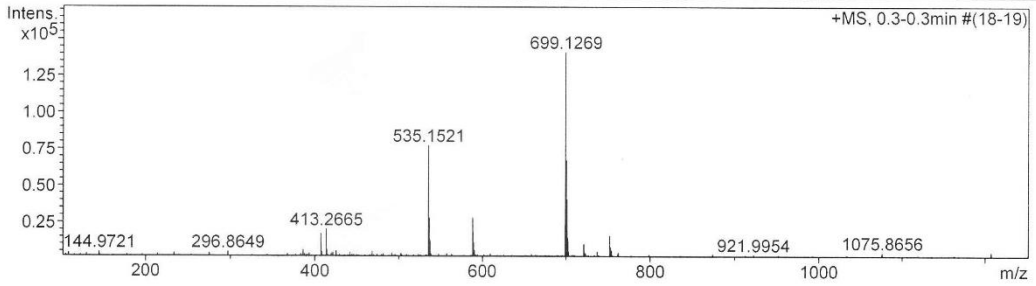

#	m/z	I	I %	S/N	FWHM	Res.
1	144.9721	4651	3.3	8.8	0.0110	13214
2	296.8649	4916	3.5	10.5	0.0138	21441
3	386.0516	5945	4.2	12.9	0.0884	4365
4	407.1270	17316	12.3	38.8	0.0981	4149
5	408.1279	4956	3.5	10.5	0.0898	4543
6	413.2665	20117	14.3	45.1	0.0940	4397
7	414.2701	6338	4.5	13.7	0.0866	4784
8	425.2224	5233	3.7	11.1	0.1211	3510
9	468.0398	5049	3.6	10.4	0.0887	5279
10	535.1521	77467	55.0	170.4	0.1118	4786
11	536.1546	28299	20.1	61.5	0.1151	4660
12	537.1534	12821	9.1	27.2	0.1121	4791
13	588.0628	28436	20.2	62.6	0.1175	5006
14	589.0655	11035	7.8	23.6	0.1307	4508
15	590.0590	5697	4.0	11.6	0.1122	5259
16	699.1269	140909	100.0	326.1	0.1404	4979
17	700.1303	67440	47.9	155.5	0.1425	4913
18	701.1260	40746	28.9	93.4	0.1451	4833
19	702.1263	14419	10.2	32.2	0.1502	4676
20	703.1290	5223	3.7	10.8	0.1520	4625
21	721.1067	10212	7.2	22.6	0.1530	4713
22	722.1113	5091	3.6	10.6	0.1409	5124
23	737.0792	5059	3.6	10.6	0.1457	5058
24	752.0390	16013	11.4	36.6	0.1477	5092
25	753.0455	8038	5.7	17.7	0.1567	4805
26	754.0319	5851	4.2	12.6	0.1367	5517
27	1398.2561	4809	3.4	11.2	0.2464	5675
28	1443.2119	4759	3.4	11.1	0.0708	20390
29	2338.9548	5042	3.6	12.0	0.0378	61825
30	2339.1576	5682	4.0	13.5	0.0342	68317

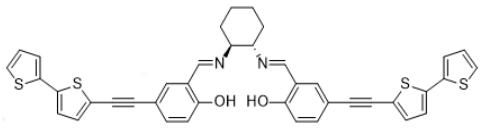

H_2S-CC-2T

Chemical Formula: $C_{40}H_{30}N_2O_2S_4$

Exact Mass: 698.1150

[$(M+H)^+$]: 699.1263

Figure A–26: HR-ESI spectrum of compound **H_2S-CC-2T**

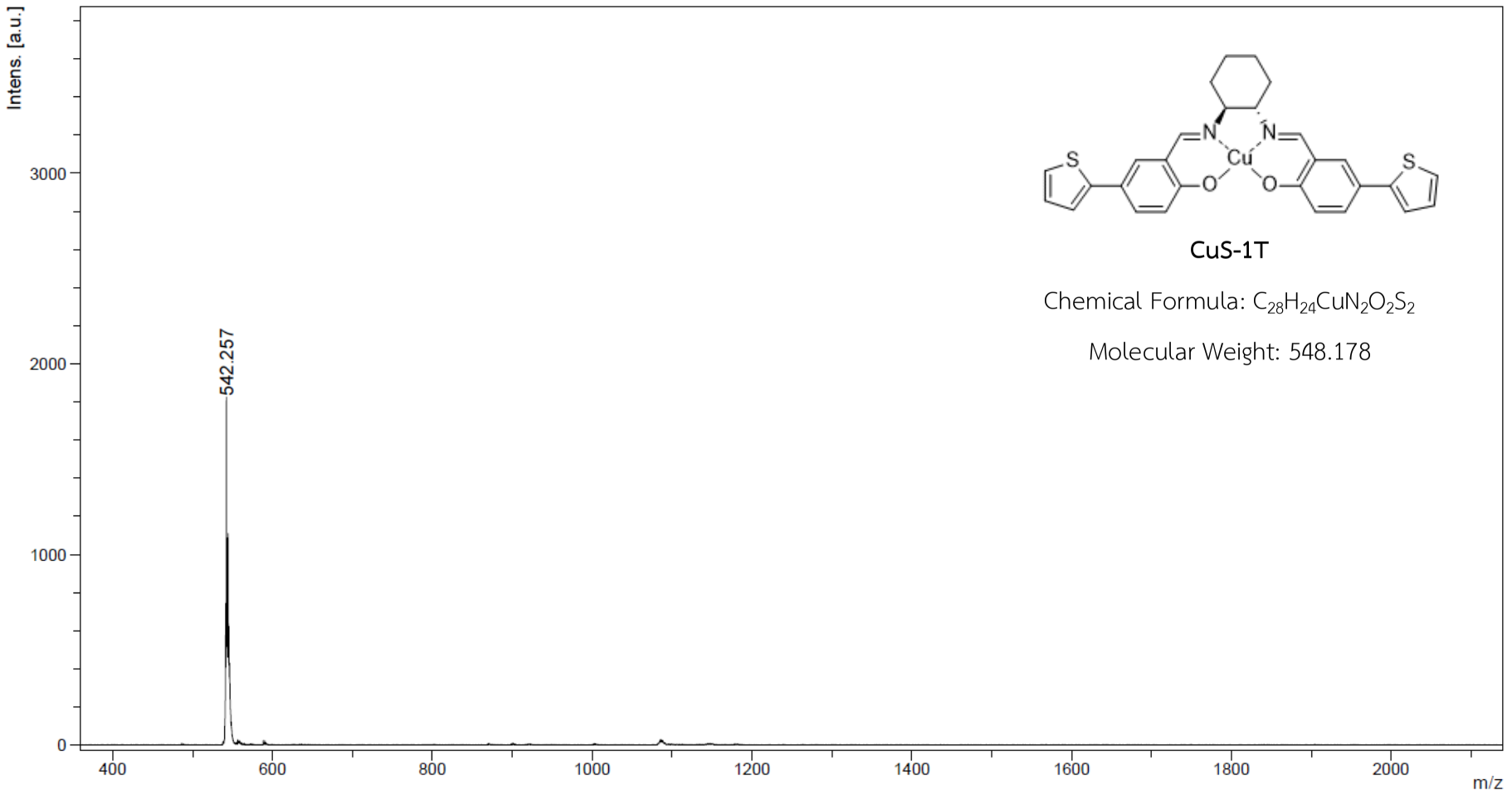

Figure A–27: MALDI-TOF spectrum of compound **CuS-1T**

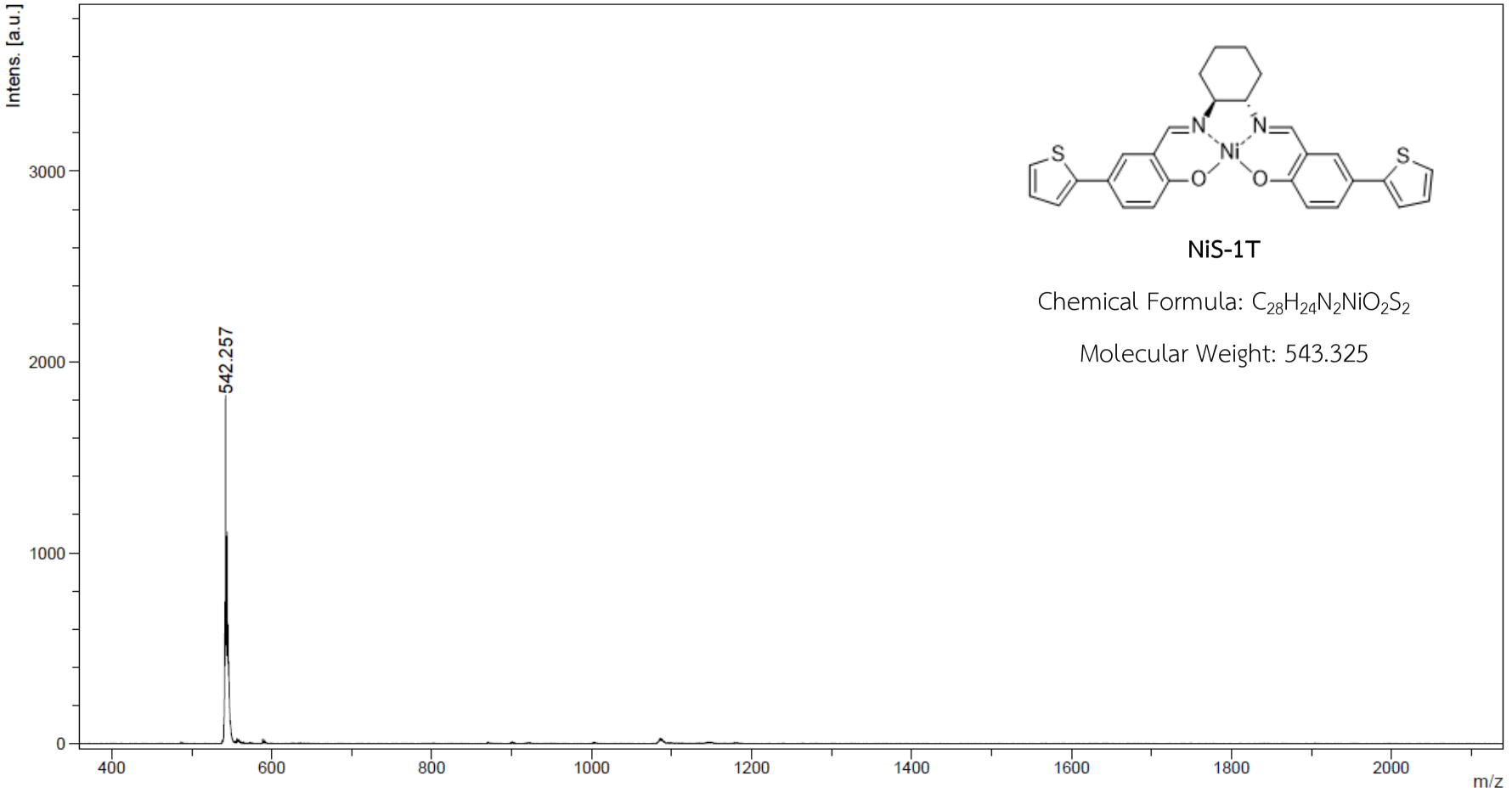

Figure A–28: MALDI-TOF spectrum of compound **NiS-1T**

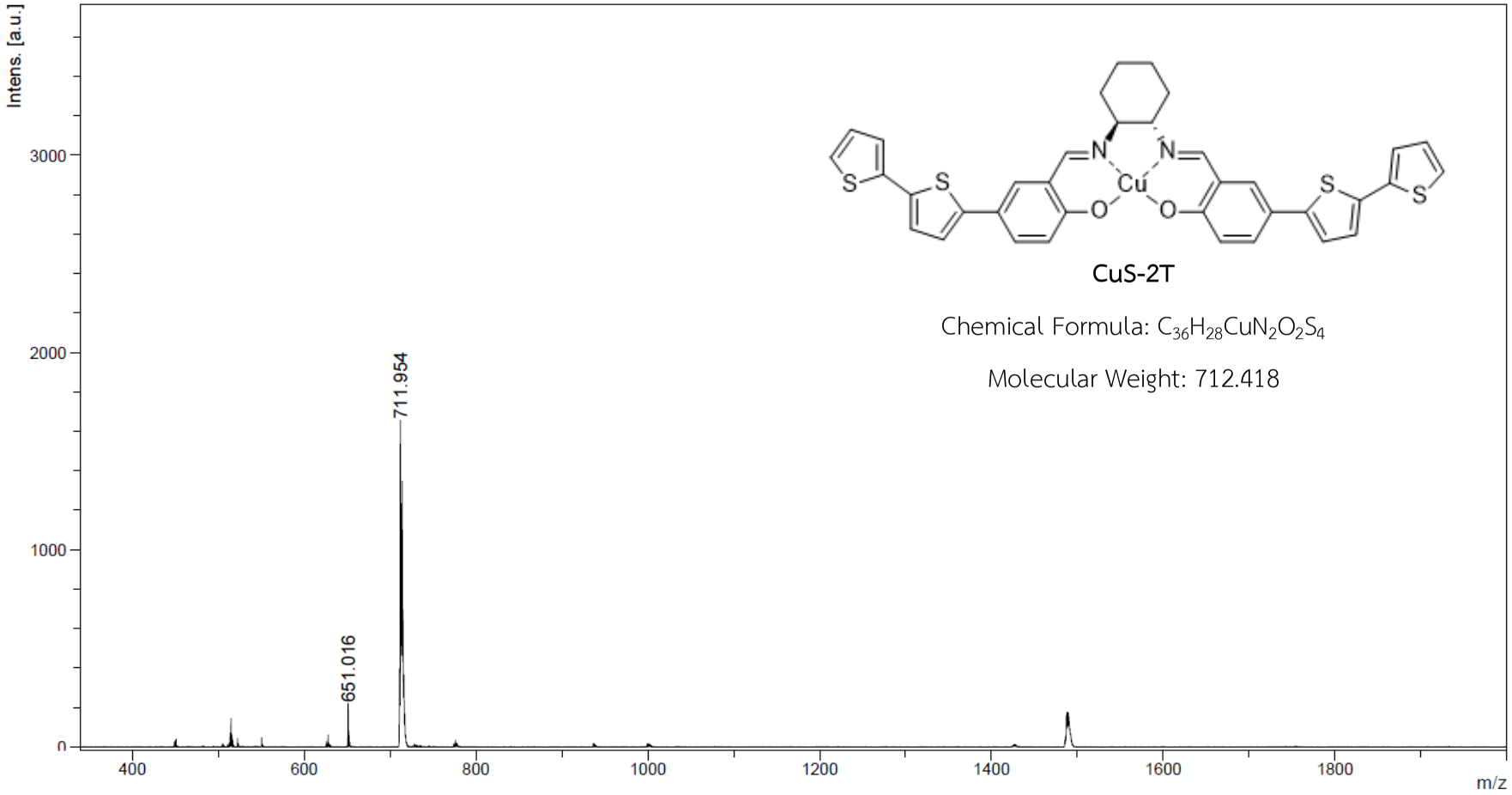

Figure A–29: MALDI-TOF spectrum of compound **CuS-2T**

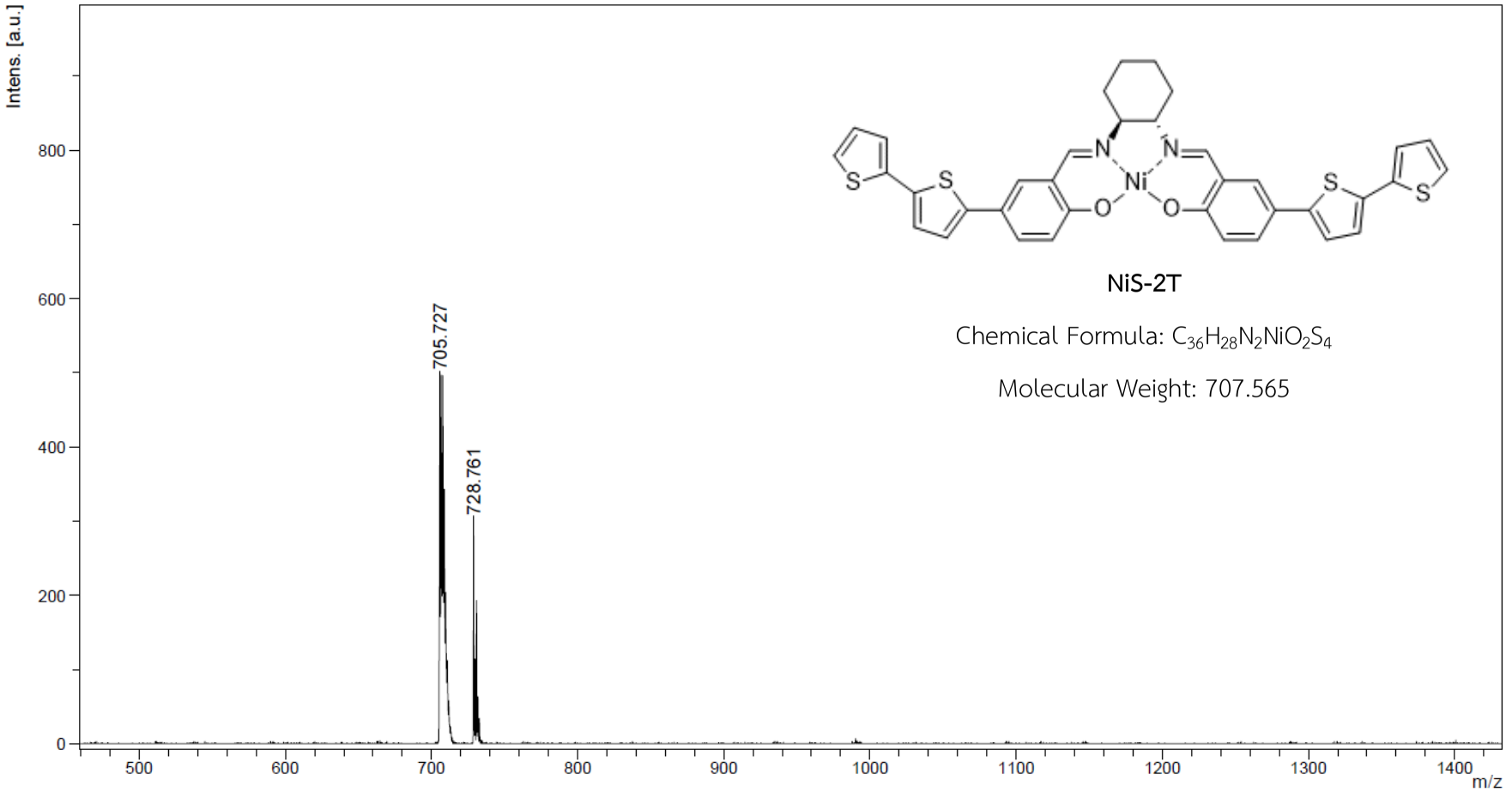

Figure A–30: MALDI-TOF spectrum of compound **NiS-2T**

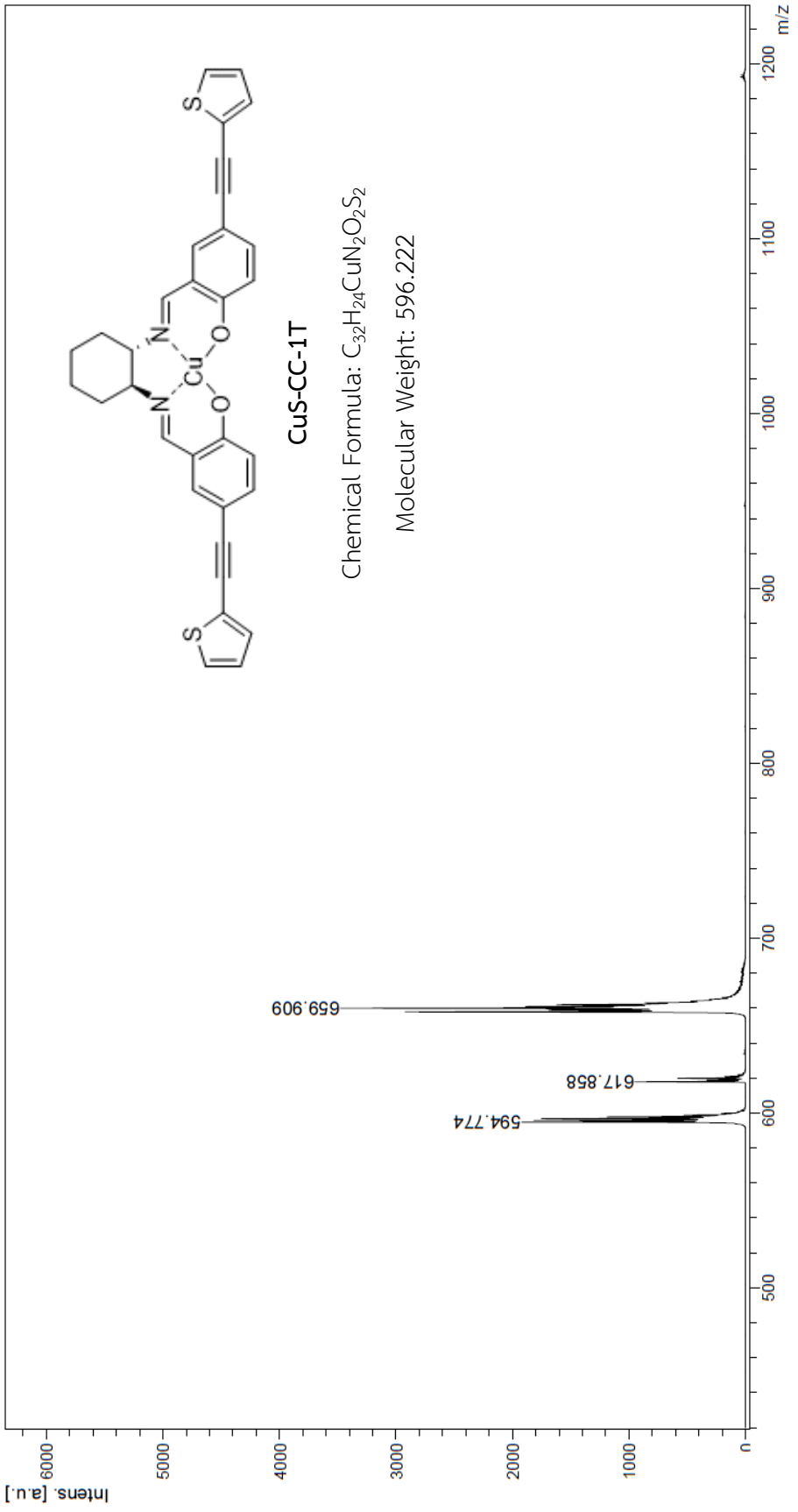

Figure A–31: MALDI-TOF spectrum of compound **CuS-CC-1T**

Mass Spectrum List Report

Analysis Info

Analysis Name	OSCK00531005_1.d	Acquisition Date	6/2/2017 10:42:06 AM
Method	Tune_wide_POS_pin_600.m	Operator	Administrator
Sample Name	CuS-CC-1Th	Instrument	micrOTOF 72
	CuS-CC-1Th		

Acquisition Parameter

Source Type	ESI	Ion Polarity	Positive	Set Corrector Fill	50 V
Scan Range	n/a	Capillary Exit	180.0 V	Set Pulsar Pull	337 V
Scan Begin	50 m/z	Hexapole RF	600.0 V	Set Pulsar Push	337 V
Scan End	3000 m/z	Skimmer 1	75.0 V	Set Reflector	1300 V
		Hexapole 1	25.0 V	Set Flight Tube	9000 V
				Set Detector TOF	2295 V

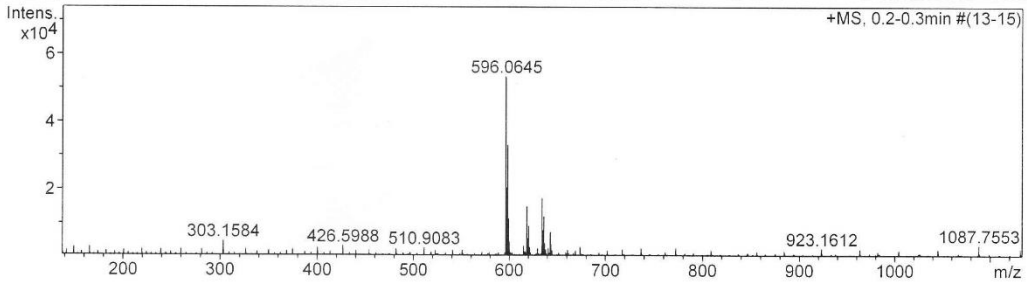

#	m/z	I	I %	S/N	FWHM	Res.
1	303.1584	4761	8.9	25.0	0.0128	23630
2	596.0645	53310	100.0	258.0	0.1052	5665
3	597.0670	20474	38.4	98.5	0.1059	5640
4	598.0633	33087	62.1	159.8	0.1037	5767
5	599.0651	11441	21.5	54.6	0.1051	5701
6	600.0624	4601	8.6	21.4	0.1051	5707
7	618.0458	15000	28.1	72.4	0.1016	6086
8	619.0496	5586	10.5	26.3	0.1037	5969
9	620.0433	9213	17.3	44.1	0.1001	6193
10	634.0190	17454	32.7	84.9	0.1119	5666
11	635.0231	7978	15.0	38.2	0.0951	6674
12	636.0180	12034	22.6	58.2	0.1094	5816
13	642.6283	7459	14.0	35.8	0.1127	5704
14	1191.1206	26167	49.1	126.6	0.1973	6037
15	1192.1227	20614	38.7	99.6	0.2007	5940
16	1193.1193	34865	65.4	169.3	0.2013	5927
17	1194.1219	23043	43.2	111.6	0.2011	5939
18	1195.1206	18142	34.0	87.7	0.1999	5979
19	1196.1184	9565	17.9	45.8	0.2009	5954
20	1197.1182	4921	9.2	23.1	0.1941	6168
21	1213.1039	7641	14.3	36.9	0.1966	6170
22	1214.1109	5620	10.5	26.9	0.2172	5590
23	1215.1038	10133	19.0	49.3	0.2006	6058
24	1216.1086	6805	12.8	32.8	0.2045	5947
25	1217.1006	5489	10.3	26.3	0.1913	6361
26	1229.0783	9981	18.7	49.1	0.2027	6065
27	1230.0793	7635	14.3	37.3	0.2102	5853
28	1231.0755	13998	26.3	69.3	0.2101	5859
29	1232.0808	9171	17.2	45.1	0.2109	5841
30	1233.0733	7616	14.3	37.3	0.2033	6066

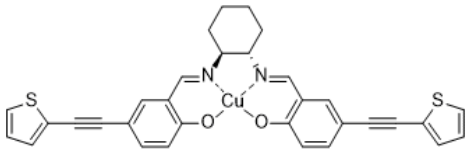

CuS-CC-1T

Chemical Formula: $C_{32}H_{24}CuN_2O_2S_2$

Exact Mass: 595.0575

$[(M+H)^+]$: 596.0648

Figure A–32: HR-ESI spectrum of compound **CuS-CC-1T**

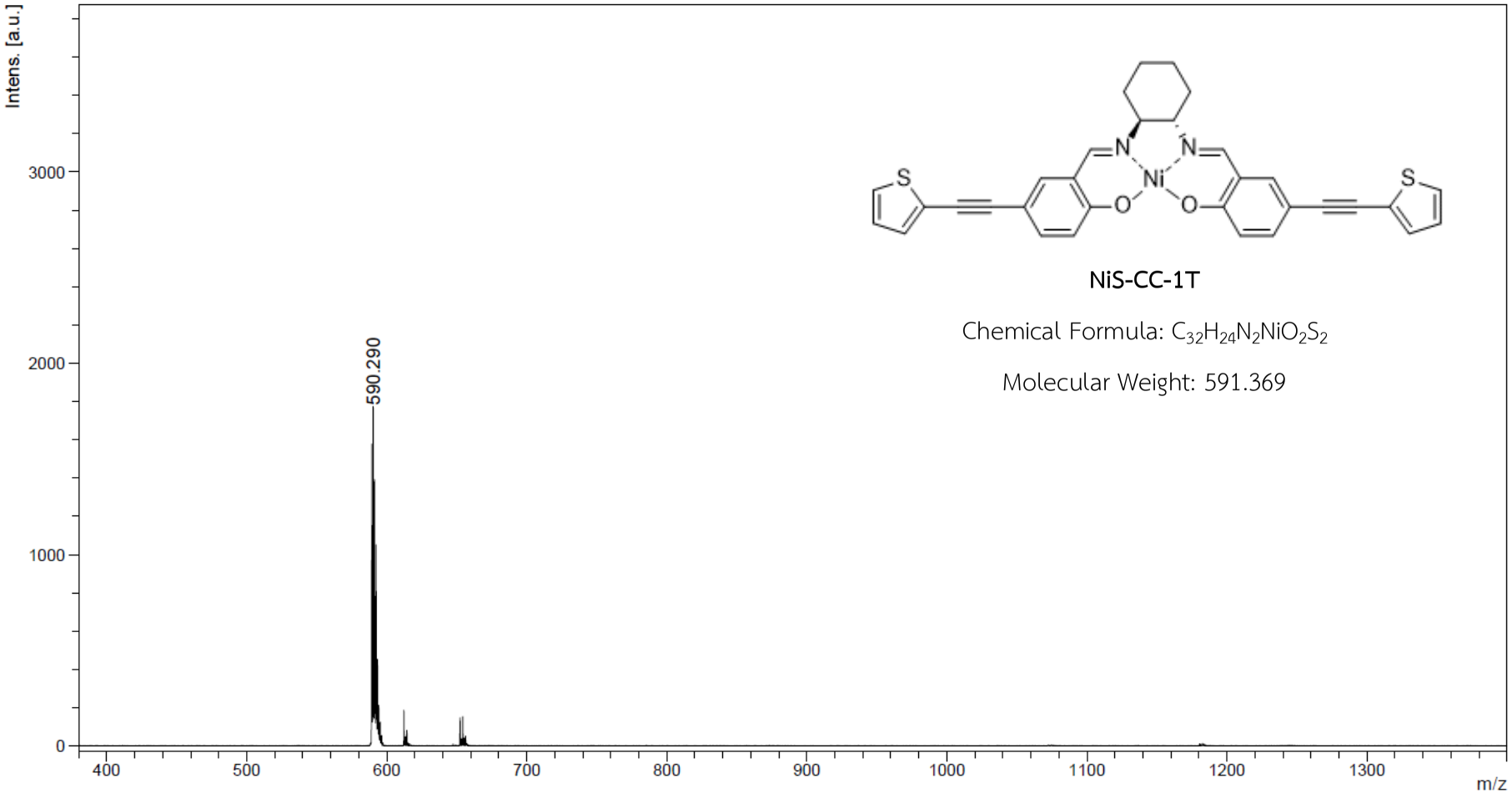

Figure A–33: MALDI-TOF spectrum of compound **NiS-CC-1T**

Mass Spectrum List Report

Analysis Info

Analysis Name	OSCK005310010.d	Acquisition Date	6/2/2017 10:08:26 AM
Method	Tune_wide_POS_pin_600.m	Operator	Administrator
Sample Name	NiS-CC-1TH	Instrument	micrOTOF 72
	NiS-CC-1TH		

Acquisition Parameter

Source Type	ESI	Ion Polarity	Positive	Set Corrector Fill	50 V
Scan Range	n/a	Capillary Exit	200.0 V	Set Pulsar Pull	337 V
Scan Begin	50 m/z	Hexapole RF	600.0 V	Set Pulsar Push	337 V
Scan End	3000 m/z	Skimmer 1	75.0 V	Set Reflector	1300 V
		Hexapole 1	25.0 V	Set Flight Tube	9000 V
				Set Detector TOF	2295 V

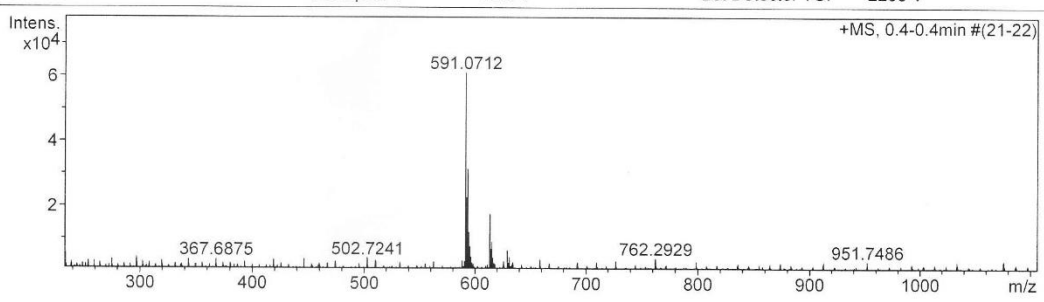

#	m/z	I	I %	S/N	FWHM	Res.
1	233.5807	5424	8.9	10.3	0.0113	20610
2	591.0712	61071	100.0	130.6	0.1128	5240
3	592.0766	22752	37.3	48.3	0.1158	5113
4	593.0682	31545	51.7	67.3	0.1203	4930
5	594.0692	12083	19.8	25.4	0.1163	5110
6	595.0687	7619	12.5	15.8	0.1238	4807
7	613.0521	17489	28.6	37.4	0.1114	5503
8	614.0565	6946	11.4	14.5	0.1364	4502
9	615.0542	8990	14.7	18.9	0.1221	5037
10	629.0255	6428	10.5	13.5	0.1179	5337
11	1181.1314	12273	20.1	26.4	0.2076	5689
12	1182.1320	9479	15.5	20.2	0.2035	5809
13	1183.1298	15002	24.6	32.4	0.2020	5857
14	1184.1284	9623	15.8	20.5	0.2339	5062
15	1185.1258	8568	14.0	18.2	0.2381	4976
16	1186.1312	5595	9.2	11.6	0.2192	5410
17	1203.1146	24292	39.8	53.3	0.2138	5628
18	1204.1190	17966	29.4	39.2	0.2275	5292
19	1205.1160	28786	47.1	63.3	0.2217	5436
20	1206.1189	20108	32.9	44.0	0.2129	5666
21	1207.1082	17797	29.1	38.9	0.2212	5458
22	1208.1069	11178	18.3	24.1	0.2324	5199
23	1209.1171	8124	13.3	17.3	0.2290	5280
24	1210.1154	5201	8.5	10.8	0.2603	4649
25	1219.0853	5014	8.2	10.4	0.2362	5162
26	1221.0907	5751	9.4	12.1	0.2255	5415
27	1443.1389	5173	8.5	11.3	0.0552	26164
28	2339.0648	7268	11.9	15.9	0.0342	68384
29	2339.2434	5448	8.9	11.8	0.0624	37516
30	2868.2412	4933	8.1	10.1	0.0669	42844

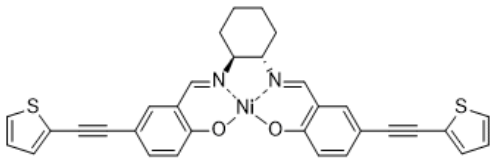

NiS-CC-1T

Chemical Formula: $C_{32}H_{24}N_2NiO_2S_2$

Exact Mass: 590.0633

$[(M+H)^+]$: 591.0705

Figure A–34: HR-ESI spectrum of compound **NiS-CC-1T**

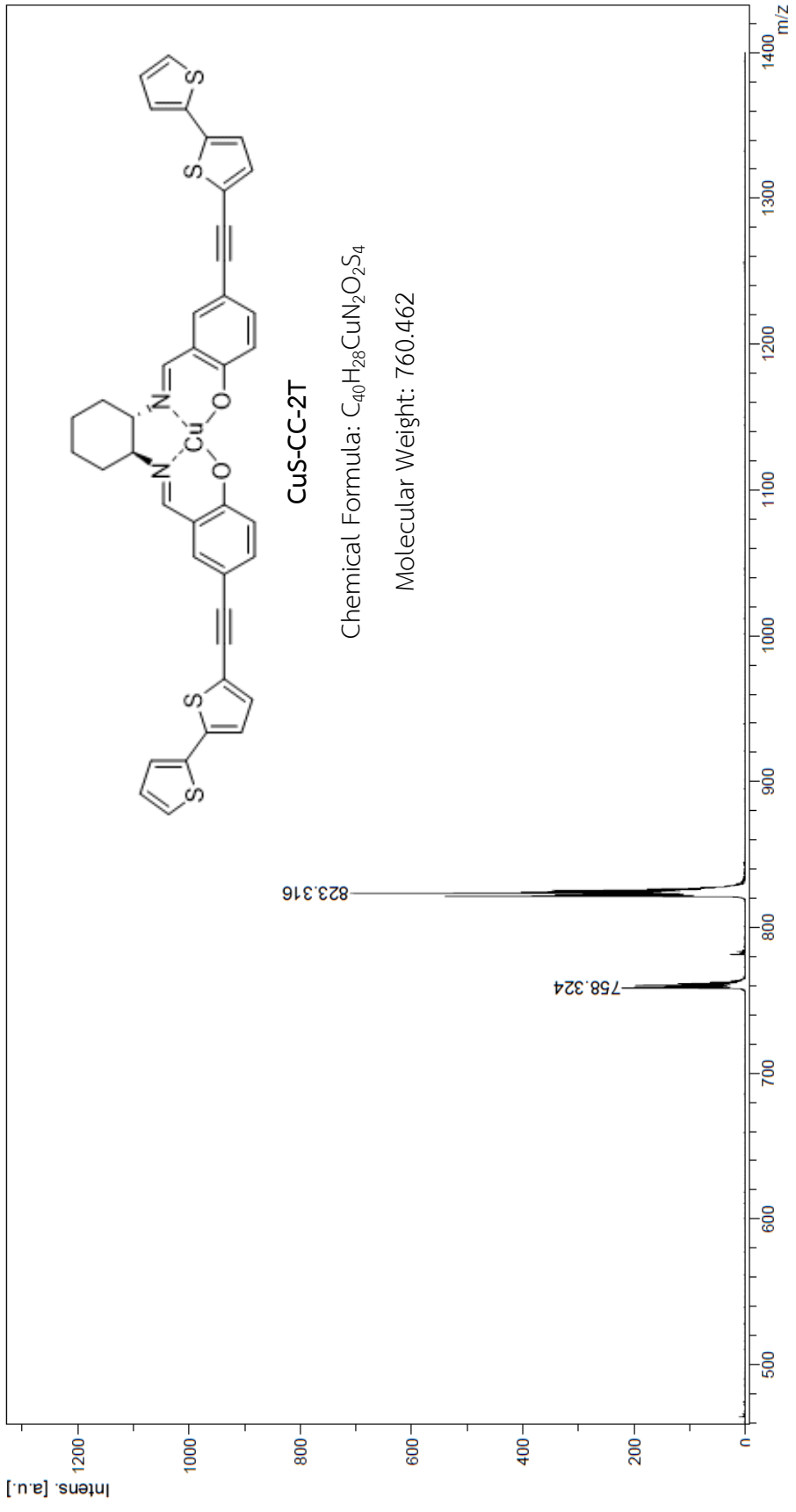

Figure A–35: MALDI-TOF spectrum of compound **CuS-CC-2T**

Mass Spectrum List Report

Analysis Info

Analysis Name	OSCK00531006_1.d	Acquisition Date	6/2/2017 10:47:12 AM
Method	Tune_wide_POS_pin_600.m	Operator	Administrator
Sample Name	CuS-CC-2Th	Instrument	micrOTOF 72
	CuS-CC-2Th		

Acquisition Parameter

Source Type	ESI	Ion Polarity	Positive	Set Corrector Fill	50 V
Scan Range	n/a	Capillary Exit	200.0 V	Set Pulsar Pull	337 V
Scan Begin	50 m/z	Hexapole RF	600.0 V	Set Pulsar Push	337 V
Scan End	3000 m/z	Skimmer 1	75.0 V	Set Reflector	1300 V
		Hexapole 1	25.0 V	Set Flight Tube	9000 V
				Set Detector TOF	2295 V

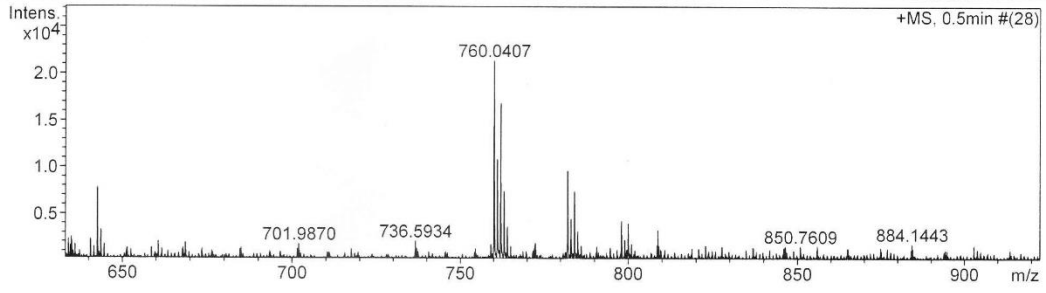

#	m/z	I	I %	S/N	FWHM	Res.
1	105.6029	3605	16.9	15.6	0.0073	14506
2	119.3619	3538	16.6	15.3	0.0084	14200
3	119.4258	3318	15.5	14.3	0.0085	13980
4	303.1535	4261	19.9	21.4	0.0118	25798
5	400.2273	4231	19.8	21.6	0.0131	30448
6	453.7892	12806	59.9	64.4	0.1018	4458
7	471.7971	4176	19.5	20.3	0.0920	5126
8	596.0670	12372	57.9	57.4	0.1173	5083
9	597.0668	5072	23.7	22.9	0.1221	4892
10	598.0639	7877	36.8	36.1	0.1208	4951
11	614.5966	3299	15.4	14.4	0.1266	4855
12	618.0482	7652	35.8	34.7	0.1074	5754
13	620.0453	4439	20.8	19.6	0.1128	5496
14	642.6290	7820	36.6	35.0	0.1299	4949
15	760.0407	21377	100.0	92.5	0.1470	5172
16	761.0402	10839	50.7	46.3	0.1484	5129
17	762.0407	16831	78.7	72.6	0.1423	5357
18	763.0399	7470	34.9	31.6	0.1427	5348
19	764.0363	3683	17.2	14.9	0.1512	5053
20	782.0220	9649	45.1	41.7	0.1505	5196
21	783.0262	4503	21.1	18.8	0.1612	4857
22	784.0206	7460	34.9	32.0	0.1507	5203
23	797.9955	4295	20.1	18.1	0.1456	5479
24	799.9927	4034	18.9	16.9	0.1617	4947
25	808.7113	3317	15.5	13.8	0.0253	32002
26	1456.7275	3735	17.5	20.8	0.0283	51452
27	1879.7358	4331	20.3	24.2	0.0327	57505
28	2356.5784	5574	26.1	30.6	0.0337	70011
29	2356.7966	3955	18.5	21.6	0.0601	39193
30	3100.2135	3357	15.7	19.1	0.0374	82796

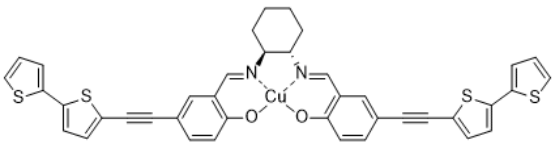

CuS-CC-2T

Chemical Formula: $C_{40}H_{28}CuN_2O_2S_4$

Exact Mass: 759.0330

$[(M+H)^+]$: 760.0402

Figure A–36: HR-ESI spectrum of compound **CuS-CC-2T**

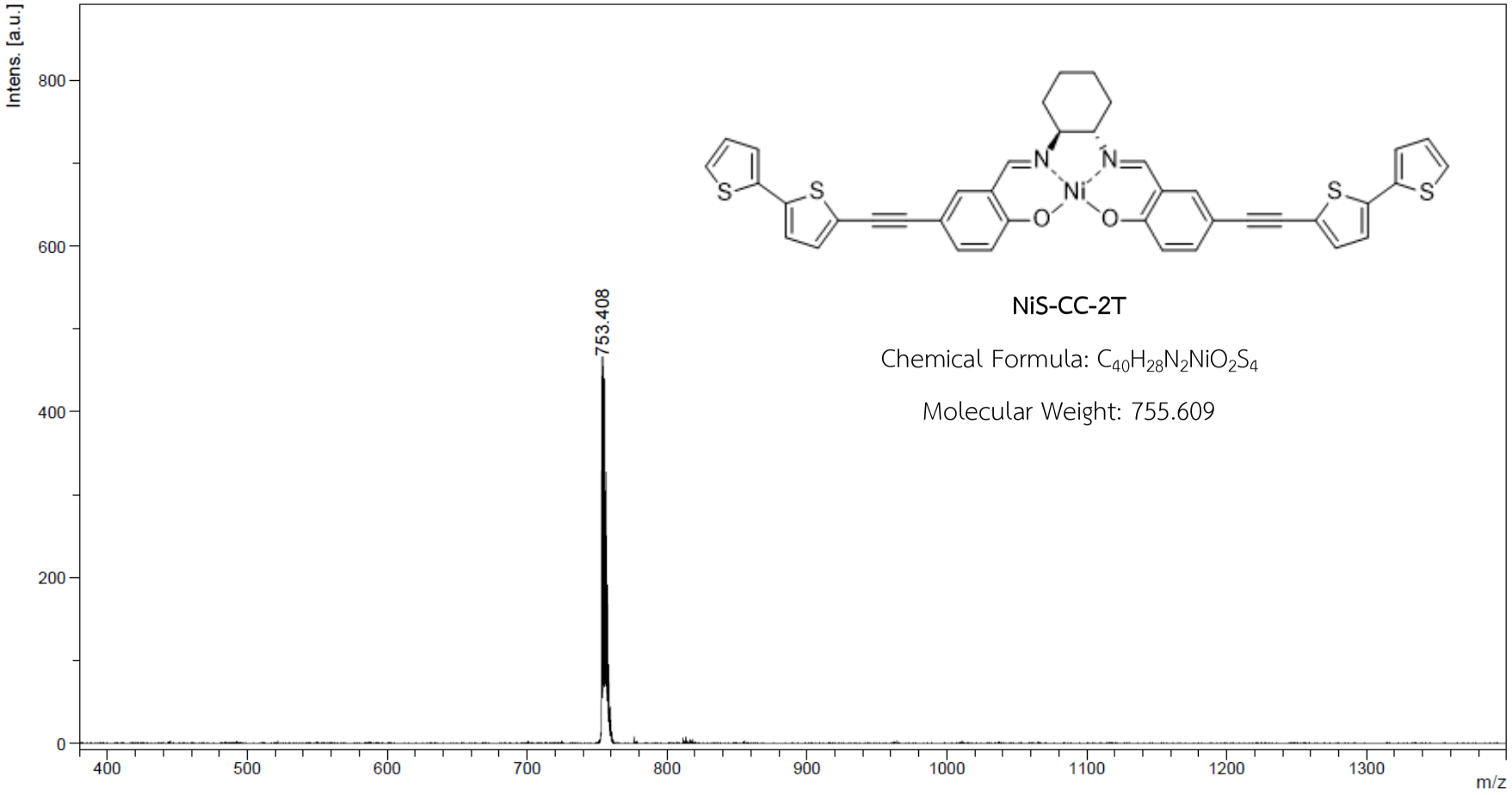

Figure A–37: MALDI-TOF spectrum of compound **NiS-CC-2T**

Mass Spectrum List Report

Analysis Info

Analysis Name	OSCK00531009_4.d	Acquisition Date	6/2/2017 10:04:17 AM
Method	Tune_wide_POS_pin_600.m	Operator	Administrator
Sample Name	NiS-CC-2TH	Instrument	micrOTOF 72
	NiS-CC-2TH		

Acquisition Parameter

Source Type	ESI	Ion Polarity	Positive	Set Corrector Fill	50 V
Scan Range	n/a	Capillary Exit	180.0 V	Set Pulsar Pull	337 V
Scan Begin	50 m/z	Hexapole RF	600.0 V	Set Pulsar Push	337 V
Scan End	3000 m/z	Skimmer 1	75.0 V	Set Reflector	1300 V
		Hexapole 1	25.0 V	Set Flight Tube	9000 V
				Set Detector TOF	2295 V

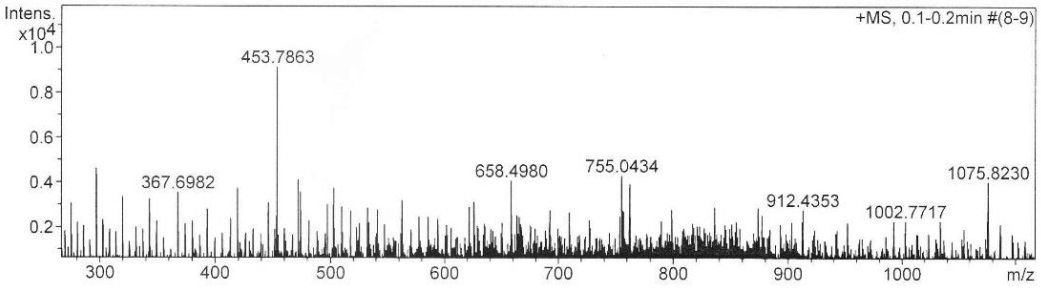

#	m/z	I	I %	S/N	FWHM	Res.
1	77.3910	4186	45.8	8.3	0.0064	12013
2	89.2873	4184	45.8	8.3	0.0114	7858
3	105.1938	3423	37.5	6.7	0.0086	12256
4	129.7633	4889	53.5	9.8	0.0091	14248
5	144.9735	4035	44.2	8.0	0.0137	10599
6	145.0418	4047	44.3	8.0	0.0166	8727
7	214.2697	3423	37.5	7.2	0.0182	11743
8	233.5843	3527	38.6	7.6	0.0114	20462
9	296.8582	4604	50.4	10.7	0.0141	21095
10	296.9512	4324	47.3	10.0	0.0322	9233
11	367.6982	3548	38.8	8.4	0.0132	27845
12	419.1169	3494	38.3	8.1	0.0148	28310
13	453.7863	9135	100.0	21.7	0.0947	4792
14	471.7985	4118	45.1	9.4	0.0878	5372
15	473.9308	3575	39.1	8.1	0.0149	31812
16	502.7254	3737	40.9	8.3	0.0259	19446
17	658.4980	4083	44.7	8.6	0.0220	29866
18	755.0434	4305	47.1	9.0	0.1440	5242
19	762.1728	3797	41.6	7.8	0.0220	34661
20	762.3039	3942	43.1	8.2	0.0264	28907
21	1075.8230	4036	44.2	9.3	0.0397	27118
22	1207.0209	4652	50.9	11.2	0.0262	45998
23	1442.9802	4115	45.0	10.3	0.0536	26915
24	1443.1364	5338	58.4	13.6	0.0533	27071
25	1864.3170	3657	40.0	9.1	0.0370	50342
26	2339.0689	5576	61.0	14.7	0.0371	63044
27	2339.1587	3929	43.0	10.1	0.1055	22174
28	2339.2511	5133	56.2	13.5	0.0468	50027
29	2798.8477	3528	38.6	8.9	0.0375	74695
30	2868.2201	4524	49.5	11.8	0.0505	56850

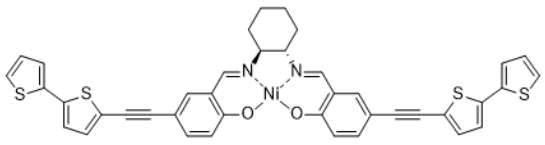

NiS-CC-2T

Chemical Formula: $C_{40}H_{28}N_2NiO_2S_4$

Exact Mass: 754.0387

$[(M+H)^+]$: 755.0460

Figure A–38: HR-ESI spectrum of compound **NiS-CC-2T**

VITA

Mr. Cherawat Kaewyai was born on Sunday 19th September, 1993, in Bangkok, Thailand. In 2015, he graduated with a Bachelor's degree of Science in Chemistry, from Srinakharinwirot University. Next, he has been studied for a Master's degree of Science in Petrochemical and polymer science, Faculty of Science, Chulalongkorn University in 2015. His poster presentation and proceeding "Synthesis of Thiophene-substituted Metallosalen for Reduction of Carbon Dioxide" have been submitted at The 44th National Graduate Research Conference (NGRC 44) in Ubon Ratchathani University, 19-20th October, 2017, Thailand.